SECRET

CENTRAL RESEARCH LIBRARY
DOCUMENT COLLECTION

ORNL-1108
Progress
9a

OAK RIDGE NATIONAL LABORATORY LIBRARY
3 4456 0022841 1

METALLURGY DIVISION

QUARTERLY PROGRESS REPORT

FOR PERIOD ENDING JULY 31, 1951

LABORATORY RECORDS
1951

AEC RESEARCH AND DEVELOPMENT REPORT

CENTRAL RESEARCH LIBRARY
DOCUMENT COLLECTION
LIBRARY LOAN COPY
DO NOT TRANSFER TO ANOTHER PERSON
If you wish someone else to see this document, send in name with document and the library will arrange a loan.

OAK RIDGE NATIONAL LABORATORY
OPERATED BY
CARBIDE AND CARBON CHEMICALS COMPANY
A DIVISION OF UNION CARBIDE AND CARBON CORPORATION
UCC
POST OFFICE BOX P
OAK RIDGE, TENNESSEE

DECLASSIFIED
CLASSIFICATION CHANGED TO:
BY AUTHORITY OF: AEC 10-9-57
BY: Beerman 6-19-68

SECRET

SECRET

ORNL-1108

This document consists of 94 pages.

Copy 9 of 140 copies. Series A.

Contract No. W-7405, eng 26

METALLURGY DIVISION

J. H. Frye, Jr., Director

QUARTERLY PROGRESS REPORT

for Period Ending July 31, 1951

Edited by:

E. C. Miller and W. H. Bridges

Date Issued JAN 23 1952

OAK RIDGE NATIONAL LABORATORY LIBRARY
3 4456 0022841 1

OAK RIDGE NATIONAL LABORATORY
operated by
CARBIDE AND CARBON CHEMICALS COMPANY
A Division of Union Carbide and Carbon Corporation
Post Office Box P
Oak Ridge, Tennessee

RESTRICTED DATA

This document contains restricted data as defined in the Atomic Energy Act of 1946.

CAUTION

This document contains information affecting the National Defense of the United States. Its transmission or the disclosure of its contents in any manner to any unauthorized person is prohibited and may result in severe criminal penalties under applicable Federal laws.

SECRET

DISTRIBUTION LIST

ORNL 1108
Progress

INTERNAL DISTRIBUTION

1 G. T. Felbeck (C&CCC)
2-3 Chemistry Library
4 Physics Library
5 Biology Library
6 Health Physics Library
7 Metallurgy Library
8-9 Training School Library
10-13 Central Files
14 C. E. Center
15 C. E. Larson
16 W. B. Humes (K-25)
17 W. D. Lavers (Y-12)
18 A. M. Weinberg
19 E. H. Taylor
20 E. J. Murphy
21 E. D. Shipley
22 J. H. Frye, Jr.
23 F. C. VonderLage
24 R. C. Briant
25 J. A. Swartout
26 S. C. Lind
27 F. L. Steahly
28 A. H. Snell
29 A. Hollaender
30 M. T. Kelley
31 K. Z. Morgan
32 J. S. Felton
33 A. S. Householder
34 C. S. Harrill
35 C. E. Winters
36 D. S. Billington
37 D. W. Cardwell
38 E. M. King
39 C. E. Ellis
40 D. D. Cowen
41 P. M. Reyling
42 W. H. Bridges
43 A. G. H. Andersen
44 L. K. Jetter
45 E. J. Boyle
46 W. D. Manly
47 C. D. Susano
48 W. W. Parkinson
49 R. J. Gray
50 B. S. Borie
51 C. D. Smith
52 D. E. Hamby
53 E. E. Stansbury
54 G. P. Smith
55 J. E. Cunningham
56 Anton Brasunas
57 R. S. Crouse
58 R. E. Adams
59 J. H. Erwin
60 J. O. Betterton, Jr.
61 R. C. Williams
62 G. M. Adamson
63 E. S. Bomar
64 L. A. Abrams
65 R. B. Day
66 T. W. Fulton
67 F. W. Drosten
68 R. B. Oliver
69 P. Patriarca

RESTRICTED DATA

This document contains restricted data as defined in the Atomic Energy Act of 1946.

CAUTION

This document contains information affecting the National Defense of the United States. Its transmission or the disclosure of its contents in any manner to any unauthorized person is prohibited and may result in severe criminal penalties under applicable Federal laws.

70 J. T. Howe
71 T. H. Blewitt
72 W. E. Taylor
73 J. H. Crawford, Jr.
74 A. F. Cohen
75 J. C. Wilson
76 H. W. Savage
77 Carnegie Institute of Technology (E. C. Creutz)
78 Princeton University (E. P. Wigner)
79 Phillips Petroleum, Idaho Falls (Attn: Librarian)

EXTERNAL DISTRIBUTION

80-82 Aircraft Nuclear Propulsion Project, Oak Ridge
83-90 Argonne National Laboratory
91-98 Atomic Energy Commission, Washington
99 Battelle Memorial Institute
100-103 Brookhaven National Laboratory
104-107 Carbide and Carbon Chemicals Company (Y-12)
108-109 Knolls Atomic Power Laboratory
110-111 General Electric Company, Richland
112 Hanford Operations Office
113-116 Los Alamos
117 Massachusetts Institute of Technology (Kaufmann)
118-119 New York Operations Office
120 Patent Branch, Washington
121 Savannah River Operations Office, Wilmington
122-136 Technical Information Service, Oak Ridge
137-140 University of California Radiation Laboratory

RESTRICTED DATA
This document contains restricted data as defined in the Atomic Energy Act of 1946.

CAUTION
This document contains information affecting the National Defense of the United States. Its transmission or the disclosure of its contents in any manner to any unauthorized person is prohibited and may result in severe criminal penalties under applicable Federal laws.

Reports previously issued in this series are as follows:

ORNL-28	Period Ending March 1, 1948
ORNL-69	Period Ending May 31, 1948
ORNL-407	Period Ending July 31, 1949
ORNL-511	Period Ending October 31, 1949
ORNL-583	Period Ending January 31, 1950
ORNL-754	Period Ending April 30, 1950
ORNL-827	Period Ending July 31, 1950
ORNL-910	Period Ending October 31, 1950
ORNL-987	Period Ending January 31, 1951
ORNL-1033	Period Ending April 30, 1951

TABLE OF CONTENTS

	PAGE NO.
SUMMARY	1
1. THORIUM RESEARCH PROGRAM	3
Mechanical Testing	3
Physical Properties	4
Density	4
Crystal Structure	7
Fabrication	7
Swaging, rolling, and drawing	8
Extrusion cladding of uranium and thorium	8
Thorium Alloy Development	10
2. PREFERRED ORIENTATION AND ANISOTROPY IN PROPERTIES OF METALS	12
3. ANP PROGRAM	20
Corrosion Testing	20
Liquid metal corrosion	20
Fluoride corrosion	27
Hydroxide corrosion	29
Powder Metallurgy Laboratory	33
Fabrication group	33
Hot rolling	33
Mechanically formed matrix	36
Loose-powder bonding	37
Rubberstatic pressing	38
Control rods	47
Cladding beryllium oxide	47
Compatibility	48
Refractory metals	48
Creep-Ruture Laboratory	48
Stress-relaxation testing	55
Welding Laboratory	55
Welding of inconel	55
Mechanical properties of welds	55
All-weld-metal tensile tests	57
Inspection	58
Corrosion of welds	58
Special tests	58
Ceramics Laboratory	59
Physical Chemistry of Liquid Metals	61
Interaction of solid and liquid metals	61

SECRET

4. X-RAY-DIFFRACTION LABORATORY 64
Recovery from Cold Work in Copper 64
Low-Temperature X-Ray Diffraction 64

5. TENSILE PROPERTIES OF PURE METALS 66
The Stress-Strain-Time Curve at Infinite Time 66
Empirical Stress, Strain, Strain Rate, Time Relations in Pure Metals 67

6. FUNDAMENTAL STUDIES OF ALLOYING 72

7. METALLOGRAPHY OF ZIRCONIUM AND ITS ALLOYS 77

8. FUEL ELEMENT FABRICATION 82
Idaho Units 82
Bulk Shielding Facility Units 82
LITR Unit 82
RaLa Units 82

9. SERVICE WORK 83
Melting, Casting, and Fabrication Facility 83
Rolling Mill 83
X-Ray-Diffraction Laboratory 84
Creep-Ruture Laboratory 84

SECRET

LIST OF TABLES

TABLE NO.	TITLE	PAGE NO.
1.1	Effect of Strain Rate on Yield and Tensile Strength of Ames Thorium	3
1.2	Tensile-Test Data for Ames Extruded Thorium	4
1.3	Results of Torsion Tests on Various Materials	4
1.4	Extrusion Cladding of Thorium	9
1.5	Extrusion Cladding of Uranium	10
3.1	Corrosion and Operational Data on Lead- and Lithium-Containing Thermal Convection Loops	22
3.2	Summary of Fluoride Corrosion Data Obtained in 100 hr at 1000°C (1830°F)	32
3.3	Summary of Hydroxide Corrosion Data Obtained in 100-hr Tests at 815°C (1500°F) and 1000°C (1830°F)	40
3.4	Summary of Results of Investigation on ZrO_2	48
3.5	Room-Temperature Tensile Properties of Inconel Tube-to-Header "Pairs"	57
3.6	Inconel All-Weld-Metal Tensile Values	60
7.1	Analyses for Gases in Crystal-Bar Zirconium	77
7.2	Diamond Pyramid Hardness Values of Zirconium Alloys, 10 kg Load	77

LIST OF FIGURES

FIG. NO.	TITLE	PAGE NO.
1.1	Broken Tensile Specimens of Extruded Ames Thorium	5
1.2	Broken Tensile Specimens of Extruded Ames Thorium	6
1.3	Experimental Arc Furnace Used for Preparation of Small Amounts of High-Purity Alloys	11
2.1	Photomicrographs Showing Deformed Grain Structure in the Middle of the Length of 1½-in.-Diameter α-Extruded Rod in the As-Extruded Condition	13
2.2	Photomicrographs Showing Completely Recrystallized Grain Structure in the Middle of the Length of 1½-in.-Diameter α-Extruded Rod After Annealing 1 hr at 550°C	14
2.3	Preferred Orientation Plot — (110) — 1½-in.-Diameter α-Extruded Uranium Rod	15
2.4	Preferred Orientation Plot — (021) — 1½-in.-Diameter α-Extruded Uranium Rod	15
2.5	Preferred Orientation Plot — (002) — 1½-in.-Diameter α-Extruded Uranium Rod	16
2.6	Preferred Orientation Plot — (111) — 1½-in.-Diameter α-Extruded Uranium Rod	16
2.7	Preferred Orientation Plot — (112) — 1½-in.-Diameter α-Extruded Uranium Rod	17
2.8	Preferred Orientation Plot — (131) — 1½-in.-Diameter α-Extruded Uranium Rod	17
2.9	Preferred Orientation Plot — (040) — 1½-in.-Diameter α-Extruded Uranium Rod	18
2.10	Preferred Orientation Plot — (200) — 1½-in.-Diameter α-Extruded Uranium Rod	18
2.11	Preferred Orientation Plot — (041) — 1½-in.-Diameter α-Extruded Uranium Rod	19
3.1	Outer Surface of 316 Stainless Steel After 400 hr of Exposure to Sodium at 1000°C	21
3.2	Sections Showing Formation of Metal Crystals Adjacent to Cold-Leg Wall of V-36 Thermal-Convection Loop Containing Lead After 84 hr of Operation	24

3.3 Hot-Leg Failure After 7 hr of Operation at 1500°F of 316 Stainless Steel Thermal-Convection Loop Containing Lead 25

3.4 Highly Magnified View of Internal Surface of 446 Stainless Steel Cold Leg from Thermal-Convection Loop Operated With Lead (Area at Approximately 1300°F) 26

3.5 View of Cold Zone of 446 Stainless Steel Loop Showing Attacked Surface and Metal Crystals Which Form in Lead (Dark Areas), Thereby Restricting Convective Flow 27

3.6 View of Cold-Zone Weld in 1010 Steel Loop Showing Metal Crystal Formation Adjacent to Pipe Wall Covered with Iron Oxide, Presumably Formed During Loop Fabrication 28

3.7 Surface of Nickel A Specimen After 100 hr of Exposure To a Na-Be-U Ternary Fluoride Mixture at 1000°C 29

3.8 Surface of 310 Stainless Steel Specimen After 100 hr of Exposure to a Na-Be-U Fluoride Mixture at 1000°C 30

3.9 Surface of Hastelloy B Specimen After 100 hr of Exposure to a Na-Be-U Fluoride Mixture at 1000°C 31

3.10 Surface of Inconel After 100 hr of Exposure at 1000°C to $3NaF \cdot UF_4$ 33

3.11 Surface of 347 Stainless Steel After 100 hr of Exposure at 1000°C to $3NaF \cdot UF_4$ 34

3.12 Surface of Inconel Specimen After 100 hr of Exposure to Strontium Hydroxide at 1000°C 35

3.13 Surface of Inconel Specimen Severely Oxidized After 100 hr of Exposure to Sodium Hydroxide at 815°C (1500°) 36

3.14 Surface of Inconel Specimen After 100 hr of Exposure to Sodium Hydroxide + 3% Sodium Hydride at 815°C (1500°F) 37

3.15 Surface of Nickel A Apparently Unattacked After 100 hr of Exposure to Sodium Hydroxide at 815°C (1500°F) 38

3.16 Surface of 304 Stainless Steel After 100 hr of Exposure to Barium Hydroxide at 1000°C 39

3.17 Effect of Cold-Rolling 30% UO_2—70% 302 Stainless Steel (-325 Mesh) 42

3.18 Effect of Cold-Rolling 30% UO_2—70% Iron (10 μ) 43

3.19 Effect of UO_2 Particle Size 44

3.20 Effect of Surface Preparation on the Bonding of Loose Powders Containing UO_2 to a 316 Stainless Steel Plate 45

3.21	Difference in Sintering in Stack of Eleven 316 Stainless Steel Plates with Bonded Powder	46
3.22	Rubberstatic Die Assembly	47
3.23	Four of the Eight Installations for Creep Testing in Vacuum	49
3.24	Units for Creep Testing in Purified Argon	50
3.25	Centralized Instrument Panel in Creep Laboratory	51
3.26	Furnace for Creep-Rupture Testing in Vacuum or Inert Atmosphere	52
3.27	Eutectic Melting of Uranium in Contact with Fe-Ni-Cr Alloys	53
3.28	Strain-Time Curves for Natural Uranium	54
3.29	Relaxation Curves of 316 Stainless Steel at 1500°F	56
3.30	Fatique-Testing Apparatus	58
3.31	Effect of Penetration on Fatigue Life of Inconel Tube-to-Header Joints	59
4.1	Root-Mean-Square Change in Length vs. Length for Cold-Worked Copper Filings During Recovery	64
5.1	True Stress-Natural Strain Diagram, Logarithmic	66
5.2	Creep Curves of OFHC Copper	69
5.3	Relations Between Creep Curves and Level Curves of the $(\sigma)_v$ Surface	70
7.1	1-in. Westinghouse Crystal Bar as Received	78
7.2	Zirconium Crystal Bar	79
7.3	Zirconium-Nickel Alloy, 2.07 wt % Nickel	80
7.4	Zirconium-Nickel Alloy, 4.08% Nickel	81

SUMMARY

The effect of strain rate on the tensile properties of thorium is being investigated. It has been found that the yield strength increases slightly with increasing strain rate, and that tensile strength increases but to a less extent. The shear modulus has been determined to be 4.26×10^6 psi. A precision measurement of the lattice parameter of iodide-process thorium has been made, giving a value of 5.0871 ± 0.0002 A. Studies on the fabrication of thorium by extrusion and drawing have continued, as have studies on the extrusion cladding of thorium and uranium with zirconium.

In order to determine whether or not the type of preferred orientation developed in α-extruded uranium rod was dependent on the actual extrusion temperature, X-ray-diffraction studies were made of completely recrystallized and unrecrystallized extruded uranium. The results show that the texture developed upon deformation is not always retained upon recrystallization.

The corrosion testing of various metals and alloys in liquid sodium, lead, and lithium and in molten fluorides and hydroxides has been continued. The interaction of sodium with 316 stainless steel appears negligible during static testing. The testing of the molten media in thermal convection loops continues to be plagued by failures other than corrosion.

The investigation of means of fabrication of solid fuel elements by powder metallurgy techniques has progressed. Only minor segregation of UO_2 in an iron matrix was noted after hot rolling. Stainless steel matrices, on the other hand, displayed considerable segregation. Rubberstatic pressing has been added as a technique for the fabrication of fuel elements and control rods.

The Creep Laboratory is essentially complete. The study of thermocouple stability in vacuum has shown that chromel-alumel couples give consistent checks with control and reference temperatures, whereas iron-constantan and platinum—10% rhodium couples gave erratic results. Some preliminary results have been obtained on uranium, thorium, 316 stainless steel, inconel, and columbium.

The evaluation of welded tube-to-header joints of inconel has received considerable attention. Tests in tension have shown that the joint is of the same order of magnitude as the original material, the failures occurring in the zone adjacent to the weld. A rotating tubular beam fatigue test apparatus has been developed, and preliminary tests show that joints with complete penetration have better fatigue life than joints with 70% penetration.

The establishment of a ceramics laboratory has proceeded satisfactorily. Basic research, engineering development, and service work will be done.

In the research on the fundamentals of liquid metal—solid metal interaction, the immersion of copper in liquid bismuth has resulted in the deposition of copper crystals removed from the specimen. This might be the

result of one or more mechanisms: thermal gradients, thermal cycling, or free energy changes. Further work is being done to elucidate the phenomenon.

A program to investigate the alloys of the transition elements in order to reconcile the theories of Mott and Jones, and Pauling concerning these elements has been initiated. At present the program will concern itself with Group IV-A elements: titanium, zirconium, and hafnium. These will be studied in the pure state as well as in the form of their alloys with other elements.

The metallography laboratory has joined with several other installations to study the metallography of zirconium and its alloys. Zirconium alloyed with nickel and with tungsten is being studied here. Thus far the nickel alloy up to 4.08% by weight of nickel quenched in various ways has been studied.

. . . . .

1. THORIUM RESEARCH PROGRAM

MECHANICAL TESTING

Ames thorium was tested at various rates of loading to determine the effect of strain rate upon the tensile properties of the metal. The analysis of the particular lot of metal used for these tests was as follows: carbon 0.15%, beryllium 0.3%, silicon 0.4%, thorium 98.7%. Sheet-metal type specimens 0.226 in. thick and 0.500 in. wide were machined from cold-rolled sheet and fully annealed by heating at a temperature of 750°C for ½ hr. Tests were made at strain rates of 0.01, 0.05, and 0.20 in./min. None of the specimens showed a definite yield point. The yield strength, calculated at 0.2% offset, was found to increase slightly with increasing strain rate. The tensile strength was affected to an even less extent by the strain rate, the greater strain rates resulting in higher values of tensile strength. The data are given in Table 1.1.

During the investigation of fabrication techniques for thorium, tensile-test specimens were prepared from each extrusion of thorium rod by machining the extruded rod and annealing at 750°C for ½ hr. The results of tests on these specimens were intended to provide one means of evaluating extrusion conditions.

The specimens were tested at a constant cross-head speed of 0.1 in./min. No correlation between tensile properties and extrusion conditions was found, but the tensile properties of the extruded material showed a definite relation to the original ingots from which the extrusions were made. Analyses of the various lots of material are being made to determine the cause of the wide variation of strength found in the different specimens. The tensile data for these specimens are shown in Table 1.2. The fractured specimens are shown in Figs. 1.1 and 1.2.

The torsion machine used in determining shear modulus has been modified to permit more accurate measurement of twist. An average value of 4.26×10^6 was obtained for the shear modulus of Ames thorium. The data are shown in Table 1.3.

TABLE 1.1

Effect of Strain Rate on Yield and Tensile Strength of Ames Thorium

SPECIMEN NO.	STRAIN RATE (in./min)	YIELD STRENGTH, 0.2% OFFSET (psi)	TENSILE STRENGTH (psi)
1	0.20	25,400	36,500
3	0.05	23,000	34,600
4	0.05	21,600	34,600
2	0.01	20,900	33,200

TABLE 1.2

Tensile-Test Data for Ames Extruded Thorium

SPECIMEN NO.	ELONGATION (%)	REDUCTION IN AREA (%)	YIELD POINT (psi)	TENSILE STRENGTH (psi)	AVERAGE TRUE BREAKING STRENGTH (psi)
223A	50	75	22,100	30,500	58,000
222C	52	71	20,750	30,300	60,300
227A	51	74	21,100	29,800	52,000
234A	52	74	22,700	31,100	58,000
231A	54	74	28,000	34,200	72,500
231B	48	74	27,500	34,800	75,000
231C1	50	71	27,600	34,300	64,300
231C2	52	73	27,400	34,500	72,300
239C1	48	70	33,100	38,200	77,500
239D2	46	70	31,900	38,900	79,400
239D	49	72	31,400	37,800	73,300
239B	48	65	32,100	38,800	70,500
239A	49	69	31,300	39,000	78,500

TABLE 1.3

Results of Torsion Tests on Various Materials

MATERIAL	SHEAR MODULUS (psi)	
	EXPERIMENTAL VALUE	HANDBOOK VALUE
Steel	11,540,000	
Steel	11,300,000	
Steel	11,250,000	
Average	11,360,000	11,700,000
Aluminum	3,860,000	
Aluminum	3,850,000	
Average	3,855,000	3,850,000
Ames thorium	4,210,000	
Ames thorium	4,270,000	
Ames thorium	4,300,000	
Average	4,260,000	

Steel and aluminum specimens were tested to check the known values of shear modulus for these materials. The average experimental value of shear modulus for steel was about 3% below the ASM Metals Handbook (1948) value, while the experimental value for aluminum agrees almost exactly with the handbook value.

PHYSICAL PROPERTIES

Density. The density of various types of thorium after different treatments was determined by immersion. The samples were weighed in carbon tetrachloride or distilled water and then weighed in air, the difference in weight being the weight of an equal volume of the liquid. If M_a is the

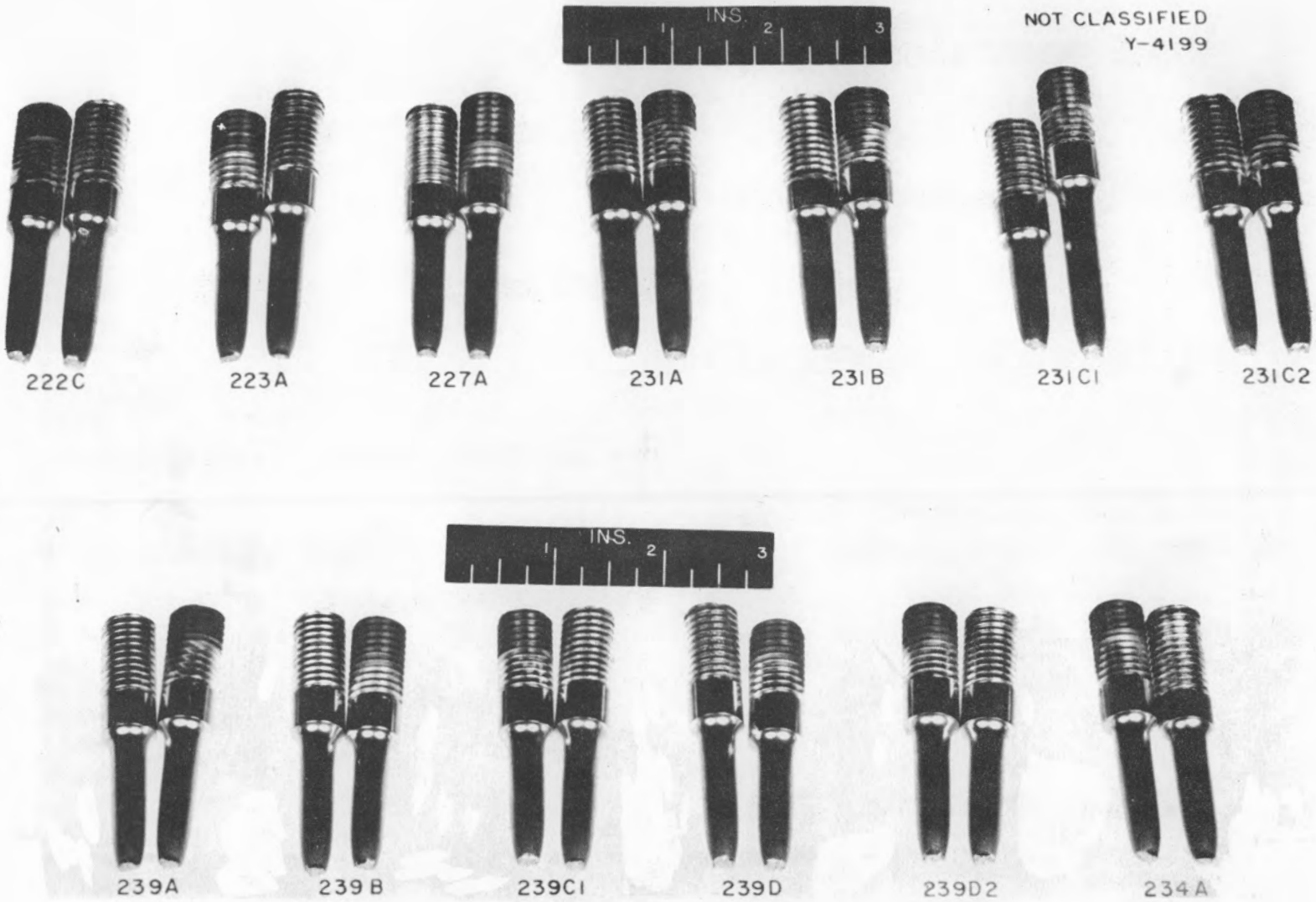

Fig. 1.1 - Broken Tensile Specimens of Extruded Ames Thorium.

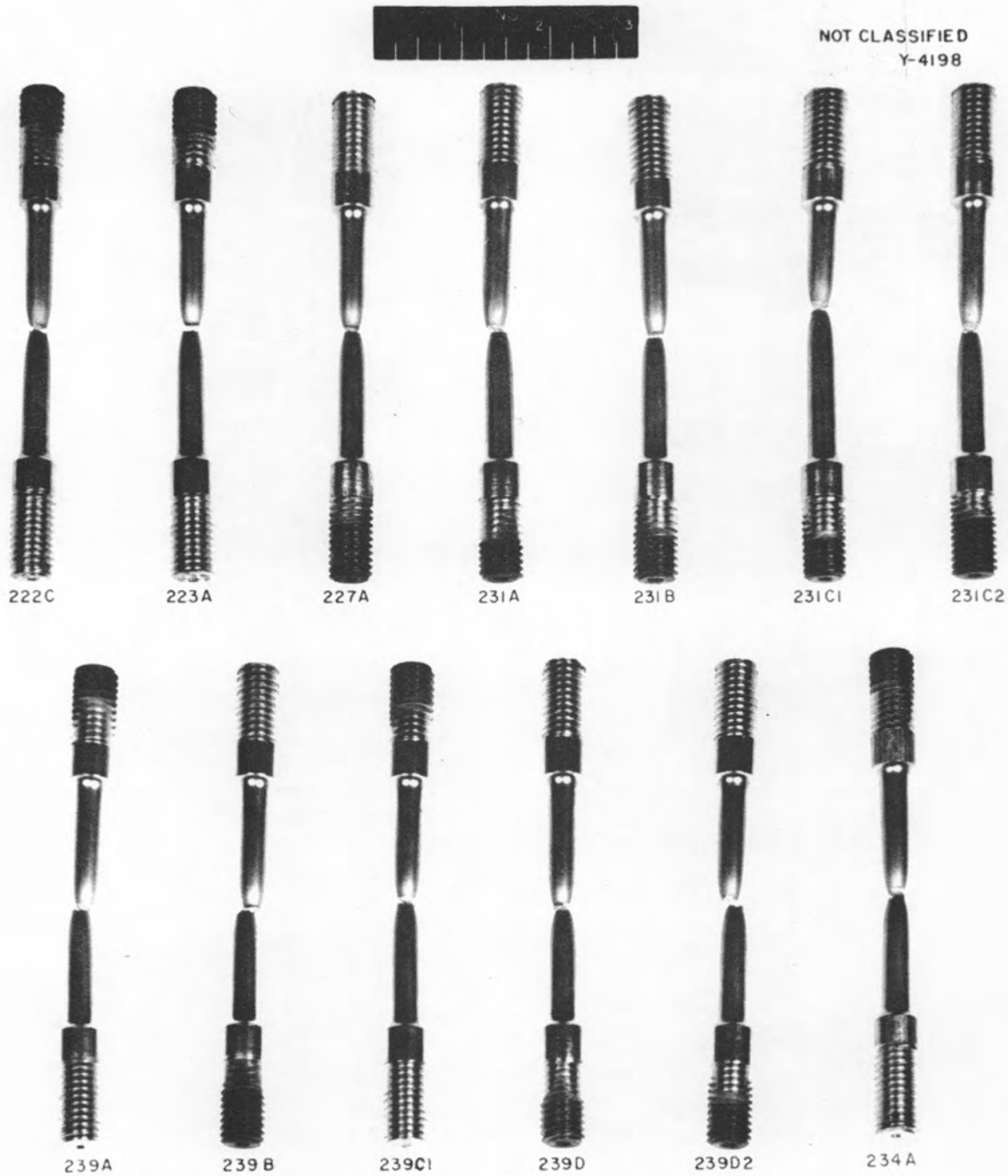

Fig. 1.2 - Broken Tensile Specimens of Extruded Ames Thorium.

weight in air and M_f the weight in fluid, then $M_a - M_f = M_w$ where M_w is the weight of an equal volume of liquid. Thus the relative density is $M_a/(M_a - M_f)$.

The values for the density of the fluid at the testing temperature were obtained, and the density of the thorium was calculated in grams per cubic centimeter. The average experimental values were as follows:

	DENSITY (g/cc)
Ames cast thorium	11.632
Ames cold-rolled thorium	11.638
Ames extruded thorium	11.644
Iodide-process deposited thorium	11.490
Iodide-process arc-melted thorium	11.664
Iodide-process arc-melted and rolled thorium	11.750
Westinghouse sintered thorium	10.354

A precision lattice parameter measurement of iodide-process thorium was made by B. S. Borie who reported a value of 5.0871 ± 0.0002 A at a temperature of 26.2°C. The theoretical density, calculated using this value for A_0, was found to be 11.710 g/cc.

Crystal Structure. Thorium is face-centered-cubic with lattice parameter of 5.0871 ± 0.0002 A at a temperature of 26.2°C. A precision lattice parameter measurement was made using iodide-process thorium which had been arc-melted and rolled into sheet. The sheet was vacuum-annealed, and powder was prepared by filing. The filings were passed through a 100-mesh screen and then annealed for ½ hr at 750°C and furnace-cooled. A Debye-Scherrer needle was prepared with Duco cement, and the diffraction pattern was recorded with a North American Philips 114.6-mm camera. Room temperature during the exposure was recorded at the camera with a mercury thermometer. Copper Kα radiation (λ_{α_1} = 1.54050 A, λ_{α_2} = 1.54434 A) filtered through nickel foil was used.

The α doublet was observed to be resolved for the 440, 531, 600, 620, and 533 lines.

The values for 2θ for these lines were measured with a traveling microscope and corrected for film shrinkage. These data were used to make a graphical extrapolation by the method of Bradley and Joy. The lattice parameter was determined as 5.0871 ± 0.0002 A at 26.2°C.

FABRICATION

An investigation of the effect of preworking upon the extrusion of Ames thorium was begun by extruding billets which had been forged or previously extruded. Both rod and tubing were extruded from forged and extruded billets with no noticeable improvement in the surface quality of the extruded material. Four cast Ames ingots 4 in. in diameter were forged into 3-in.-diameter billets at Battelle Memorial Institute. The forged billets were extruded into rod ½, 7/8, and 1 in. in diameter and into tubing 7/8 in. o.d. by 5/8 in. i.d. There appeared to be little if any improvement in the extrusion produced from a forged billet as compared to a cast billet. Ames cast billets 4 in. in diameter were extruded into 2½-in.-diameter bars. These bars were cut into about 4-in. lengths for further extrusion. These

preworked billets were extruded into rod, 7/8-in.-diameter tubing, and zirconium-lined tubing 7/8 in. o.d. by 3/8 in. i.d.

The above extrusions were made under conditions nearly identical with those previously reported for extrusions of as-cast Ames billets.[1] Although some improvement was expected in the surface quality as a result of the breaking up of the cast structure, no improvement could be detected.

Three Ames cast billets were extruded into 2- by 1-in. rectangular bars for flat rolling stock. These extrusions indicate that no particular difficulty would be experienced in extruding thorium into any desired shape.

Swaging, Rolling, and Drawing. A new oil motor drive was installed on the drawbench. This installation provides drawing speeds from 2.5 to 40 ft/min. Dies have been obtained which provide reduction in approximately 25% steps from 5/8 in. diameter to 0.005 in. diameter. Drawing studies will be started in the near future. No work was done in connection with rolling and swaging.

Extrusion Cladding of Uranium and Thorium. Studies of cladding uranium and thorium were continued in connection with the MTA development work. However, very little was done to check the quality of bonds obtained between the tubes and the inside cladding of zirconium because of a change in emphasis from tubing to solid rods.

Data from the extrusion of five zirconium-lined thorium tubes are presented in Table 1.4. Good tube surfaces were obtained by extrusion of the thorium-zirconium billets at 850°C. Although good surfaces were obtained on the thorium at lower temperatures, the zirconium appeared to have more of a tendency to seize the mandrel. No tests of the bond between the thorium and zirconium have been carried out except to conduct a back-bend on one sample. This sample was reversed through approximately 120° before the sample broke, but the treatment did not strip the zirconium from the thorium.

The thorium-zirconium extrusion billets consisted of a standard 3-in. cast thorium billet with a 1-in.-diameter zirconium core. The parts were cleaned individually in a degreaser, dried, and then forced together and welded in a dry box under an argon atmosphere. This assembly procedure provides a relatively clean interface between the zirconium and thorium and presents the possibility of salt admission during the salt-bath heating period.

Data from the extrusion of four zirconium-lined uranium tubes and one zirconium-clad uranium rod are presented in Table 1.5. The extrusion billets were prepared in the same manner as the thorium-zirconium billets. However, the uranium-zirconium bond appears to be more difficult to make than the thorium-zirconium bond, and it requires more care in the preparation of the billet. This is probably due to the lower extrusion temperature and the increased oxidation of the uranium. Electropolishing of the uranium appears to have improved the bond obtained from one extrusion, and

---

[1] *Metallurgy Division Quarterly Progress Report for Period Ending April 30, 1951*, ORNL-1033 (in press).

SECRET

TABLE 1.4

Extrusion Cladding of Thorium

BILLET NO.	BILLET SIZE (in.)	TEMPERATURE (°C)	HEATING TIME	EXTRUSION SIZE (in.)	REDUCTION RATIO	SPEED (ft/min)	DIE TYPE	EXTERIOR SURFACE QUALITY	INTERIOR SURFACE QUALITY	REMARKS
241-3	3 x 3-9/16	725	3 hr 70 min	7/8 x 5/8	22.7/1	72	30° Bell	Excellent	Fair	Sample taken from center of rod took 120° back-bending before breaking; zirconium did not strip from thorium
241-A4	3 x 3-1/2	725	1 hr 30 min	7/8 x 1/2	16.8/1	31	30° Bell	Good	Fair	Billet was heated in Ex-O-Gas atmosphere after being coated with sodium silicate and graphite; thorium surface appeared about same as usual from salt bath
234-32	3 x 4-7/16	800	3 hr 35 min	7/8 x 3/8	13.9/1	38	30° Bell	Good	Fair	This zirconium core was drilled 9/16 in. diameter for ½ in. diameter bore but was extruded 3/8 in. bore owing to failure of ½-in. mandrel in previous extrusion; the relative flow of zirconium and thorium was erratic; bend appears fair
228-A2	2-1/2 x 4	850	1 hr 40 min	7/8 x 3/8	9.3/1	33	15° Bell	Good	Good	Bend between thorium and zirconium appears to be good, but zirconium cladding was thick on both ends even though zirconium core was 1 in. shorter than thorium billet
228-A3	2-1/2 x 4	850	1 hr 44 min	7/8 x 3/8	9.3/1	35	15° Bell	Good	Good	Extrusion good except for uneven thickness of zirconium cladding

SECRET

TABLE 1.5

Extrusion Cladding of Uranium

BILLET NO.	BILLET SIZE (in.)	TEMP. (°C)	HEATING TIME	EXTRUSION SIZE (in.)	REDUCTION RATIO	SPEED (ft/min)	DIE TYPE	SURFACE QUALITY EXT.	SURFACE QUALITY INT.	REMARKS
704-1	3 X 4	575	3 hr 10 min	7/8 X 5/8	22.7/1		Shear	Good	Poor	Zirconium cladding was too thin after flowing out at both ends
704-2	3 X 4	575	3 hr 15 min	7/8 X 1/2	16.8/1		Shear	Good	Poor	Bond between uranium and zirconium appears extremely weak
704-3	3 X 2-3/4	600	25 min	3/4 X 1/2	27.8/1		10° Bell			Would not extrude
705-4	3 X 3-7/8	600	2 hr 45 min	3/4 X 3/8	20.6/1	20	10° Bell	Good	Fair	Bond appears to be good between uranium and zirconium inner cladding
None	3 X 3-3/4	620	2 hr 23 min	3/4	16/1		45° Bell	Fair		Bond appears to be good between uranium and zirconium; uranium core evacuated; zirconium thin on lead end

this bond was further improved by evacuating the joint prior to welding of the billet for one rod extrusion.

No attempt has been made to control the thickness of the zirconium cladding. The thickness of cladding on both the uranium and thorium has varied considerably from leading to lagging end of the extrusion produced. Control of this variable thickness will be attempted when satisfactory bonds are produced.

THORIUM ALLOY DEVELOPMENT

In order to become thoroughly familiar with the metal thorium and its existing alloys, a search was made of the available technical literature dealing with the properties and characteristics of this metal and its alloys. Particular emphasis was placed on the systems carbon-thorium, oxygen-thorium, and nitrogen-thorium. All the data found relating to these systems appear to be influenced by the impurities or contaminants originally present in the thorium metal or introduced in the process of preparing the alloys. No data were found, for instance, of the extent of solubility of carbon in thorium in the absence of oxygen and nitrogen. Therefore, it appeared highly desirable to prepare alloys of carbon and relatively pure thorium (iodide-process) in an arc furnace, under conditions that would exclude contaminants. When such alloys become available, a study will be made of the solubility of carbon as a function of temperature. The relation of carbon content to cold deformation and to recrystallization will also be studied.

Preliminary melts of carbon and thorium in a vacuum arc furnace were not successful because a stable arc could not be maintained. Later attempts necessitated the introduction of argon

gas (oxygen and nitrogen free) to stabilize and maintain the arc. After further trials, it was found that carbon can best be introduced into the thorium by melting the latter in a relatively pure graphite crucible. Three such melts were prepared which will serve as the master alloy for the introduction of carbon into thorium (iodide-process).

The experimental arc furnace used for the preparation of small amounts of the high-purity alloys is shown in Fig. 1.3.

UNCLASSIFIED

Y-3994

Fig. 1.3 - Experimental Arc Furnace Used for Preparation of Small Amounts of High-Purity Alloys.

. . . . .

2. PREFERRED ORIENTATION AND ANISOTROPY IN PROPERTIES OF METALS

It was shown in a previous report[1] that the type of preferred orientation developed in some high-α-extruded uranium rod in the as-extruded condition varied with extrusion ratio and from the front end to the back end of a given extruded length. The texture was predominantly a duplex [010]-[410]fiber texture with minor components [031], [321], [001], and [100], but the intensity of the [410] relative to that of the [010] component increased with increase in extrusion ratio and decreased from the front end to the back end of the extruded length. Since the degree of recrystallization changed correspondingly with these variables, it was suggested that the texture depended upon the degree of recrystallization in that the intensity of the [410] relative to that of the [010] component increased with increase in degree of recrystallization.

It was pointed out, however, that the textures might be dependent upon the actual extrusion temperature, the intensity of the [410] relative to that of the [010] component increasing with increasing temperature, assuming that the texture developed upon deformation was not altered by recrystallization. The textures developed in uranium rod swaged at various temperatures have been rationalized on this basis.[2]

To check the assumption that uranium rod upon recrystallization retains the texture developed upon deformation, the preferred orientation in a sample that was unrecrystallized in the as-extruded condition was compared with that in a similar sample that was deliberately annealed to bring about complete recrystallization.

A 1½-in.-diameter rod was extruded through a 25° conical die from a 3-1/8-in.-diameter ingot at 500°C billet temperature (extrusion ratio 4.3). The extruded length was water-spray-quenched as it emerged from the die to retain the as-extruded structure. A sample was taken from near the middle of the extruded length and examined, and an adjacent sample was annealed 1 hr at 550°C and then examined. The former was unrecrystallized, whereas the latter was completely recrystallized, as shown in Figs. 2.1 and 2.2.

A spherical diffraction specimen 0.500 in. in diameter was machined from each sample so that the center line of the specimen coincided with that of the rod. The spherical surface was lapped to smoothness and electropolished to remove the surface layers deformed by machining and lapping (the specimen was reduced approximately 0.010 in. by electropolishing).

The preferred orientation was determined by the X-ray-diffraction spectrometer technique described in previous reports.[3,4] Examination

(1) *Metallurgy Division Quarterly Progress Report for Period Ending January 31, 1951*, ORNL-987, p. 17 (June 7, 1951).

(2) A. M. Turkalo, J. E. Burke, and A. N. Holden, *Fiber Textures in Uranium*, KAPL-428 (Aug. 31, 1950).

(3) *Metallurgy Division Quarterly Progress Report for Period Ending January 31, 1950*, ORNL-583, p. 37 (March 10, 1950).

(4) *Metallurgy Division Quarterly Progress Report for Period Ending July 31, 1950*, ORNL-827, p. 35 (Dec. 4, 1950).

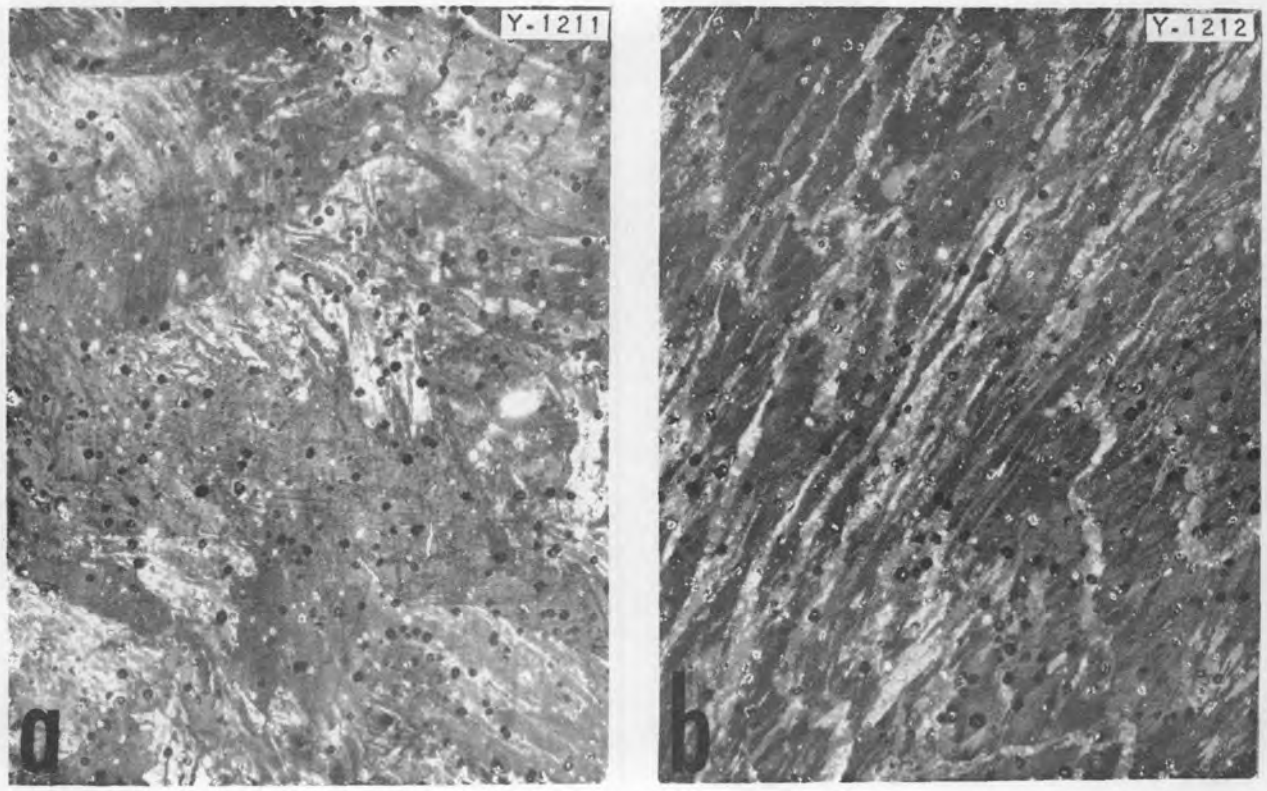

Fig. 2.1 - Photomicrographs Showing Deformed Grain Structure in the Middle of the Length of 1½-in.-Diameter α-Extruded Rod in the As-Extruded Condition. 150X. Sample U9-31; etched; observed under polarized light. (*a*) Transverse. (*b*) Longitudinal.

was made on a Norelco Type 12021 Geiger counter X-ray-diffraction goniometer employing Cu Kα radiation. The specimen was rotated at 200 rpm about its longitudinal axis (the extrusion direction) during exposure.

Plots of the intensity of diffraction vs. the angle (ϕ) between the extrusion direction and the normal to the diffracting plane for various planes for each specimen are given in Figs. 2.3 through 2.11.

Analysis of the data revealed that the unrecrystallized sample (U9-31) had a duplex [010]-[410] fiber texture with minor [031], [001], and [431] components, but the recrystallized sample (U9-26) had essentially a pure [431] fiber texture. On the graphs in Figs. 2.3 through 2.11 are indicated the positions of the intensity maxima to be expected for the various diffracting planes for these preferred directions and the shifts in the intensity maxima brought about by an inclination of 10° of the fiber axis

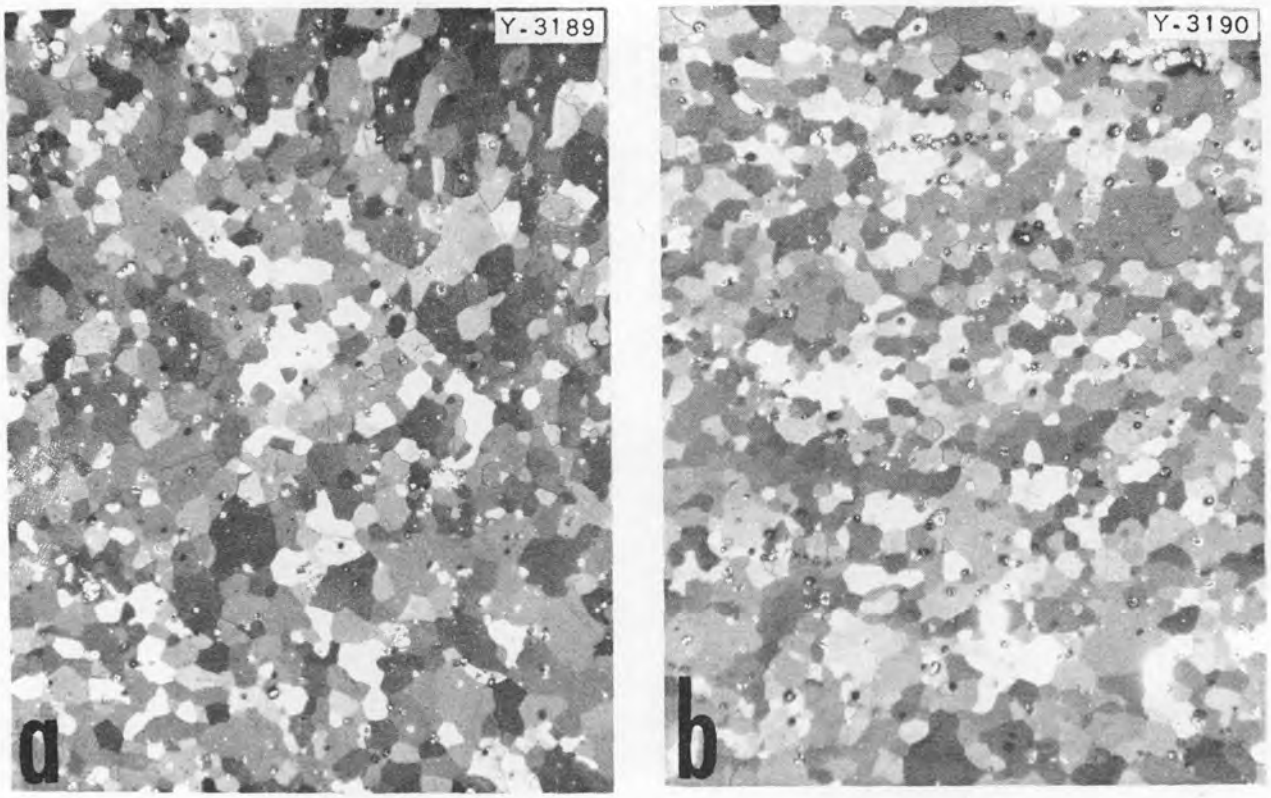

Fig. 2.2 - Photomicrographs Showing Completely Recrystallized Grain Structure in the Middle of the Length of 1½-in.-Diameter α-Extruded Rod After Annealing 1 hr at 550°C. 150X. Sample U9-26; etched; observed under polarized light. (*a*) Transverse. (*b*) Longitudinal.

if the textures are of the conical type.

These results show very definitely that uranium rod upon recrystallization does not always retain the texture developed upon deformation. Not only is the texture produced by deliberate recrystallization different from that of the structure from which it recrystallized, but also it is considerably different from that in uranium rods which had been extruded under a higher extrusion ratio and thus were recrystallized in the as-extruded condition.

The situation may be similar to that observed for some other metals, in that rod in which the deformation texture is very well developed tends to retain that texture upon recrystallization, whereas rod in which the deformation texture is not so well developed tends to assume a different texture upon recrystallization.

To check this point, rods extruded at higher extrusion ratios will be examined in the as-extruded and in the annealed conditions.

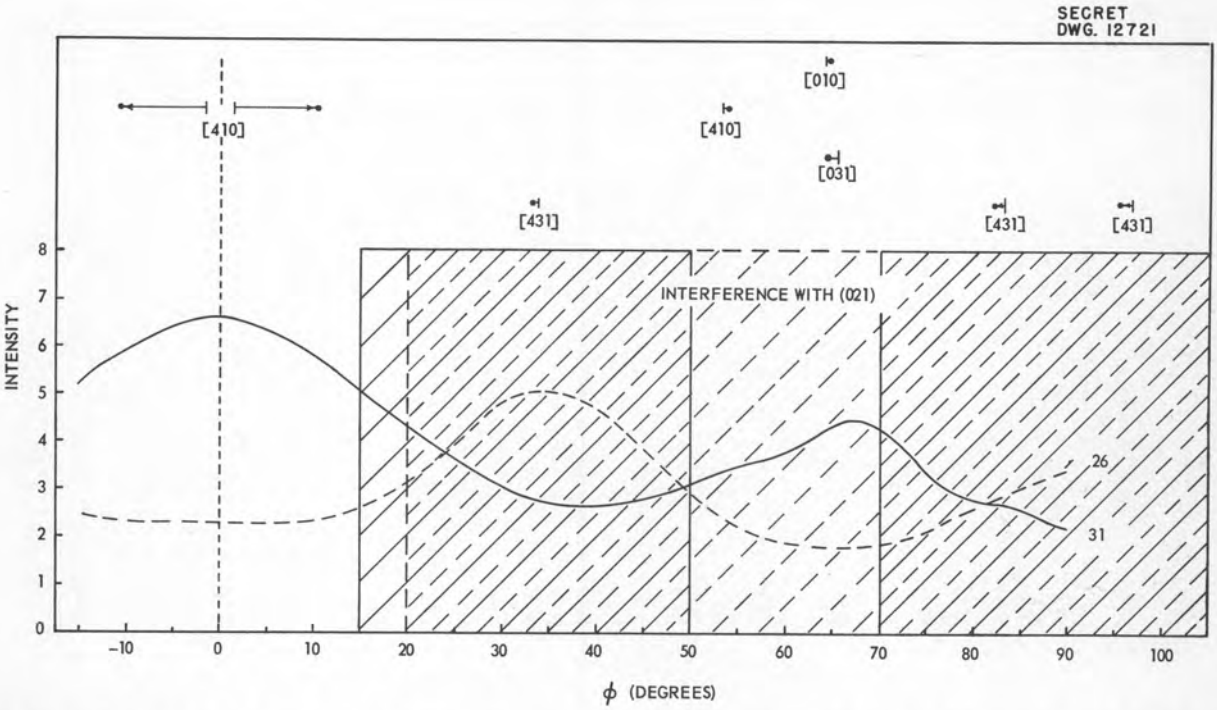

Fig. 2.3 - Preferred Orientation Plot — (110) — 1½-in.-Diameter α-Extruded Uranium Rod.

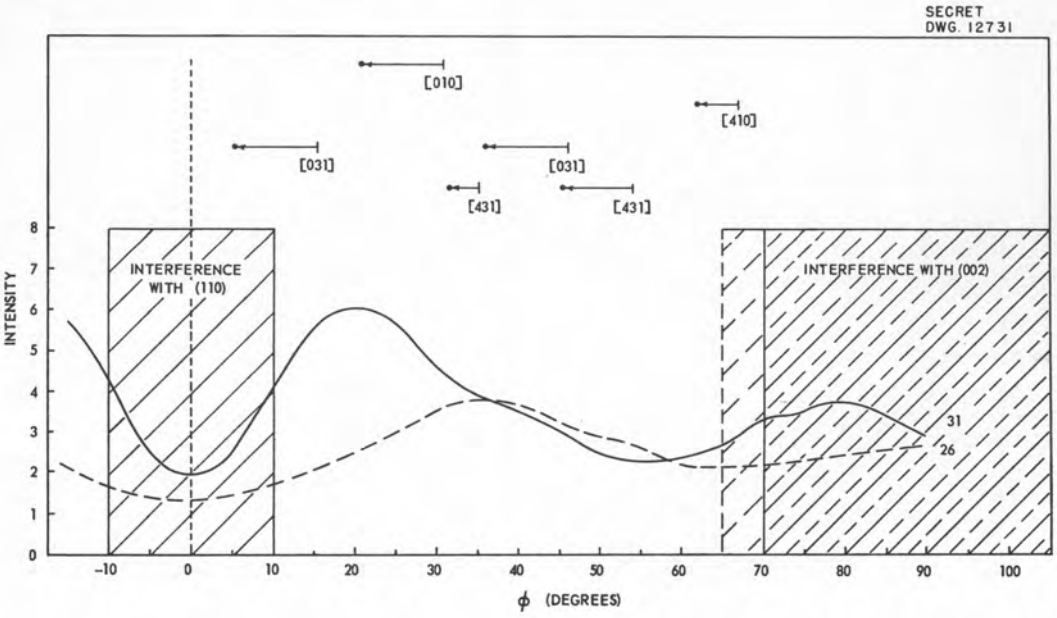

Fig. 2.4 - Preferred Orientation Plot — (021) — 1½-in.-Diameter α-Extruded Uranium Rod.

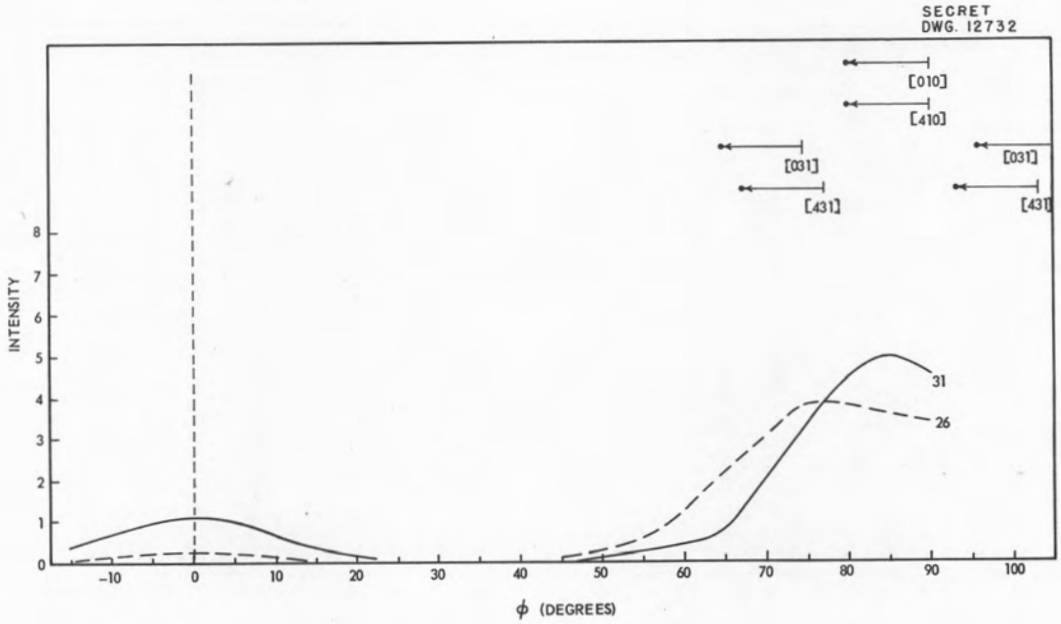

Fig. 2.5 - Preferred Orientation Plot — (002) — 1½-in.-Diameter α-Extruded Uranium Rod.

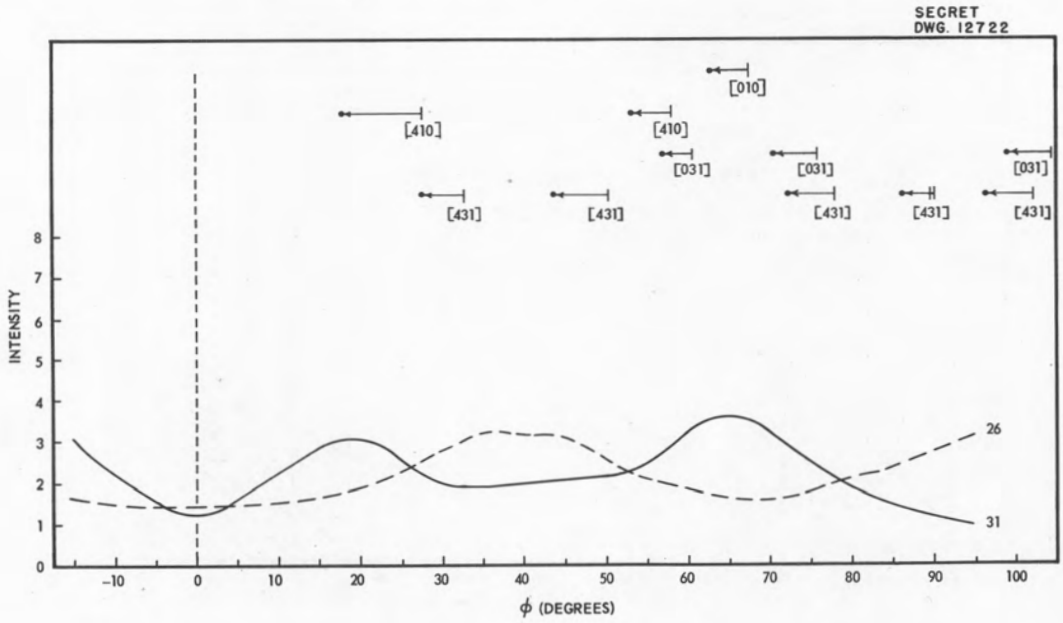

Fig. 2.6 - Preferred Orientation Plot — (111) — 1½-in.-Diameter α-Extruded Uranium Rod.

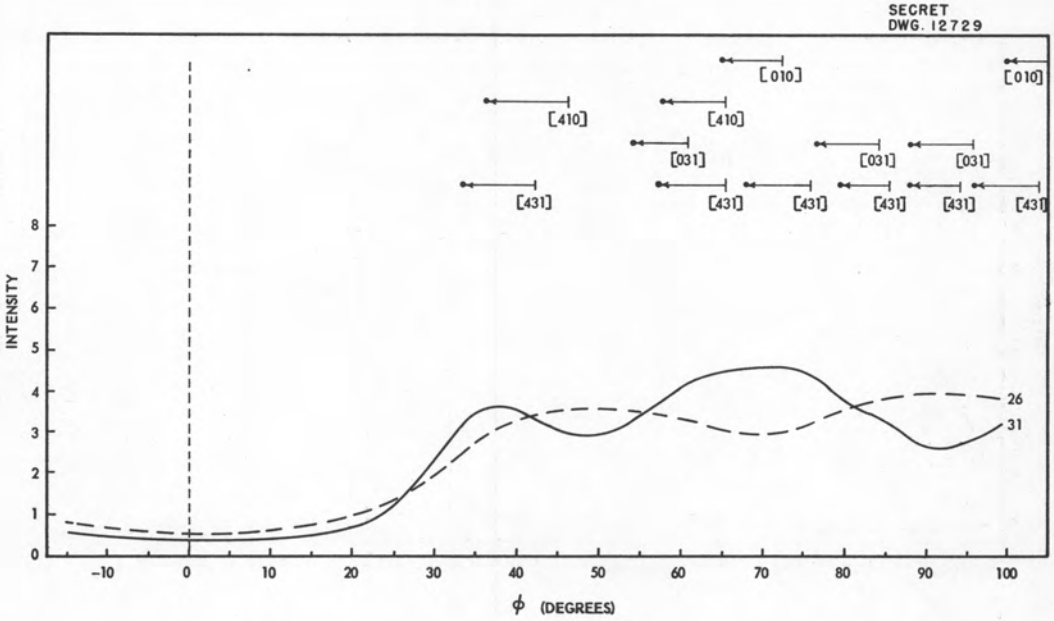

Fig. 2.7 - Preferred Orientation Plot — (112) — 1½-in.-Diameter α-Extruded Uranium Rod.

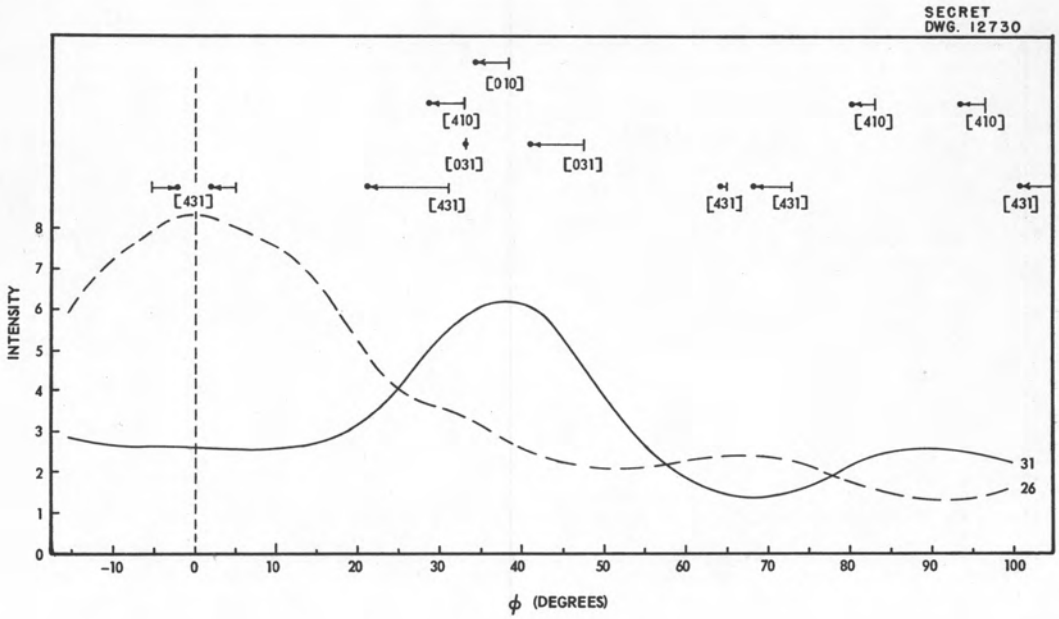

Fig. 2.8 - Preferred Orientation Plot — (131) — 1½-in.-Diameter α-Extruded Uranium Rod.

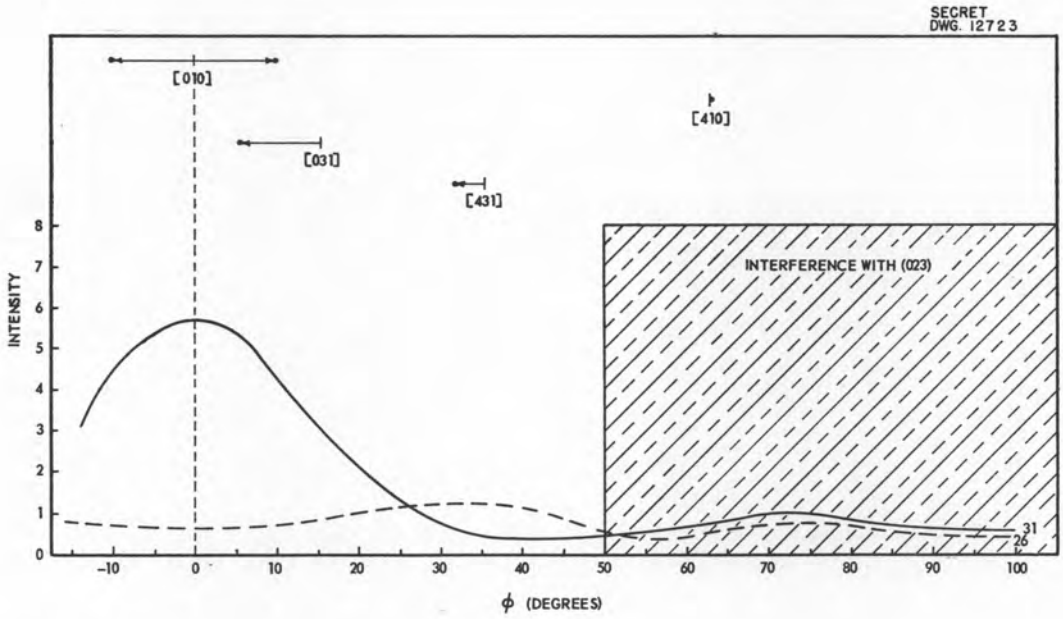

Fig. 2.9 - Preferred Orientation Plot — (040) — 1½-in.-Diameter α-Extruded Uranium Rod.

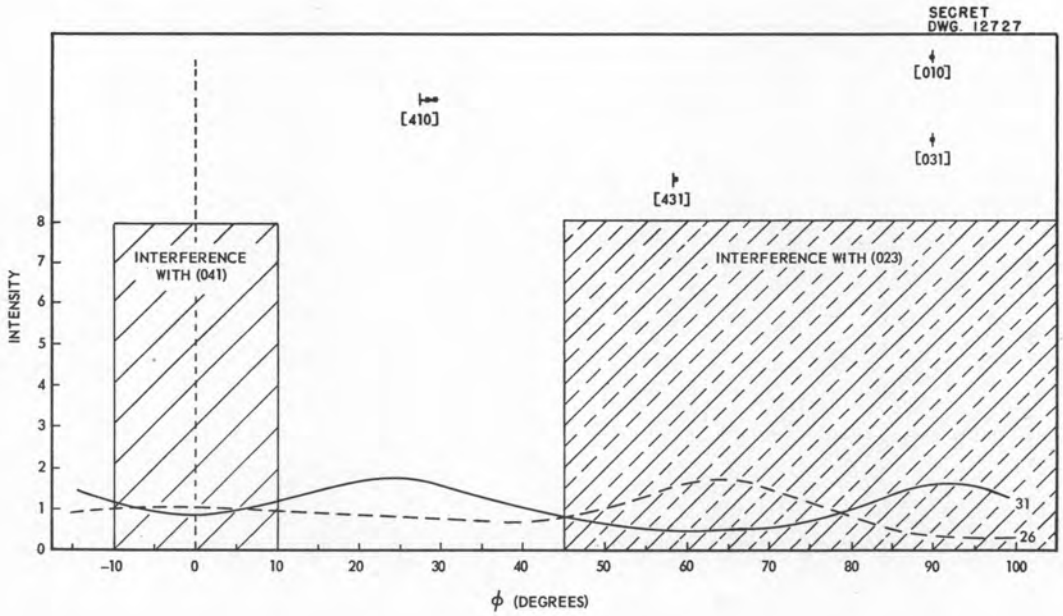

Fig. 2.10 - Preferred Orientation Plot — (200) — 1½-in.-Diameter α-Extruded Uranium Rod.

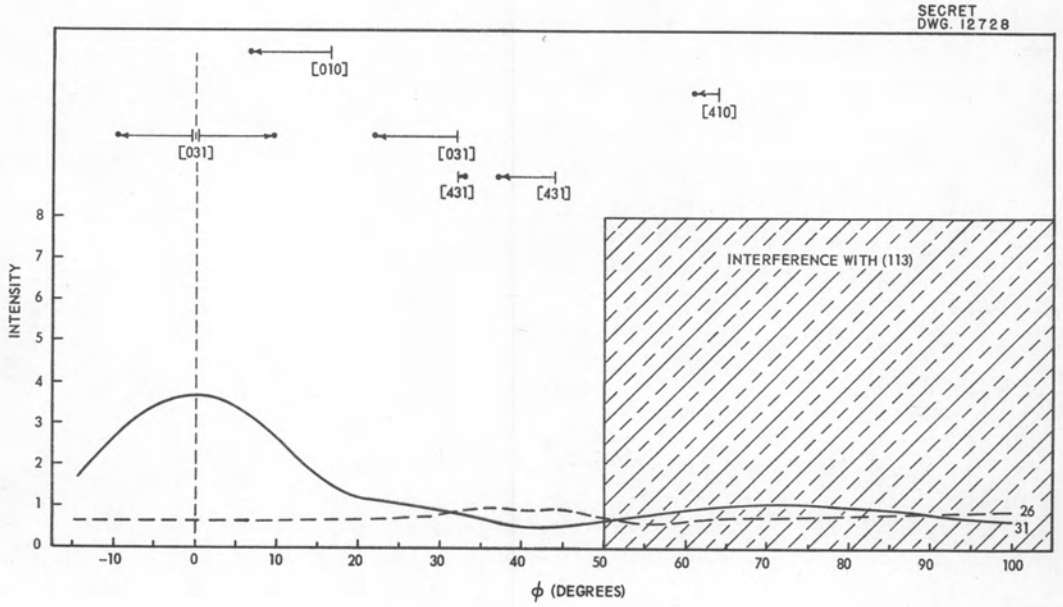

Fig. 2.11 - Preferred Orientation Plot — (041) — 1½-in.-Diameter α-Extruded Uranium Rod.

. . . . .

3. ANP PROGRAM

CORROSION TESTING

Considerable interest has arisen recently in the corrosion behavior of various metals and alloys in nonmetallic media, namely molten fluorides and hydroxides. Although static and dynamic tests are still being made using liquid metals, the major portion of our static corrosion program has shifted to these fluid media.

The hydroxides being considered at present include sodium, strontium, and barium hydroxides, whereas the fluoride mixture currently being emphasized is a ternary mixture containing sodium, potassium, and uranium fluorides.

Liquid Metal Corrosion. *Static Tests.* Liquid metal corrosion tests now are confined mainly to sodium attack. In an effort to determine the effect of time on the interaction of sodium with 316 stainless steel at 1000°C, tests were made for 1, 5, 10, 25, 50, 100, 400, and 1000 hr. Gravimetric determinations indicated no significant weight change in any of these tests. Metallographic examination of sectioned specimens revealed no subsurface reaction. Visual examination revealed a velvet-like frosted appearance after the test (these were highly polished prior to testing), which on high magnification indicated this to have been caused by a reorganization of surface metal. Grain boundaries, twin lines, and crystal faces were prominently displayed, as shown in Fig. 3.1. This surface condition is probably more stable than the original polished surface, merely readjusting itself either by surface diffusion or by the limited solubility of the metal components in the sodium.

Tests are now in progress to evaluate the behavior of Timken alloys 16-25-6 and 16-13-3 (Cr, Ni, Mo, respectively) in sodium at 815°C (1500°F) and 1000°C (1830°F). The possibility of surface carburization of inconel, 310 stainless steel, 316 stainless steel, and iron is being determined by using sodium to which a small amount of charcoal has been added.

The corrosion resistance of molybdenum-coated steels will also be evaluated using a suitable liquid metal. These materials are now being procured from the Linde Air Products Co. at Tonawanda, N. Y.

Dynamic Tests. A number of thermal convection loops which were operated with lead and lithium were examined after failure. The hot leg temperature was intended to be 1500°F, although much higher temperatures were obtained when internal plugging obstructed the natural convective flow. Failure resulted at these higher temperatures, not from internal corrosion by the molten metal, but rather from causes such as arcing from the heater windings, high-temperature air oxidation, or internal plugging. Strictly speaking, therefore, the term "liquid-metal corrosion" should not be associated with these test failures.

The lives of the various loops tested, their compositions, and metallographic observations are given in Table 3.1. The metallographic notes were made after examining random

Fig. 3.1 - Outer Surface of 316 Stainless Steel After 400 hr of Exposure to Sodium at 1000°C. 500X. Note development of crystal faces on certain grains and grain boundary attack.

samples of the hot leg, cold leg, and welded sections. The extent of corrosion was dependent upon the materials involved, the temperature, and the time of interaction. It should be kept in mind that the temperature was not actually controlled, but was merely attained by initially selecting a certain power input to obtain approximately 1500°F at the beginning of the test, when convective flow was unobstructed. When partial or complete plugging developed as a result of metal crystal formation in the cold leg, as shown in Fig. 3.2, heat losses were reduced, and the hot leg temperature increased. This increase was then compensated by decreasing the power input so that the hot leg temperature was again 1500°F. The cold leg temperature continually decreased, indicating partial plugging; it eventually became completely plugged, and the test was terminated.

SECRET

SECRET

TABLE 3.1

Corrosion and Operational Data on Lead- and Lithium-Containing Thermal Convection Loops

LOOP COMPOSITION	LOOP TEMPERATURE (°F) HOT ZONE	LOOP TEMPERATURE (°F) COLD ZONE	LOOP LIFE (hr)	REMARKS	METALLOGRAPHIC EXAMINATION	ANALYSIS OF LOAD AFTER TESTS (%) HOT ZONE CUP	HOT ZONE PIPE	COLD ZONE CUP	COLD ZONE PIPE
Loops Containing Lead									
1010 steel (loop 19)	1100	885	1 000	Temperature gradient in tube increased gradually, indicating partial plugging	Hot and cold zone tube walls showed very little evidence of attack; metal crystals formed in cold zones	Fe 0.0049	Fe 0.013	Fe 0.0081	Fe 0.0009
1010 steel, enameled exterior (loop 18)	1400	1110	62	Loop plugged internally during operation	Tube walls showed very little evidence of attack; metal crystals formed in cold zones	Fe 0.39 Cr 0.071	Fe 0.017		Fe 0.0079
316 stainless steel (loop 32)	1500	1300	7	Loop plugged internally in cold zone; failure in hot zone due to external causes	Intergranular attack to depth of 20 mils noted in hot zone; none noted in cold zone; metal crystals observed in cold zone		Fe 0.057 Ni 0.064 Cr 0.022 Mo 0.020 Mn 0.01	Fe 8.8 Ni 1.5 Cr 3.6 Mn 0.13	Fe 0.014 Ni 0.36 Cr 0.026 Mn 0.11
316 stainless steel (loop 26)	1500	1300	138	Loop plugged internally during operation	Hot zone much more severely attacked than cold zone; metal crystals observed in cold zone	Fe 0.15 Ni 0.05 Cr 0.001 Mo 0.012	Fe 0.04 Ni 0.03 Cr 0.001 Mo 0.004	Fe 4.6 Ni 0.6 Cr 1.39 Mo 0.005 O_2 0.048	Fe 11.2 Ni 5.0 Cr 0.03 Mo 0.78 O_2 0.005
446 stainless steel (loop 28)	1500	1300	62	Loop plugged internally during operation	0.003-in. intergranular attack observed in hot zone, 0.002 in. in cold; metal crystals observed in portions of cold leg	Fe 0.03 Cr <0.001	Fe 0.045 Cr <0.001	Fe 7.8 Cr 2.92	Fe 5.1 Cr 4.64

SECRET

TABLE 3.1 *(continued)*

LOOP COMPOSITION	LOOP TEMPERATURE (°C) HOT ZONE	LOOP TEMPERATURE (°C) COLD ZONE	LOOP LIFE (hr)	REMARKS	METALLOGRAPHIC EXAMINATION	ANALYSIS OF LOAD AFTER TESTS (%) HOT ZONE CUP	HOT ZONE PIPE	COLD ZONE CUP	COLD ZONE PIPE
Loops Containing Lead *(continued)*									
V-36 alloy (loop 39)	1500	1200	84	Loop plugged internally during operation	General attack in hot zone only; cold zone showed evidence of metal crystal formation	Fe 0.025 Ni 0.21 Cr 0.22 Mn 0.0048 Co 0.52	Fe 0.0014 Ni 0.11 Cr 0.022 Mn 0.0018 Co 0.06		Fe 0.046 Ni 0.39 Cr 0.61 Mn 0.017 Co 0.79
Haynes alloy No. 25 (loop 36)	1500	1290	699	Loop plugged internally; failed in hot zone	Hot zone revealed more general attack than cold; metal crystals observed in cold zone		Fe 0.0036 Ni 0.073 Cr 0.018 Mn 0.0039 Co 0.14	Fe 0.0083 Ni 0.055 Cr 0.031 Mn 0.0018 Co 0.09	Fe 0.016 Ni 0.067 Cr 0.030 Mn 0.0059 Co 0.05
Loops Containing Lithium									
1010 steel (loop 20)	1100	1020	34.5	Loop plugged(?) during operation, then failed in hot zone	Intergranular attack observed in hot and cold zones to depth of 0.020 in.; hot weld region attacked to depth of 0.040 in.; no metal crystals observed in cold zone	Fe 0.0025		Fe 0.0075	
Haynes alloy No. 25 (loop 35)	1500	1375	280	Loop plugged (?) internally and failed in hot zone	Intergranular attack noted to depth of 0.008 in. in hot zone pipe, and to 0.016 in. in hot zone weld; only 0.005 in. attack evident in the cold zone pipe, none in cold zone weld			Fe 0.01 Ni 0.05 Cr 0.75 Co 0.75 Mn 0.02	
V-36 alloy (loop 38)			0.0	Loop failed at start of test because heater element arced across hot zone pipe		Fe 0.08 Ni 0.0025 Cr 0.001 Co <0.0025		Fe 0.04 Ni 0.011 Cr 0.024 Co 0.0035	

SECRET

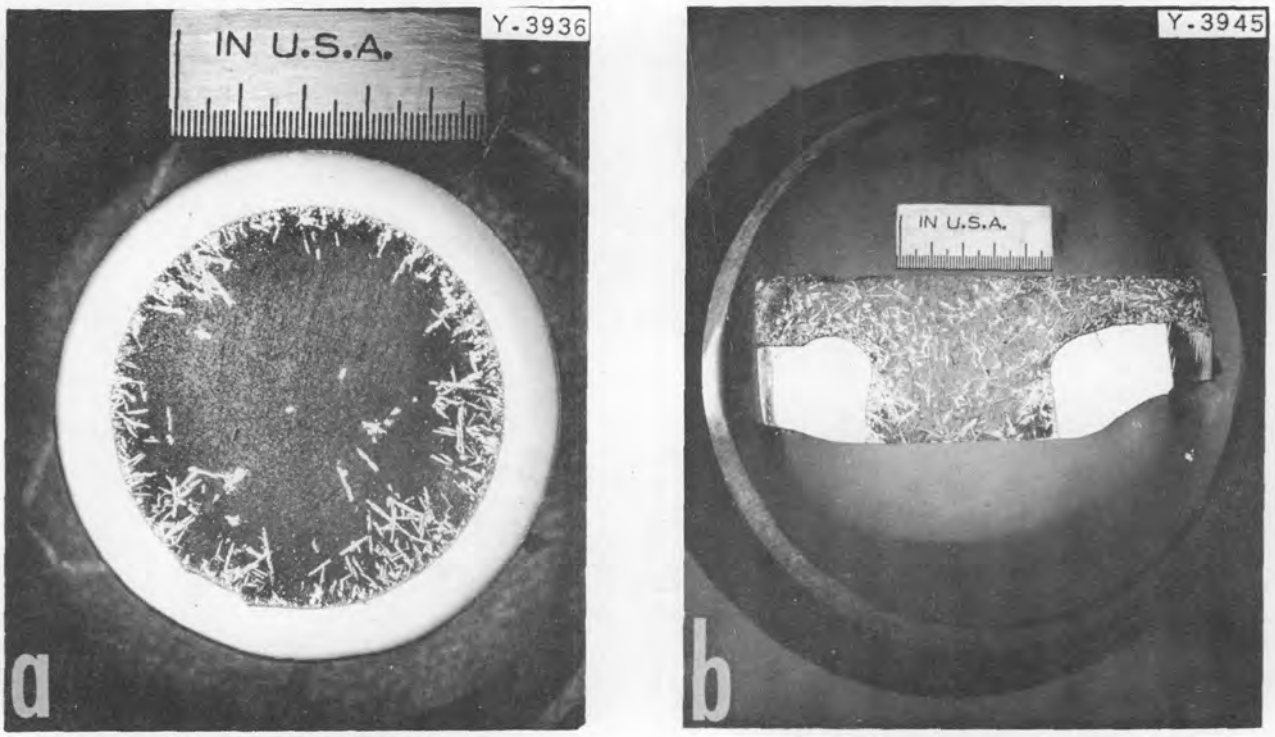

Fig. 3.2 - Sections Showing Formation of Metal Crystals Adjacent to Cold-Leg Wall of V-36 Thermal-Convection Loop Containing Lead After 84 hr of Operation. (*a*) Longitudinal. (*b*) Transverse. The smallest division on each scale shown is 1/100 in.

Occasionally a failure resulted from overheating in the hot leg, permitting the heating elements to short-circuit to the loop. Figure 3.3 illustrates such a failure.

Although it is accepted that the corrosive attack in the hot zone is appreciable, it is generally believed that attack in the cold zone is negligible, or even nonexistent. Figure 3.4 illustrates an attack in the cold zone of a 446 stainless steel loop by lead which appears to be interdendritic in nature. Such attack releases solid particles to the circulating lead stream and may cause or accelerate plugging in this manner.

A mass of metal crystals which were observed in the cold leg of a 316 stainless steel loop is shown in Fig. 3.5. These crystals need not necessarily be bonded directly to the tube walls, but may merely be trapped there. The oxide layer shown in Fig. 3.6 separates the metal crystals from the loop material, making bonding impossible.

An attempt was made to determine the composition of the metal crystals

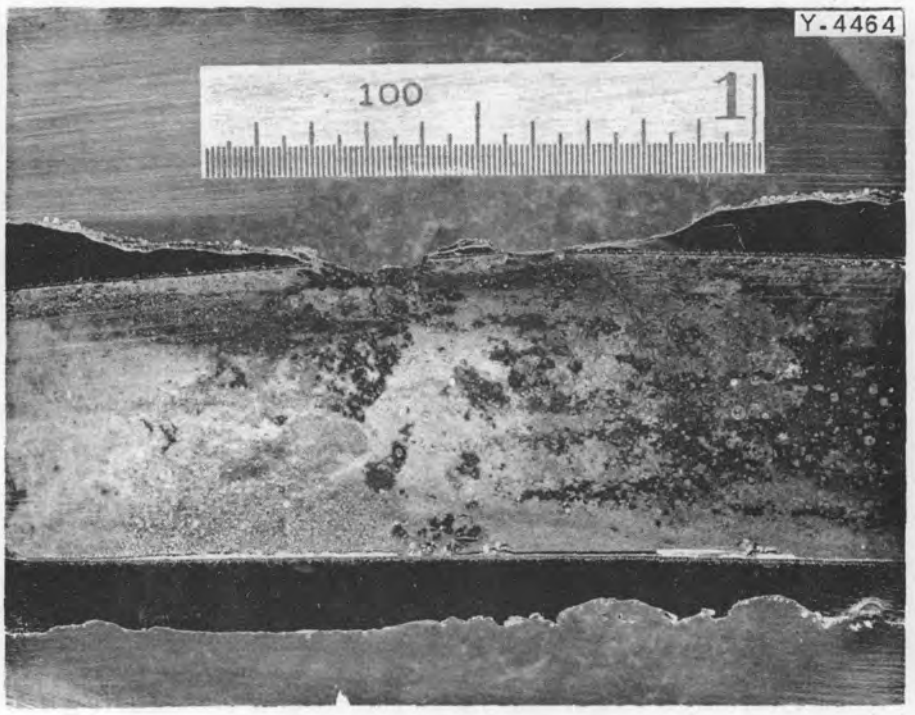

Fig. 3.3 - Hot-Leg Failure After 7 hr of Operation at 1500°F of 316 Stainless Steel Thermal-Convection Loop Containing Lead. 3X. Note that failure resulted from attack on outer surface of tube wall. The smallest division on the scale is 1/100 in.

by quantitative analysis. Neglecting lead, the following elements were detected:

1. In the cold zone of a 316 stainless steel (18% Cr-10% Ni-3% Mo) loop after 138 hr operation; 67% Fe, 6% Cr, 24% Ni, 3% Mo.
2. In the cold zone of a 446 stainless steel (26% Cr) loop after 62 hr operation, 63% Fe, 37% Cr.

These values are averages of analyses made in different areas of the cold zones. The composition varied somewhat, and these averages should be considered as approximate values.

A number of loops containing sodium have also been tested and are now being examined. Small test specimens of composition similar and dissimilar to that of the loops were suspended in the hot and in the cold leg and may provide some interesting additional data.

The attack in all cases was not severe, as shown in Figs. 3.7 through 3.9. . Some decarburization was observed, but this is not a highly objectionable type of surface instability. Only in the case of a 347 stainless steel sample (erroneously believed to be inconel) placed in an inconel tube was an appreciable weight

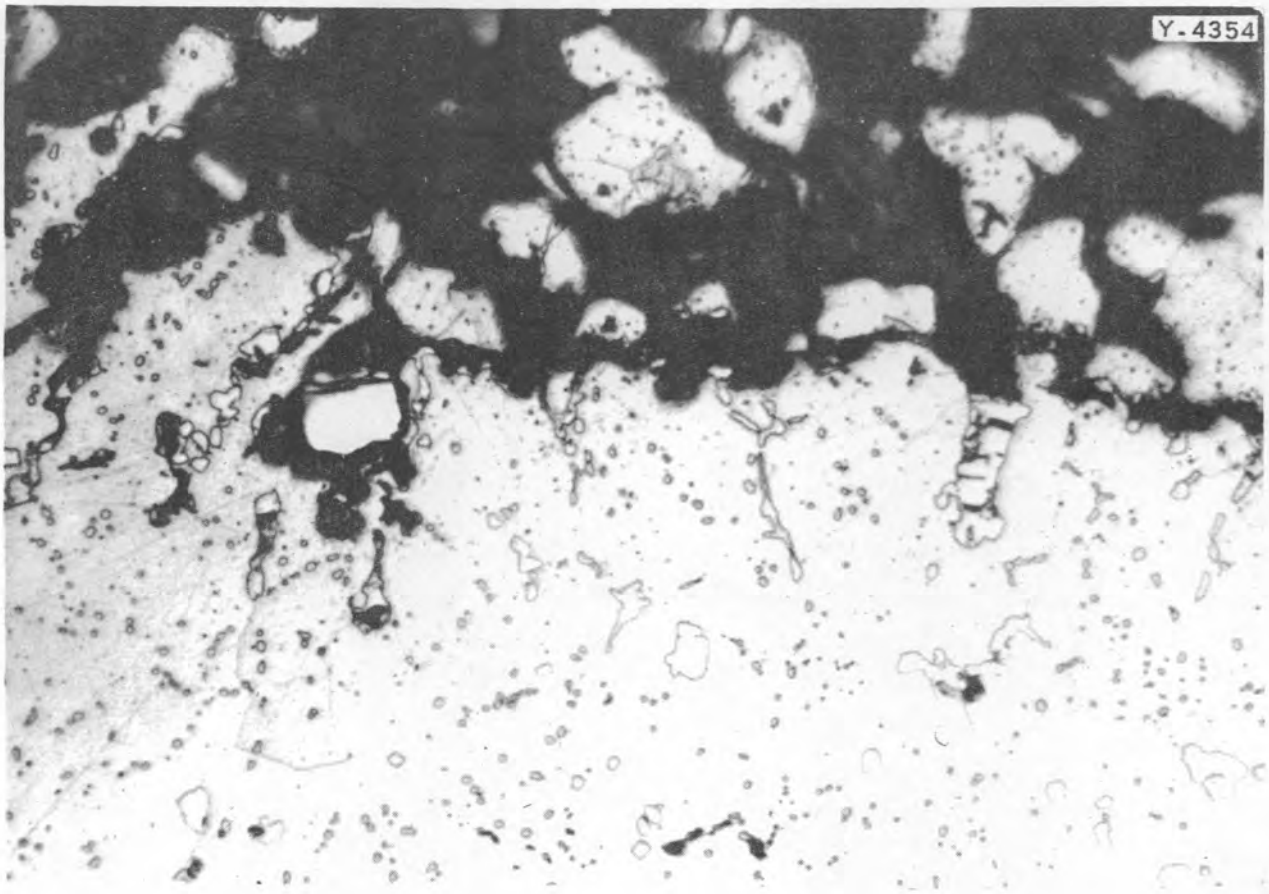

Fig. 3.4 - Highly Magnified View of Internal Surface of 446 Stainless Steel Cold Leg from Thermal-Convection Loop Operated with Lead (Area at Approximately 1300°F). 1000X. Note that interdendritic attack releases solid particles to lead stream.

loss detected. Weight changes for other samples, positive and negative, were very low.

Weight losses are undoubtedly caused by solution of the metal sample in the fluoride bath, as indicated by bath analyses, which are also reported in Table 3.2. Weight gains, in spite of some loss by solution, must be interpreted as absorption of one or more bath constituents (fluoride or metal) by the metal specimen. Analyses of the fluoride bath at various levels of the tube after test, when compared to the original fluoride analyses, indicate a definite decrease in beryllium, a slight decrease in sodium, and very little, if any, decrease in the uranium concentration. These changes in bath analyses may be directly associated with the weight gains which were observed on several test specimens.

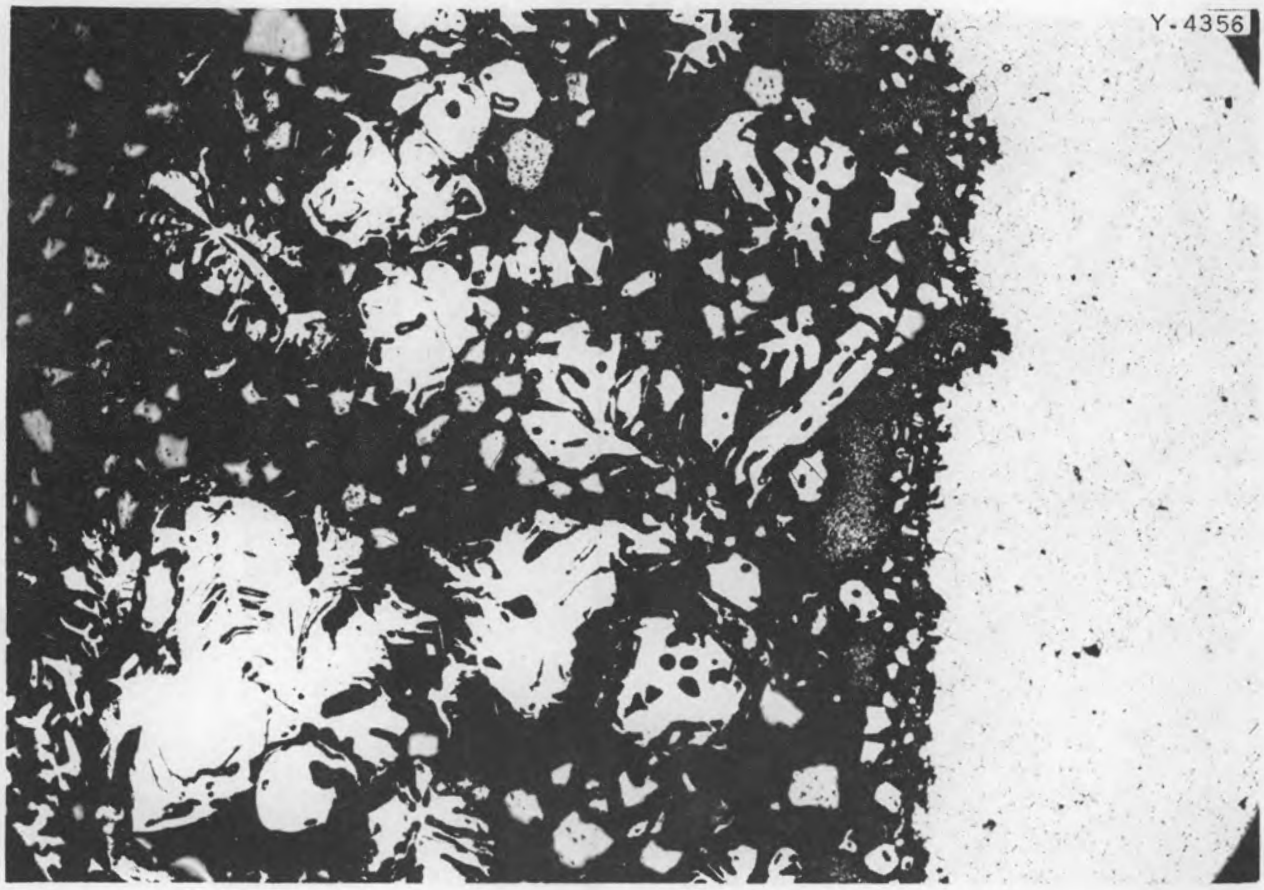

Fig. 3.5 - View of Cold Zone of 446 Stainless Steel Loop Showing Attacked Surface and Metal Crystals Which Form in Lead (Dark Areas), Thereby Restricting Convective Flow. 150X.

Fluoride Corrosion. Several preliminary corrosion tests have been made in molten fluorides. Inconel and 347 stainless steel have been exposed for 100 hr at 1830°F (1000°C) to $3NaF \cdot UF_4$ which had previously been heated in contact with metals of these compositions for 150 hr at 650°C.

The attack on inconel, in the form of subsurface voids, was noted to a depth of 0.004 in., as shown in Fig. 3.10. The 347 stainless steel was less severely attacked, as may be seen in Fig. 3.11, where the subsurface attack was limited to 0.002 in. The nature of the corrosion product has not yet been determined.

An analysis of the fluoride bath after testing gave the following results:

	Fe (%)	Ni (%)	Cr (%)
With inconel	0.25	Not detected	0.03
With 347 stainless steel	0.2	Not detected	0.05

UNCLASSIFIED

Y-4301

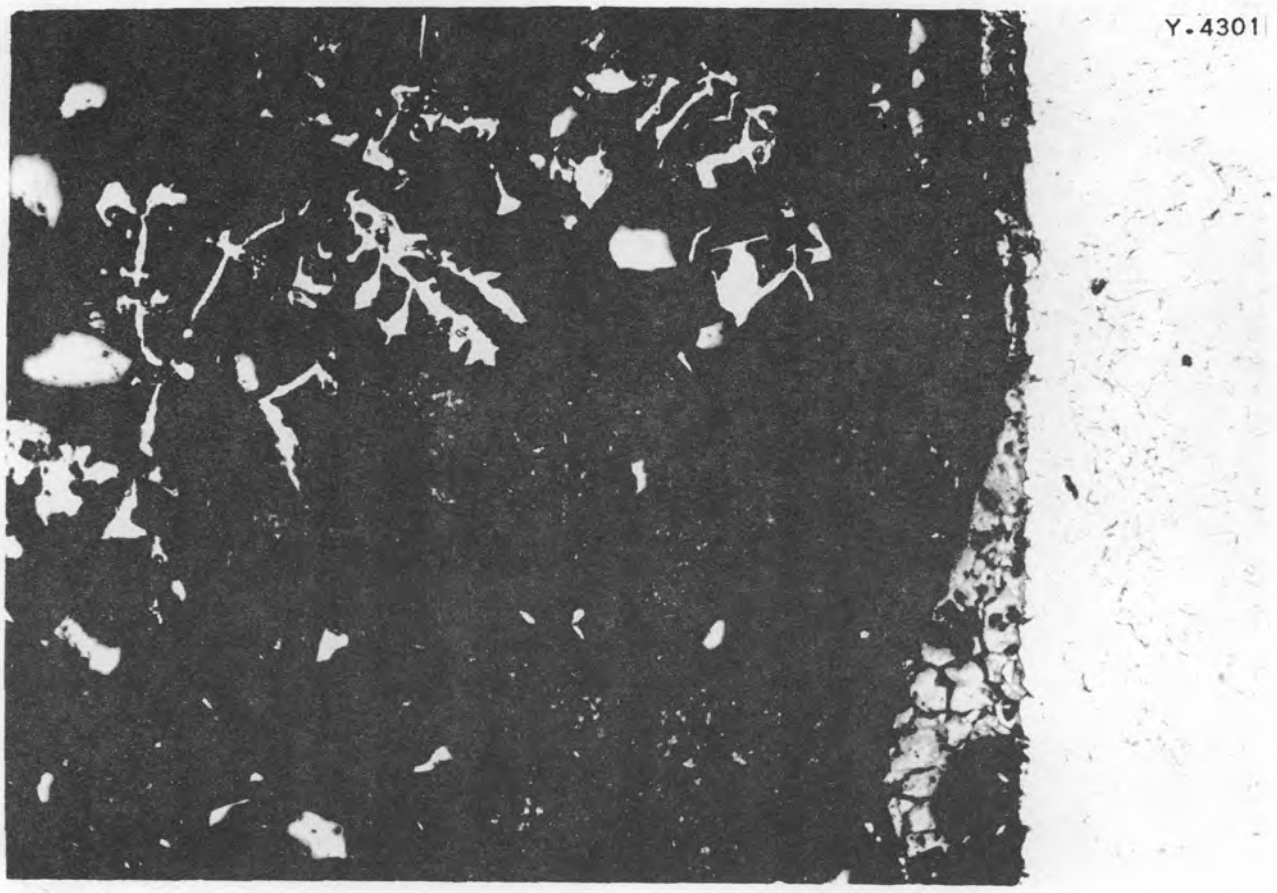

Fig. 3.6 - View of Cold-Zone Weld in 1010 Steel Loop Showing Metal Crystal Formation Adjacent to Pipe Wall Covered with Iron Oxide, Presumably Formed During Loop Fabrication. 175X.

A ternary fluoride mixture composed of 76 mole % NaF, 12 mole % BeF_4, and 12 mole % UF_4 was also used in corrosion testing. A 100-hr test with 310 stainless steel at 1500°F (815°C) showed no metallographic evidence of attack, although an analysis of the fluoride bath indicated 0.2% Fe, 0.02% Ni, and no chromium to be present. The presence of nickel and absence of chromium is the reverse of the findings listed above for the binary fluoride mixture. However, these differences may not be real because tests described below indicate that gravity segregation may exist in the container, and the composition of the fluoride mixture will depend on the location from which the test sample was obtained.

A number of fluoride corrosion tests were made on commercial alloys using a mixture of 10.7 mole % BeF_2, 68.0 mole % NaF, and 21.3 mole % UF_4. The materials tested are listed in Table 3.2 together with notes taken

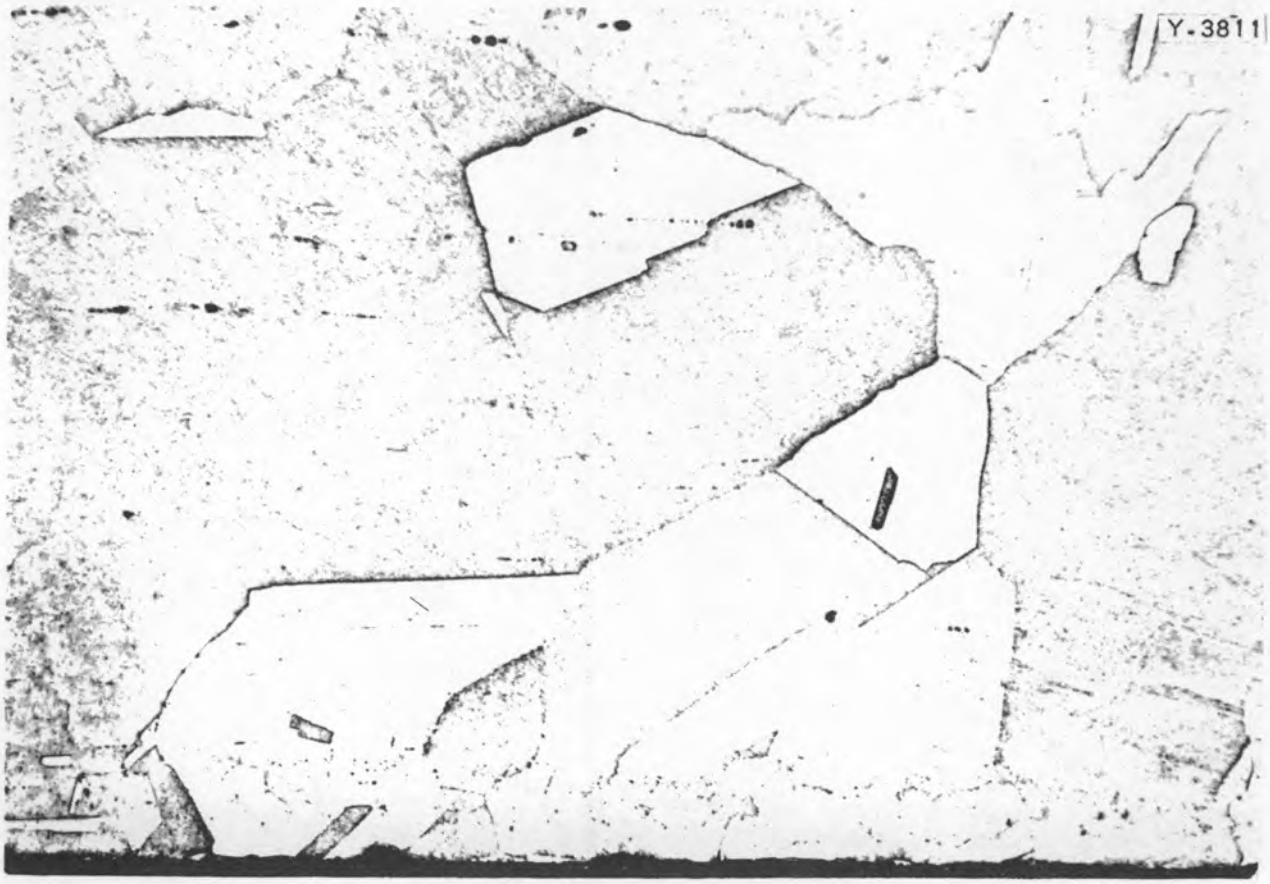

Fig. 3.7 - Surface of Nickel A Specimen After 100 hr of Exposure to a Na-Be-U Ternary Fluoride Mixture at 1000°C. 250X. Note absence of subsurface voids and presence of tiny precipitates near surface.

while the exposed specimens were being studied on the metallograph and results from fluoride bath analyses.

Preliminary results from a platinum-inconel sample exposed to the ternary fluoride mixture of 47.5 mole % NaF, 26 mole % KF, 27.5 mole % UF_4 at 1500°F (815°C) for 100 hr showed some evidence of interaction. In a similar test using sodium instead of fluoride, the platinum metal was completed consumed. These test data will be reported in detail at a later time.

Corrosion tests in molten fluoride will be undertaken on a larger scale when the apparatus for melting and and purification is completed. Close contact is being maintained with the Y-12 Corrosion Group who have undertaken a similar program.

Hydroxide Corrosion. Corrosion tests by hydroxides have been made at 1500°F, using NaOH, $Sr(OH)_2$, and $Ba(OH)_2$. Unfortunately, these materials are not available commercially in a very pure form, and initial tests

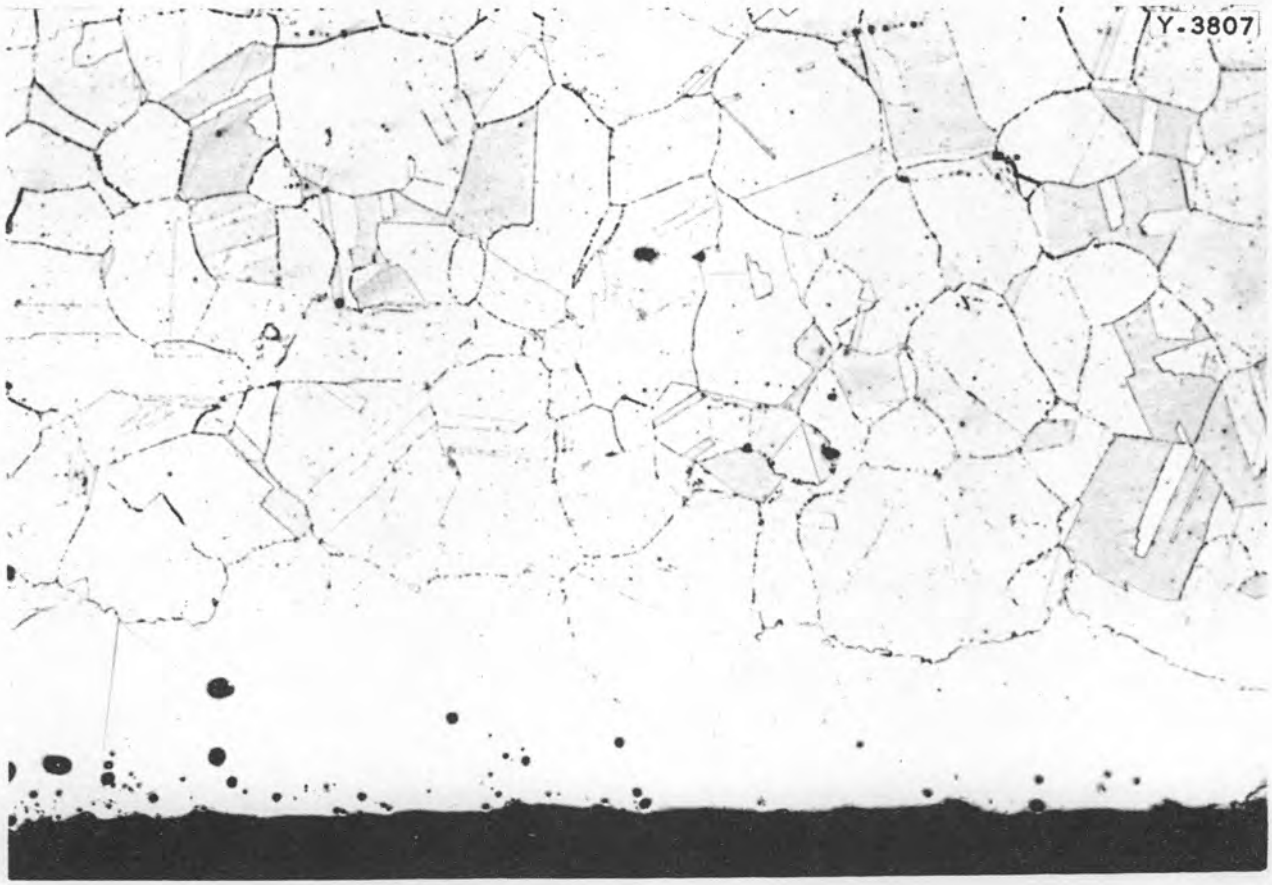

Fig. 3.8 - Surface of 310 Stainless Steel Specimen After 100 hr of Exposure to a Na-Be-U Fluoride Mixture at 1000°C. 250X. Note surface decarburization and void formation to depth of 0.002 in.

were made using as-received materials. More recent tests have used these hydroxides in various stages of dehydration, and, in some cases, substances were added to remove excess moisture, e.g., addition of Na or NaH to NaOH.

Corrosion by hydroxides is quite different from corrosion by fluorides or liquid metals in that the corrosion product is an oxide. The hydroxide-affected zone on a metal surface, however, was generally found to be quite complex. Figure 3.12 shows the surface region of an inconel sample which was exposed to $Sr(OH)_2$ at 1000°C for 100 hr. Apparently the oxidizing potential of the hydroxide bath is not sufficiently great to oxidize all the components of inconel (Fe, Ni, Cr). Since thermodynamic data indicate that nickel is more noble than either iron or chromium, it is quite probable that the metallic area in the affected layer is nickel-rich. Chemical analyses will be made in an effort to verify this belief.

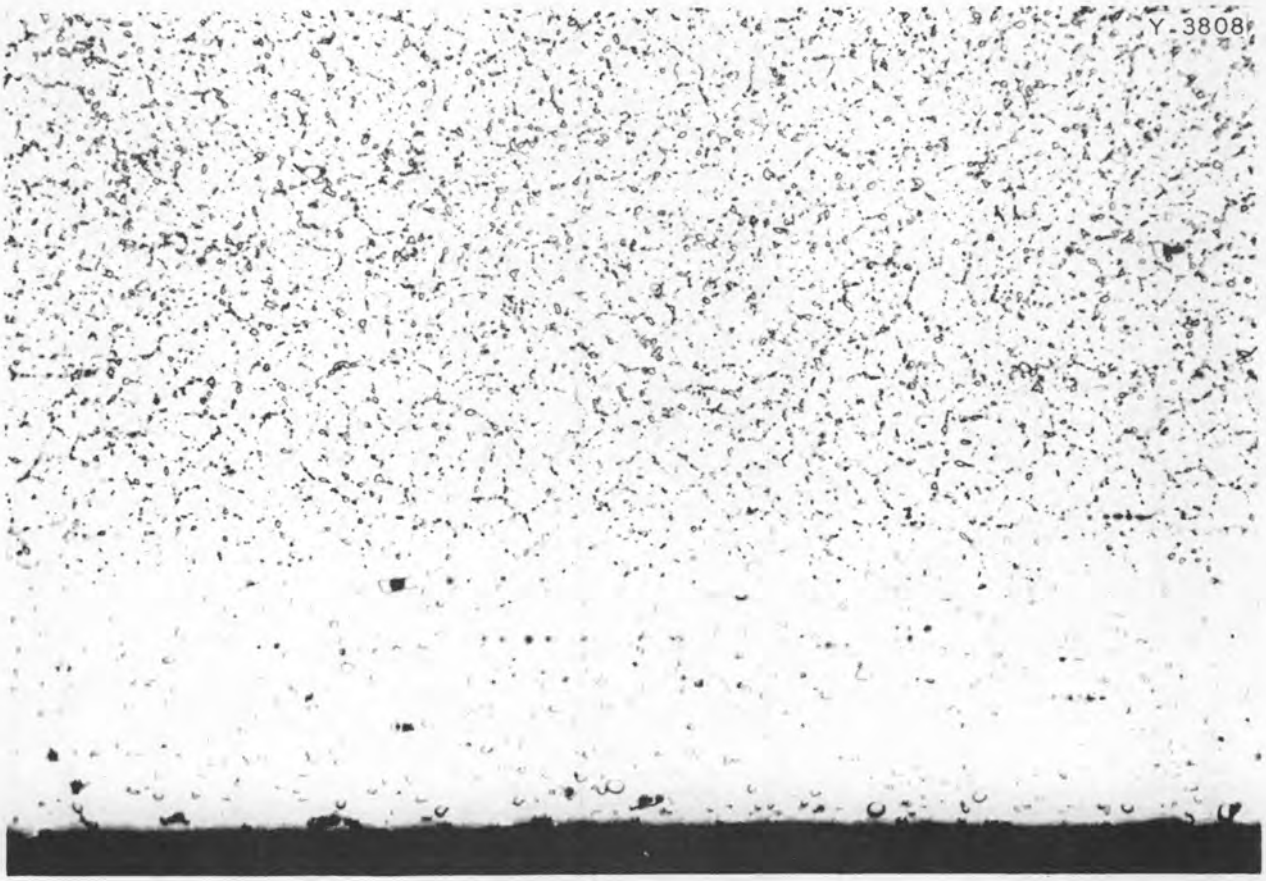

Fig. 3.9 - Surface of Hastelloy B Specimen After 100 hr of Exposure to a Na-Be-U Fluoride Mixture at 1000°C. 250X. Note decarburization to depth of 0.005 in. and retention of third phase.

Photomicrographs presented in Figs. 3.13 and 3.14 show a similar but more severe attack on inconel in NaOH and NaOH + NaH. The residual metallic area is much greater on the inconel specimen exposed to the hydroxide-hydride mixture, which would be expected since addition of NaH would be expected to lower the oxidizing potential. Nickel, however, showed no evidence of surface attack by NaOH, as is quite evident in Fig. 3.15. This is to be expected from thermodynamic considerations. The specimen did, however, show a very slight weight loss.

The attack by $Ba(OH)_2$ was found to be similar to that observed with strontium and sodium hydroxides. Figure 3.16 illustrates the appearance of a 316 stainless steel surface after a 100-hr exposure to barium hydroxide at 1000°C.

A summary of the hydroxide corrosion data obtained thus far is presented in Table 3.3. Many of these data will be

SECRET

SECRET

TABLE 3.2

Summary of Fluoride Corrosion Data Obtained in 100 hr at 1000°C (1830°F)

MATERIAL	METALLOGRAPHIC EXAMINATION	BATH ANALYSIS (ppm)		WEIGHT CHANGE ($g/in.^2$)
		TOP	BOTTOM	
Nickel A	Only evidence of attack was precipitation of fine particles along surface to depth of 0.002 in. (Fig. 3.7)	Ni 350	Ni 40	+0.002
304 stainless steel	Shallow surface voids observed to depth of <0.001 in.			-0.005
316 stainless steel	Very few shallow surface voids observed to depth of <0.001 in.	Fe 5,500 Ni 420 Cr 560	Fe 1,500 Ni 40 Cr 390	0.000
347 stainless steel	Surface voids observed to depth of 0.001 in.; no other visible attack	Fe 10,900 Cr 2,400	Fe 9,800 Cr 1,300	-0.003
310 stainless steel	Decarburized to depth of 0.002 in.; few scattered voids in this area (Fig. 3.8)			-0.003
330 stainless steel	Surface contains voids to depth of 0.001 in.	Fe 4,500 Ni 20 Cr 520	Fe 7,200 Ni 800 Cr 320	-0.003
446 stainless steel	0.002-in.-deep sigma-like precipitate throughout ferritic matrix except at surface zone; few voids observed to depth of 0.001 in.	Fe 1,440 Cr 50	Fe 7,410 Cr 190	-0.008
Hastelloy B	Decarburized to depth of 0.005 in.; lightly etched phase persistent throughout (Fig. 3.9)	Fe 5,800 Ni 310 Mo <10	Fe 1,200 Ni 70 Mo <10	+0.003
Inconel (as received)	Surface voids observed to depth of approximately 0.002 in.			
Inconel (decarburized)	Surface voids observed to depth of 0.003 in.	Fe <10 Ni 300 Cr <10	Fe 1,810 Ni 20 Cr 350	+0.003
347 stainless steel in inconel tube	Surface roughened; voids observed to depth of 0.006 in.			-0.120

Fig. 3.10 - Surface of Inconel After 100 hr of Exposure at 1000°C to $3NaF \cdot UF_4$. 250X. Voids adjacent to surface represent fluoride attack to depth of 0.004 in.

studied using more refined testing procedures and more highly purified components.

POWDER METALLURGY LABORATORY

Fabrication Group. The work on fabrication of solid-fuel elements has progressed along the lines discussed in ORNL-1033.[1] An additional fabrication technique, rubberstatic pressing, is now also being investigated. With all fabrication techniques the use of a screened fraction of sintered UO_2 seems to be desirable. Preliminary work is also underway on control rod fabrication for the ARE and on a program of alloy study involving molybdenum and columbium.

Hot Rolling. After a plate has been fabricated by hot-rolling it is desirable that it be drawn to final size. Since a suitable drawbench is

[1] *Metallurgy Division Quarterly Progress Report for Period Ending April 30, 1951*, ORNL-1033 (in press).

Fig. 3.11 - Surface of 347 Stainless Steel After 100 hr of Exposure at 1000°C to $3NaF \cdot UF_4$. 250X. Note formation of voids to depth of 0.002 in.

not available, cold-rolling was substituted. A set of plates was fabricated by the procedure outlined in ORNL-987. They were hot-rolled at 1100°C to a reduction of 75%. Six plates, each containing 30% UO_2, were made; three had matrices of iron and three of 302 stainless steel. Plates from each set were then given additional cold reductions of 10, 25, and 50% by hand-rolling. The plates with iron matrices rolled very well, showing only minor evidence of segregation of the UO_2. However, the units containing a stainless steel matrix suffered considerable segregation and striating of the UO_2. In neither case was the bond between the core and cladding material altered. Figures 3.17 and 3.18 are representative of this work.

To determine the effect of using coarse UO_2 in the fabrication of cores, a high-temperature induction furnace was assembled. A total of 330 g of a special high-purity UO_2 was sintered at 2100°C in a hydrogen atmosphere. The average weight change amounted to a loss of 0.5%. After sintering, the

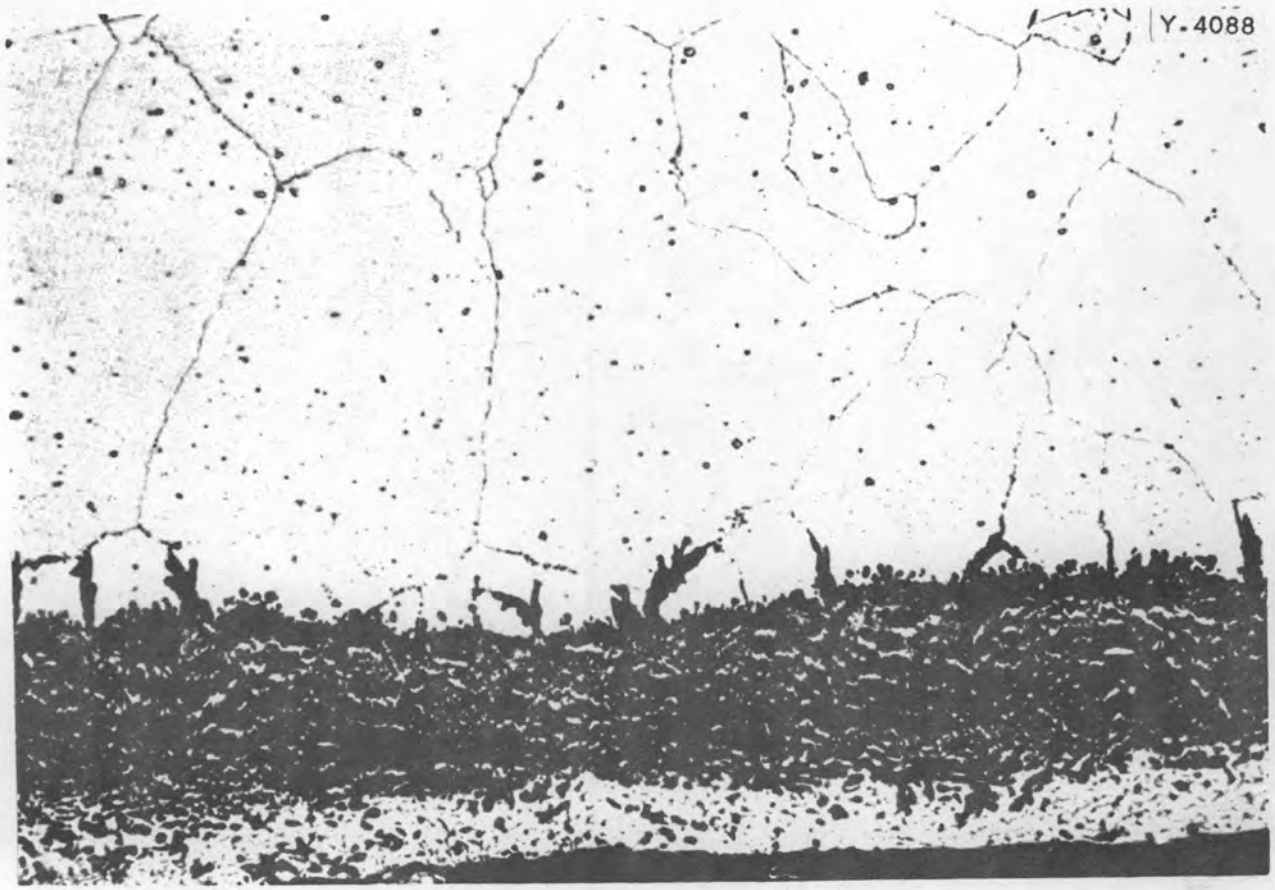

Fig. 3.12 - Surface of Inconel Specimen After 100 hr of Exposure to Strontium Hydroxide at 1000°C. 250X. Note 0.002-in. grain boundary penetration beneath 0.006-in. corroded layer.

coarse fragments of UO_2 were uniformly gray in color and quite hard. The apparent density had been increased by a factor of 3. The sintered product was then ground and divided into various size ranges by screening.

The -100, +200 mesh size fraction of the UO_2 was mixed in two batches with -100 and -325 mesh 302 stainless steel. Compacts were prepared in the usual manner and rolled at 1120°C to reductions of 50, 75, and 90%. Metallographic examination (Fig. 3.19) indicated segregation of the coarse UO_2 to be less sensitive to the particle size of the matrix stainless steel powder than is normal UO_2. However, a tendency to agglomerate into localized groups for reductions greater than 75% was noted. There was also some evidence of the UO_2 particles penetrating into the cladding layers.

To conserve on stainless steel an attempt was made to use mild steel tubing instead of stainless as the protective covering. The samples were

UNCLASSIFIED

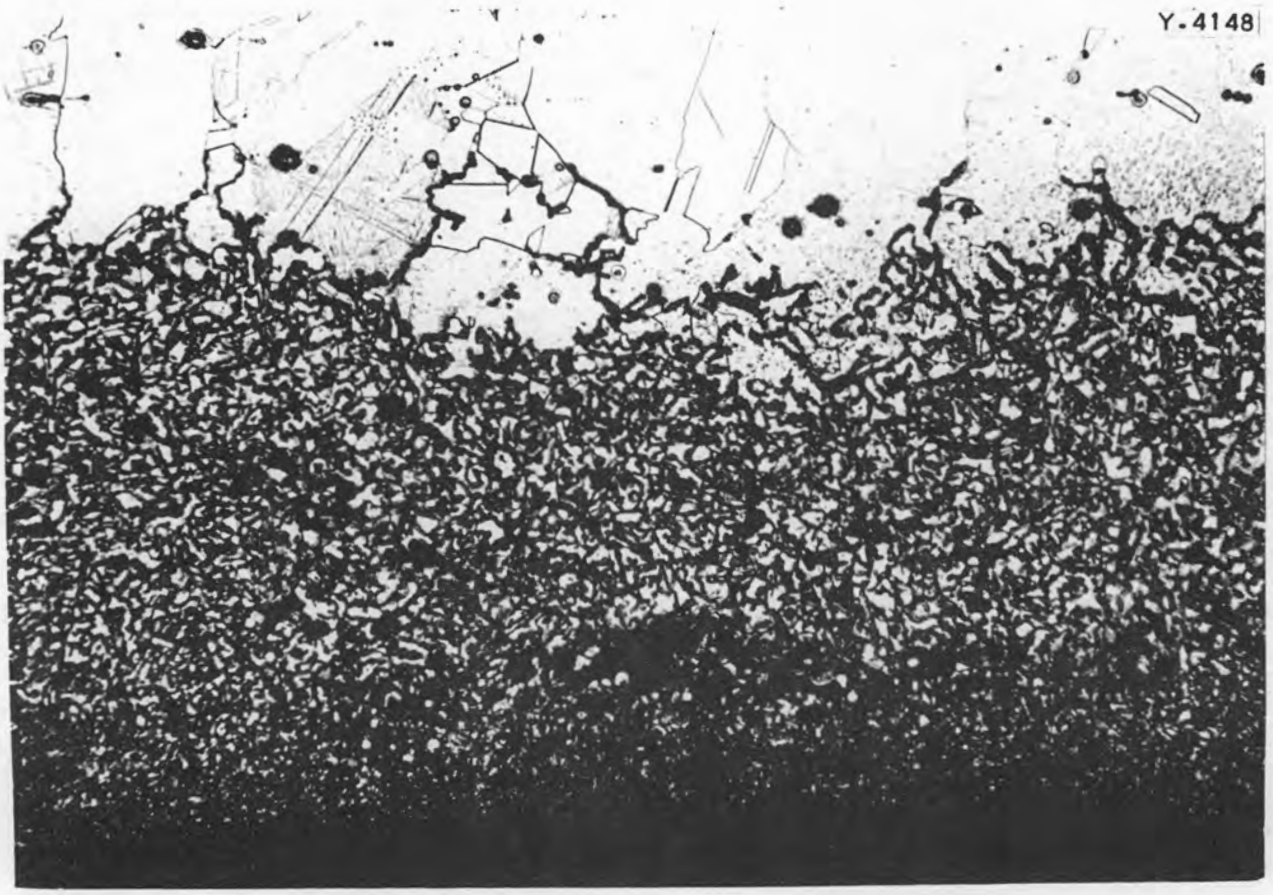

Fig. 3.13 - Surface of Inconel Specimen Severely Oxidized After 100 hr of Exposure to Sodium Hydroxide at 815°C (1500°F). 250X.

rolled at 1100°C but were heavily oxidized before receiving the first pass through the mill. On metallographic examination it was evident that the oxidizing conditions had penetrated to the compact and prevented adequate bonding. Further tests will be made, and it is hoped that a satisfactory atmosphere may be obtained by adjustment of the gas dissociator.

Mechanically Formed Matrix. The work in the X-10 shop on developing a method for punching molybdenum plates and obtaining a high percentage of open area (see ORNL-1033) has been held up waiting the delivery of carbide punches. Other methods of forming a suitable mechanical matrix are being placed on an inactive basis until the accompanying bonding problems have been solved. A low-temperature induction furnace is being assembled for these solid-phase bonding studies in which bonding will be tried both with and without load. The furnace is

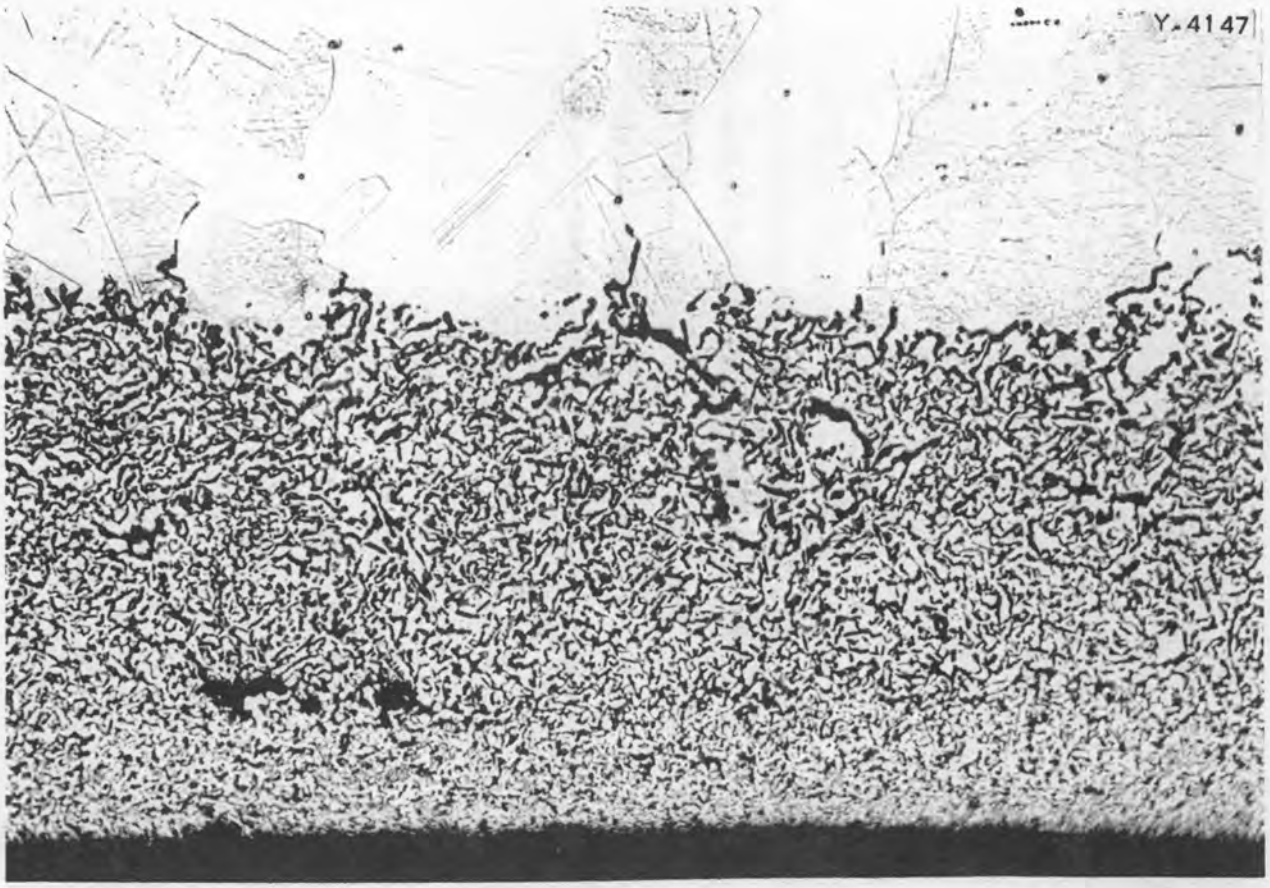

Fig. 3.14 - Surface of Inconel Specimen After 100 hr of Exposure to Sodium Hydroxide + 3% Sodium Hydride at 815°C (1500°F). 250X. Note depth of oxide formation and presence of unattacked metal in surface layer.

nearly completed and is expected to be placed in operation as soon as the induction furnaces are ready.

Loose-Powder Bonding. The microscopic examination of the samples discussed in ORNL-1033 has been completed. While the physical tests did not show any differences in bonding with various surface preparations of the base plate, Fig. 3.20 shows that under the microscope some apparent differences do exist. The as-degreased and the slightly roughed plates are more completely bonded than the others. Microscopic results on the remaining samples confirm those previously reported from the physical tests. Figure 3.21 shows that adequate bonding may be achieved by loose sintering and in addition shows how critical the variables are. The four plates in this panel were all sintered at the same time in a single stack of 11 plates. Steel spacers were used between the plates, making an overall stack height

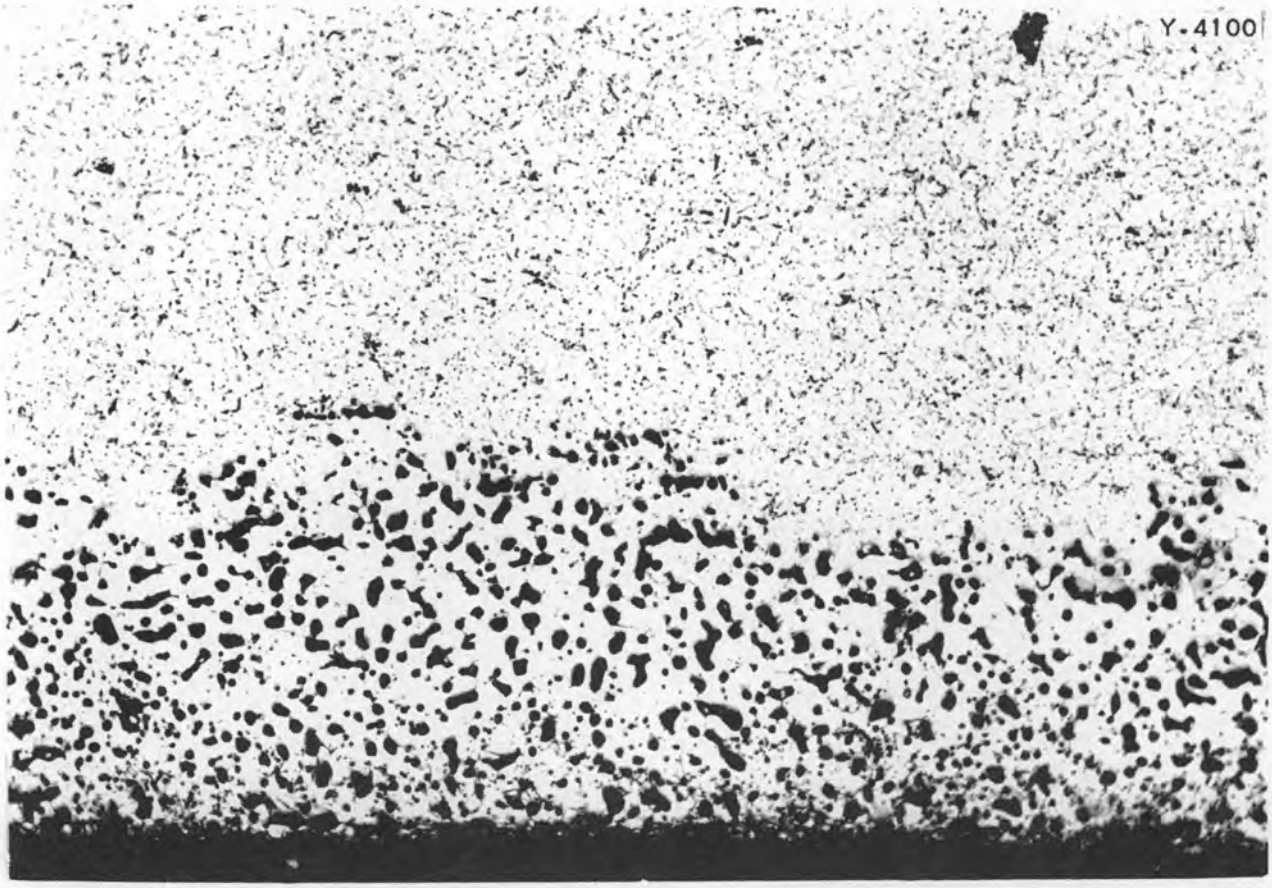

Fig. 3.15 - Surface of Nickel A Apparently Unattacked After 100 hr of Exposure to Sodium Hydroxide at 815°C (1500°F). 250X.

of slightly over 1 in. Whether the light load caused by weight of the plates and spacers or a slightly higher temperature (estimated 25°F) or both caused the improvement in bonding with lower stack position remains to be shown.

Work on the sintering of loose powders is now being carried out in our own furnaces. The first run was to be one of a series to determine optimum sintering temperature, and was to be run at 1250°C. Instead of the intended as-received UO_2 a size fraction (-100, +325 mesh) of the high-density, sintered UO_2 was used by mistake. With 30% coarse UO_2 in 302 stainless steel a fair bond was found at 1250°C. Increasing the temperature to 1280°C did not give a definite improvement in the bond. Another sample using regular UO_2 was prepared and sintered as above; however, very little bond was obtained.

Rubberstatic Pressing. Rubberstatic pressing has been used during this quarter as an additional fabrication technique. Figure 3.22 shows how this procedure may be used to press a powder

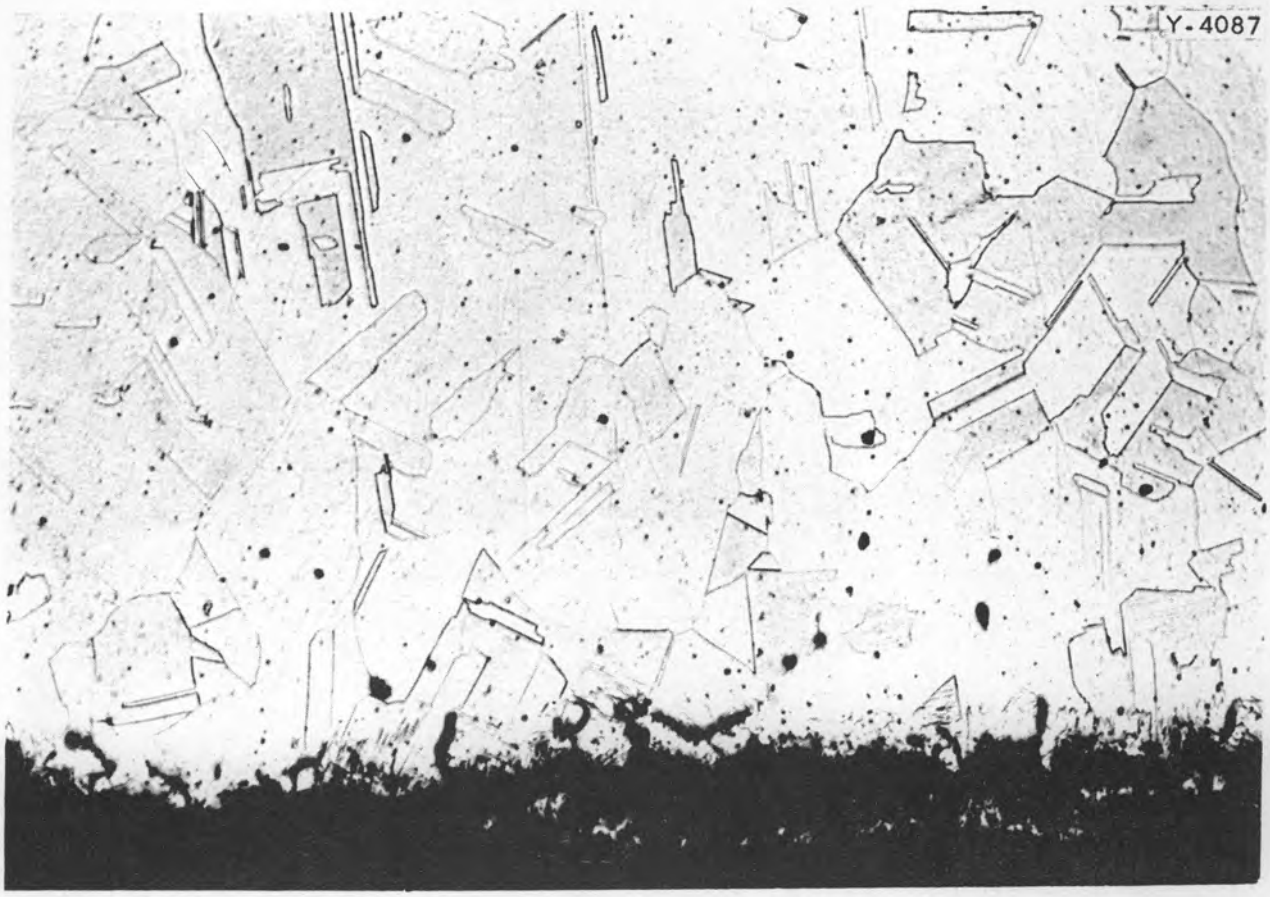

Fig. 3.16 - Surface of 304 Stainless Steel After 100 hr of Exposure to Barium Hydroxide at 1000°C. 250X. Note 0.003-in. layer of metal + oxide.

layer onto the inner surface of a tube. Pressure applied to the steel punches is transmitted through the rubber and presses the powder tightly onto the inside of the tube. This is followed by a sintering operation. This technique is being used as a fabrication method on both solid-fuel elements and control rods.

In the first specimen tried in the fuel-element work the lower half of the powder layer was 302 stainless steel while the upper half was electrolytic iron. After being pressed under 40 tsi and sintered at 1250°C, the stainless steel was well bonded but the iron had pulled away during sintering. A series of samples was then prepared using 30% by volume of high-density coarse UO_2 with various particle sizes in -325 mesh 302 stainless steel matrices. All the compacts were pressed at 30 tsi and sintered at 1250°C. The sample with -325 mesh UO_2 was not bonded, while another with -200, +325 mesh UO_2 was

SECRET

SECRET

TABLE 3.3

Summary of Hydroxide Corrosion Data Obtained in 100-hr Tests at 815°C (1500°F) and 1000°C (1830°F)

MATERIAL	HYDROXIDE	TEMPERATURE (°C)	WEIGHT CHANGE (g/in.^{2})	REMARKS	METALLOGRAPHIC NOTES
304 stainless steel	As-received $Ba(OH)_2$	1000	-0.027	Container tube failed during test; specimen not embrittled	Oxidized layer 0.003 in. thick; 0.001-in. intergranular attack beneath (Fig. 3.16)
316 stainless steel	As-received $Ba(OH)_2$	1000	-0.015	Container tube failed	0.004-in. oxidized layer; 0.001-in. intergranular attack beneath
Nickel A	As-received $Sr(OH)_2$	1000	-0.002		No visible evidence of attack
Nickel A	Degassed $Sr(OH)_2$	1000	-0.002		Occasional grain boundary attack to depth of 0.003 in.
304 stainless steel	As-received $Sr(OH)_2$	1000	-0.020		Very shallow (0.0005 in.) intergranular attack beneath 0.003-in. oxide layer; faint suggestion of thin transformation layer
304 stainless steel	Degassed $Sr(OH)_2$	1000	+0.010		0.001-in. oxide layer; 0.001-in. intergranular penetration into metal
316 stainless steel	As-received $Sr(OH)_2$	1000	+0.010		0.001-in. intergranular attack
316 stainless steel	Degassed $Sr(OH)_2$	1000	+0.034		0.001-in. intergranular attack
Inconel	As-received $Sr(OH)_2$	1000	-0.030	Container tube failed during test	0.006-in. oxidized layer; 0.001-in. grain boundary attack beneath
Inconel	Degassed $Sr(OH)_2$	1000	+0.105		0.006-in. oxidized layer; 0.002-in. intergranular attack beneath (Fig. 3.12)
316 stainless steel	As-received NaOH	815	+0.047		0.007-in. oxide layer; 0.001-in. intergranular attack beneath

SECRET

TABLE 3.3 (*continued*)

MATERIAL	HYDROXIDE	TEMPERATURE (°C)	WEIGHT CHANGE (g/in.^{2})	REMARKS	METALLOGRAPHIC NOTES
316 stainless steel	Degassed NaOH	815	+0.080		0.005-in. oxide layer; 0.002-in. intergranular attack beneath
316 stainless steel	NaOH + 3% NaH	815	+0.011		0.003-in. oxide layer; 0.001-in. intergranular attack beneath
316 stainless steel	NaOH + 30% Na	815	+0.033		0.003-in. oxide layer; 0.002-in. intergranular attack beneath
316 stainless steel	NaOH + 5 drops H_2O	815	Data not available	Tube burst from internal pressure	0.003-in. oxide layer; 0.002-in. intergranular attack beneath
Nickel A	As-received NaOH	815	-0.005		No evidence of attack
Nickel A	Degassed NaOH	815	+0.003		No evidence of attack
Nickel A	NaOH + Na	815	-0.014		No evidence of attack
Inconel	Degassed NaOH	815	+0.15	Tube failed during test	Severe attack to depth of 0.016 in. (Fig. 3.13)
Inconel	NaOH + NaH	815	+0.10		Sample severely oxidized to depth of 0.013 in.; container tube completely attacked (Fig. 3.14)
Inconel	NaOH + H_2O	815	+0.12	Tube failed	0.015-in. oxidized layer
Inconel	NaOH + Na	815	+0.08		0.012-in. oxidized layer
Inconel X	Degassed NaOH	815	Data not available	Tube failed during test	Completely oxidized (>0.018 in.)
Nichrome V	Degassed NaOH	815	Data not available	Tube failed during test	Completely oxidized (>0.018 in.)
Hastelloy B	Degassed NaOH	815	Data not available		0.012-in. severe intergranular attack (Fig. 3.15)

SECRET

SECRET

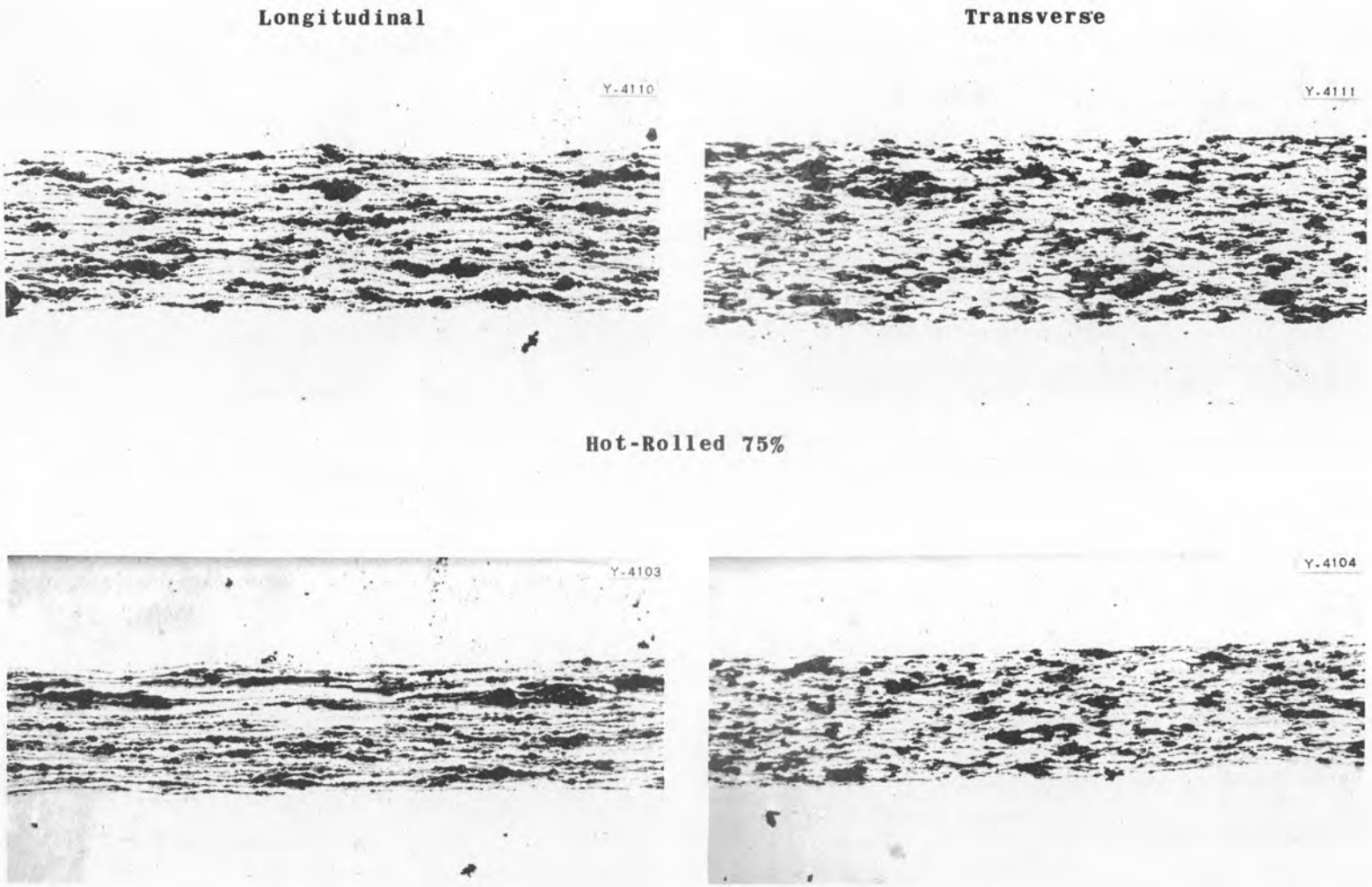

Fig. 3.17 - Effect of Cold-Rolling 30% UO_2—70% 302 Stainless Steel (-325 Mesh). Photographed at 175X; reduced 50% in reproduction.

SECRET

SECRET

Longitudinal **Transverse**

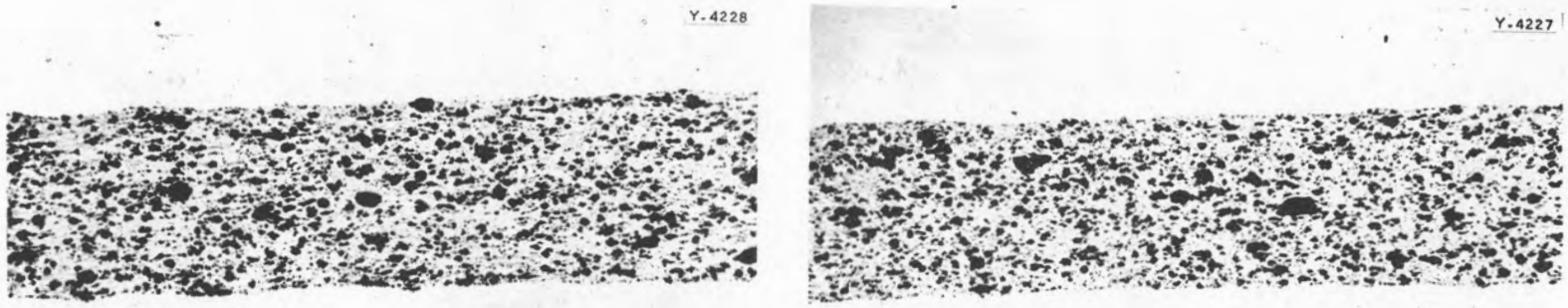

Hot-Rolled 75%

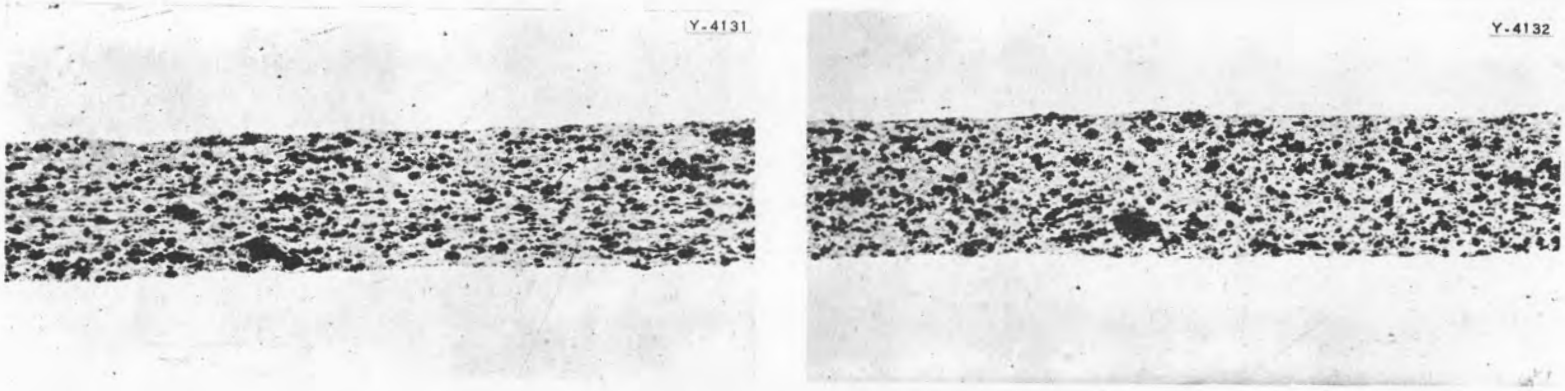

Cold-Rolled 25% After Hot-Rolling

Fig. 3.18 - Effect of Cold-Rolling 30% UO_2—70% Iron (10 μ). Photographed at 175X; reduced 50% in reproduction.

SECRET

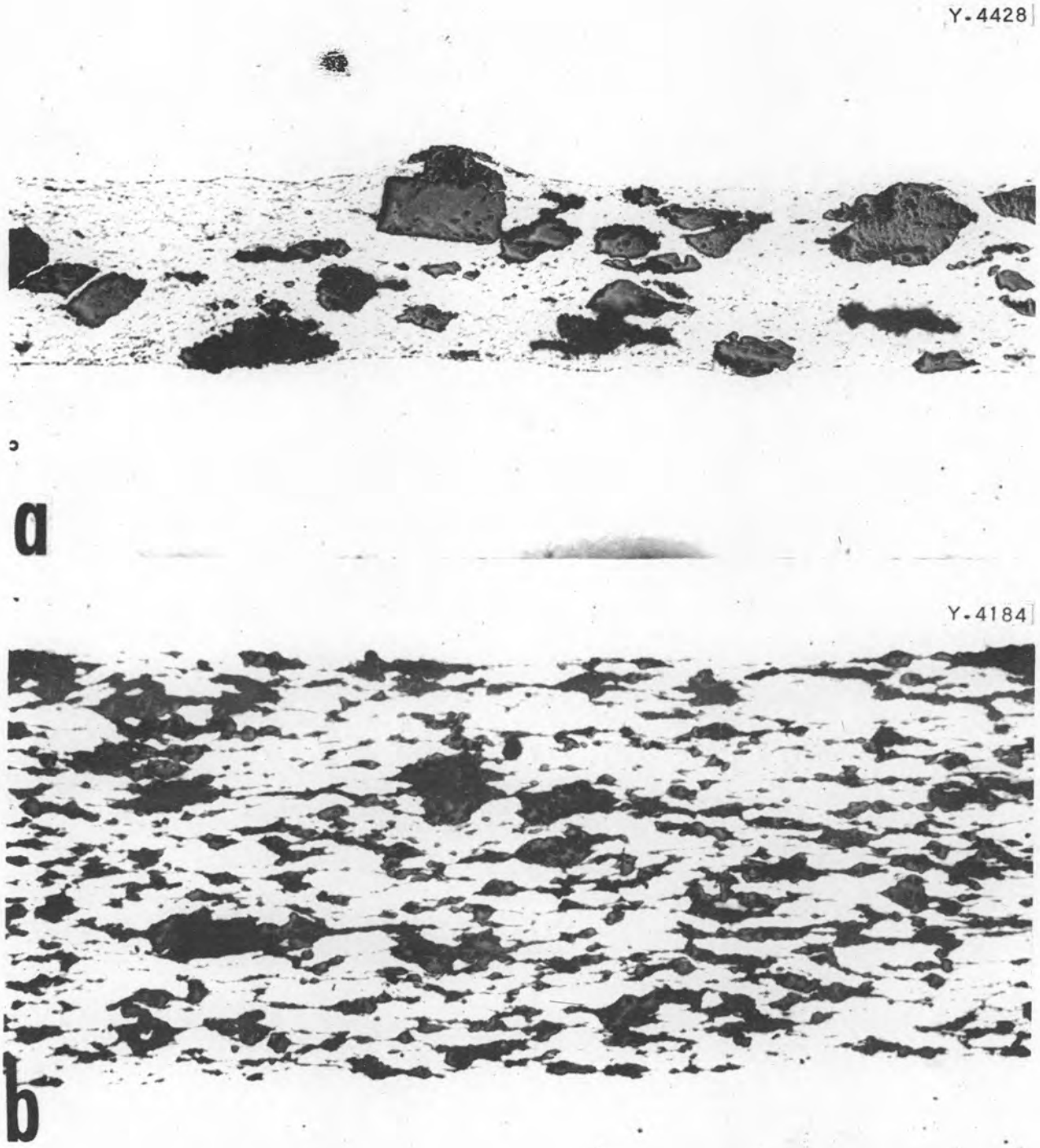

Fig. 3.19 - Effect of UO_2 Particle Size. (*a*) Coarse; 30% UO_2 (-100, +200 mesh)—70% 302 Stainless Steel (-325 mesh). 175X. (*b*) Fine; 30% UO_2 (as received)—70% 302 stainless steel (-325 mesh). 250X.

SECRET

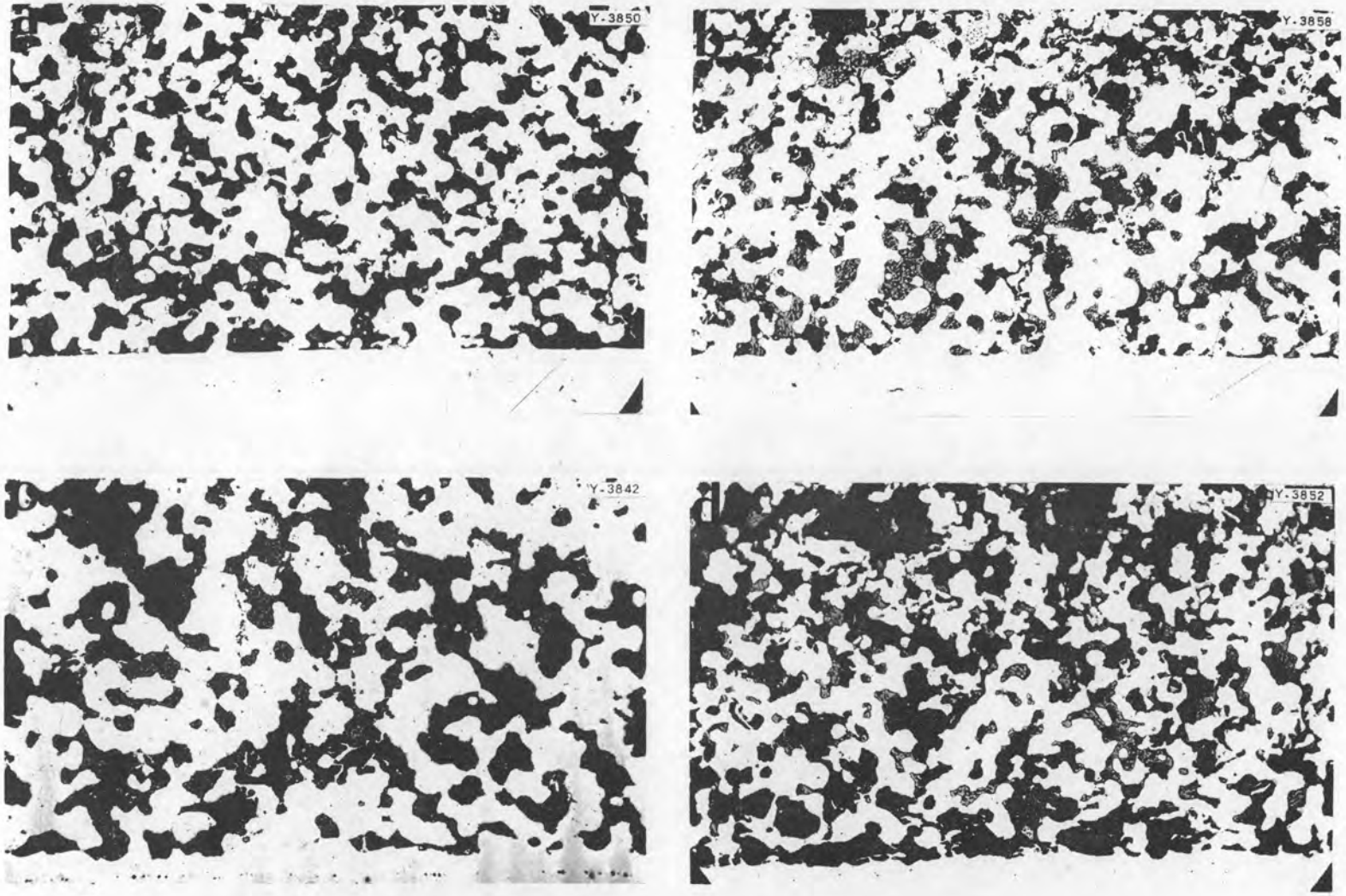

Fig. 3.20 - Effect of Surface Preparation on the Bonding of Loose Powders Containing UO_2 to a 316 Stainless Steel Plate. Photographs taken at 175X; reduced 50% in reproduction. (*a*) Electropolished. (*b*) Degreased. (*c*) Slightly roughened. (*d*) Heavily roughened.

SECRET

SECRET

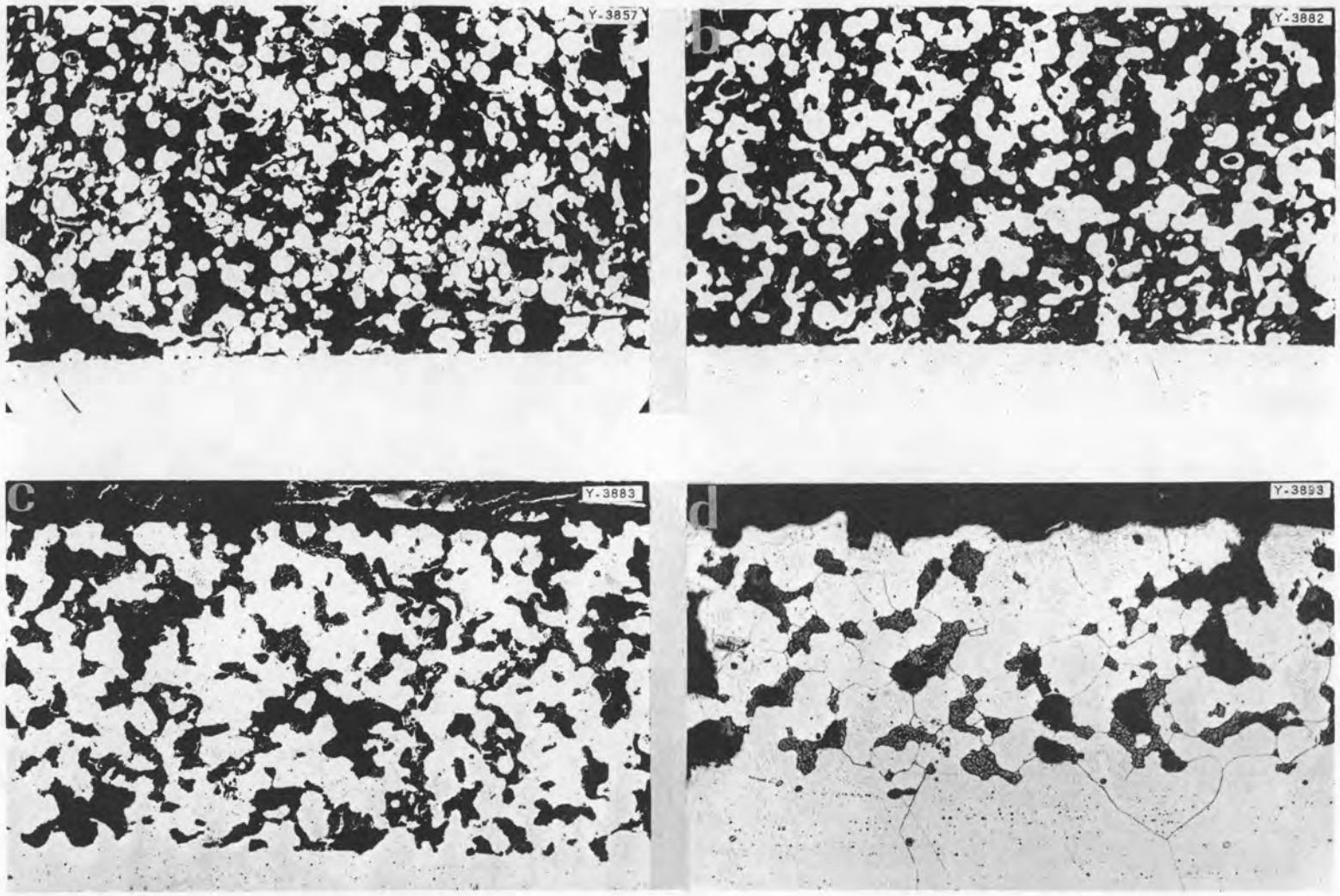

Fig. 3.21 - Difference in Sintering in Stack of Eleven 316 Stainless Steel Plates with Bonded Powder. Photographs taken at 175X; reduced 50% in reproduction. (*a*) Unetched; top plate. (*b*) Unetched; fourth plate. (*c*) Unetched; seventh plate. (*d*) Etch, aqua regia; bottom plate.

SECRET

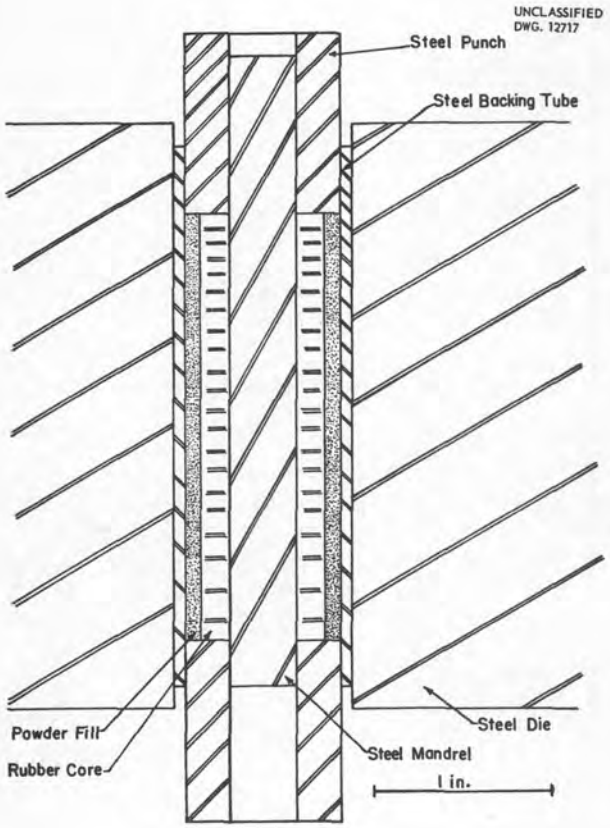

Fig. 3.22 - Rubberstatic Die Assembly.

bonded only superficially. However, two samples using -100, +200 mesh and -60, +100 mesh UO_2 were well bonded.

Control Rods. Work has started on the fabrication of control rods for the ARE. While hot-rolling and rubberstatic pressing are both being investigated as possible fabrication procedures, the most likely method, at present, seems to be a simple canning of powders. Materials now being investigated as possible control materials are B_4C and HfO_2, but the investigation is being expanded to include development of refractory boron, hafnium, or cadmium compounds.

As a preliminary investigation ZrO_2 was used as a substitute for HfO_2, and some plates were prepared with the standard hot-rolling technique. Although these two compounds are similar chemically, there is a considerable difference in their density, but this is not likely to affect the preliminary work. Cores with 30% by volume of ZrO_2 in nickel, iron, and 302 stainless steel were fabricated. They were clad with nickel or 316 stainless steel by hot-rolling at 1100°C. Table 3.4 is a summary of the results of this investigation.

Cladding Beryllium Oxide. The Gerity Michigan Co. of Adrian, Michigan has been attempting to develop a plating procedure for cladding beryllium oxide. The only oxide readily available at the beginning of this investigation was some high-fired material left from the Daniels reactor and several crucibles of low-density porous material. The high-fired material had a dark film on the surface which prevented any bonding. The porous material introduced considerable difficulty from gases and/or solutions becoming entrapped in the pores and then forming blisters during subsequent heating. If this problem can be solved, Gerity is quite optimistic that a successful cladding may be plated on. However, two samples which they gave us and which appeared to be satisfactory did not have enough mechanical bond to allow mounting for a metallographic study. They have now been asked to give this phase of the work a low priority and to push their investigation of electroforming techniques for special shapes.

TABLE 3.4

Summary of Results of Investigation on ZrO_2

CORE COMPOSITION (vol %)	CLADDING	REDUCTION (%)	BOND OF CLADDING TO CORE	REMARKS
ZrO_2 30, Ni 70	Nickel	56	Very good	Distribution of ZrO_2 good
		80	Very good	Distribution of ZrO_2 good
ZrO_2 30, Ni 70	316 stainless steel	92	Good	Tendency toward clumping of oxide particles
ZrO_2 30, Fe 70	316 stainless steel	53	Fair	Distribution good
		74	Fair	Slight tendency toward clumping
ZrO_2 30, Fe 70	316 stainless steel	92	Good	Extreme clustering of ZrO_2 particles; some penetration of ZrO_2 into cladding
ZrO_2 30, 302 stainless steel 70	316 stainless steel	77	Very good	Distribution very good

Compatibility. To determine the compatibility of UO_2-Fe or UO_2--302 stainless steel cores in contact with 316 stainless steel cladding sections of hot-rolled plates were sealed in evacuated tubes. The tube and its contents were held at 1000°C for 100 hr. Metallographic examination disclosed a diffusion of less than 0.001 in. between the iron cores and the 316 cladding and none between the 316 cladding and the 302 cores. Both these results were in agreement with earlier tests.

Refractory Metals. A survey of the literature on molybdenum and columbium has been undertaken in preparation for future work with those metals. Simple tests are being run upon available specimens to confirm or disprove some of the questionable reports.

CREEP-RUPTURE LABORATORY

The installation of equipment in the laboratory (Figs. 3.23 and 3.24) located is Building 2000 is essentially complete. The installation of equipment in the laboratory in Building 2019 for testing in liquid metal is about 70% complete and it is hoped that testing can be started by September.

The control instruments (Fig. 3.25) now have had about 6000 hr of nearly continuous operation, during which time all the 6N7 and 6SQ7 tubes have had to be replaced. About 70% of the mercury relays have required replacement, having had an average life of about two million cycles. A mechanical type relay has been placed in one control circuit for a life test.

Fig. 3.23 - Four of the Eight Installations for Creep Testing in Vacuum.

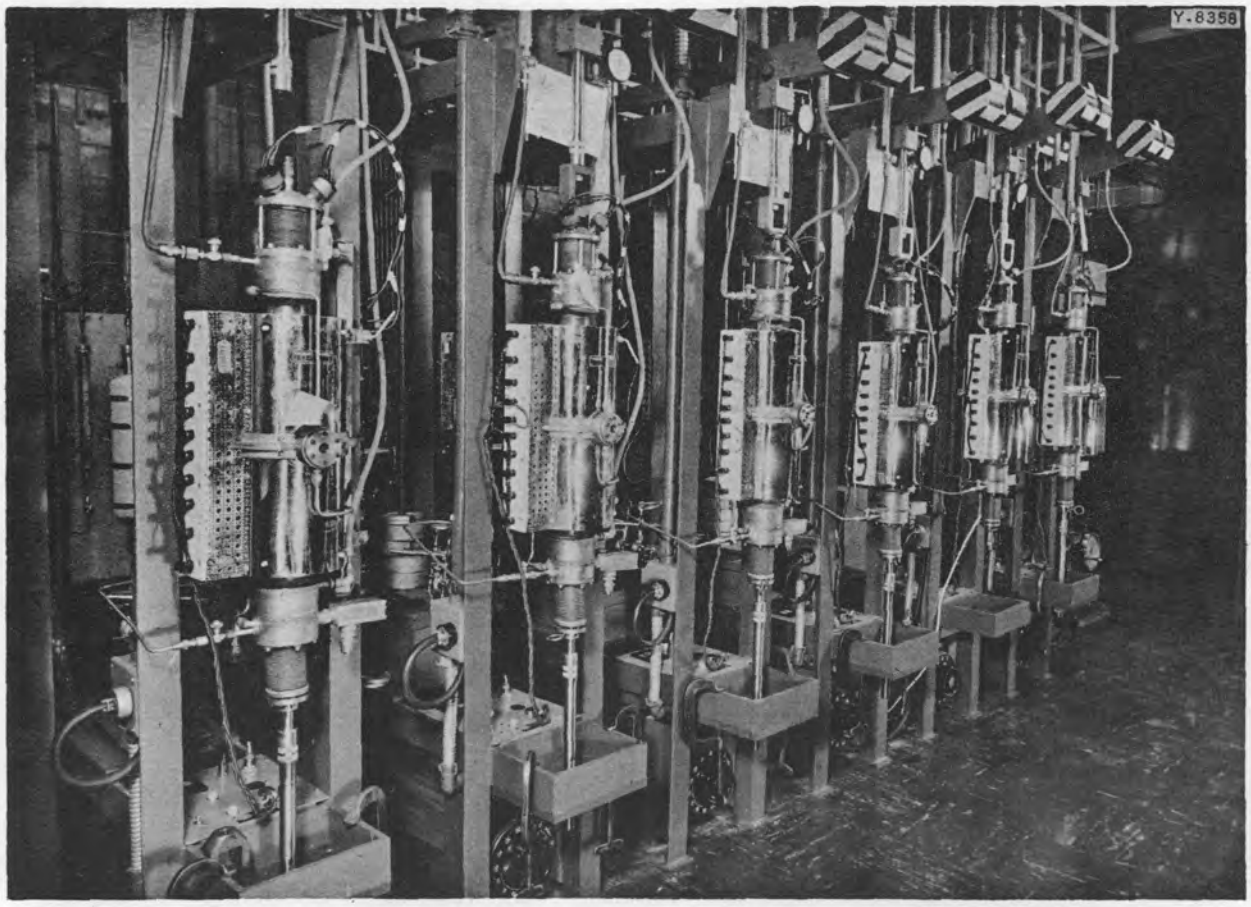

Fig. 3.24 - Units for Creep Testing in Purified Argon.

Nine technicians were hired and reported for duty during May. These men have now had sufficient training and are expected to start shift work July 30, placing the laboratory on a 24-hr basis. The principal aim of the testing during the past quarter has been to train these technicians, though acceptable test results have been obtained.

The 25-kw emergency generator has been installed and tested, the average total changeover time being 5 sec. The generator holds an essentially constant voltage even with 100% load changes.

In the early runs to study the operation of the vacuum furnaces (Fig. 3.26), vapor-deposited aluminum was observed on the specimens and pull rods. This observation raised the question of thermocouple stability in vacuums of 0.05 μ Hg or less at elevated temperature. Further testing showed by visual observation that aluminum and manganese will vaporize from the alumel wire at temperatures

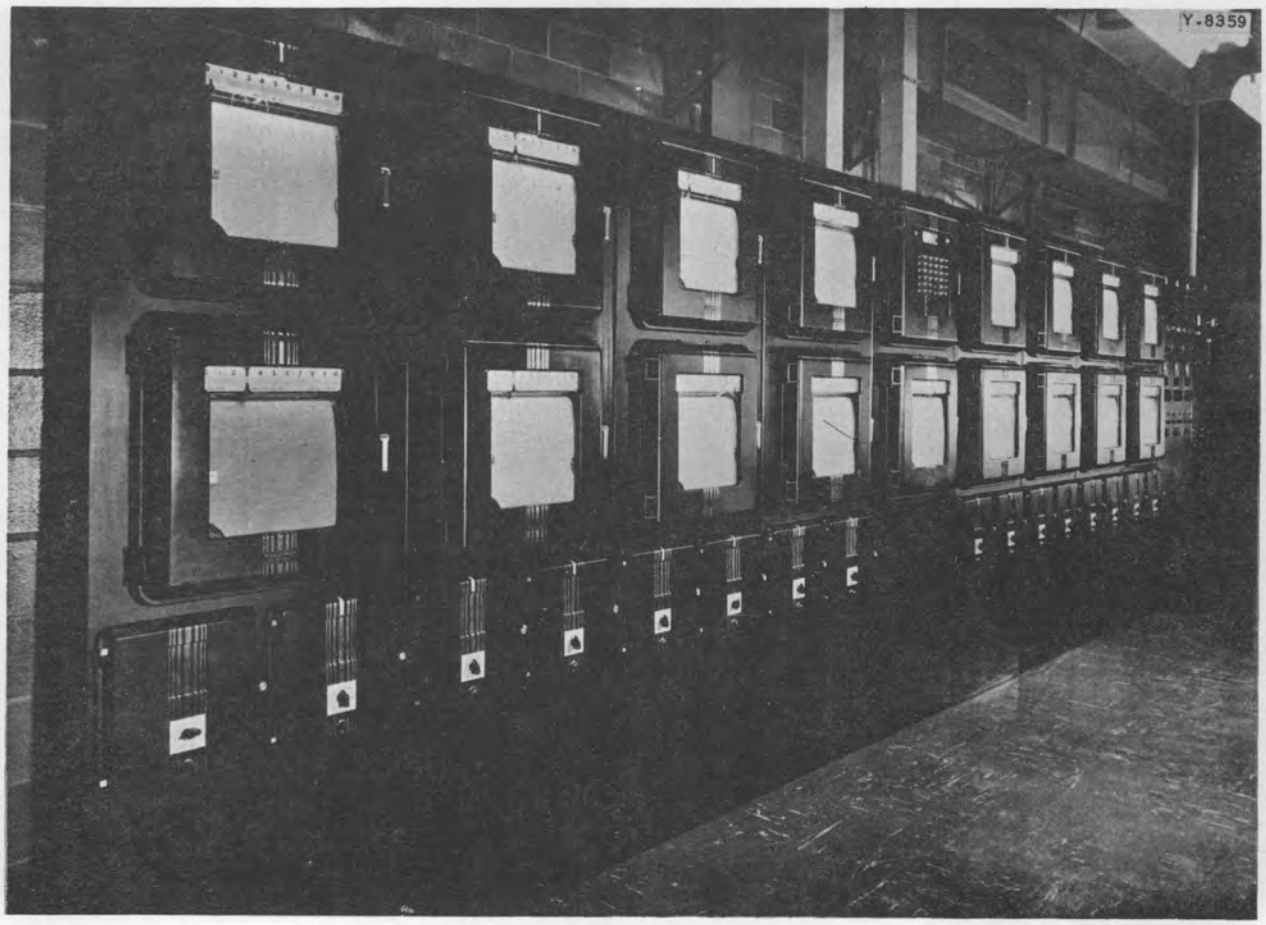

Fig. 3.25 - Centralized Instrument Panel in Creep Laboratory.

above 750°C and that chromium will vaporize from all sources in the furnace at temperatures above 850°C.

To study the effect of composition changes on thermocouple stability, chromel-alumel, iron-constantan, and platinum—10% rhodium couples were wired to a uranium bar. Two chromel-alumel couples were also brought into the system in stainless steel protection tubes; one couple controlled the furnace and the other served as a check on the temperature stability of the system. The temperature was held at 700°C for 1000 hr. The platinum and iron-constantan couples gave erratic temperatures while the chromel-alumel couple in vacuum gave consistent checks with the control and reference temperatures. Recalibration after such a run is unsuccessful unless the temperature gradient along the couple is exactly reproduced.

In an earlier attempt to check the stability of the thermocouples, chromel-alumel, platinum—10% rhodium, and iron-constantan couples were wired to the surface of a uranium bar. A

UNCLASSIFIED

PHOTO 9215

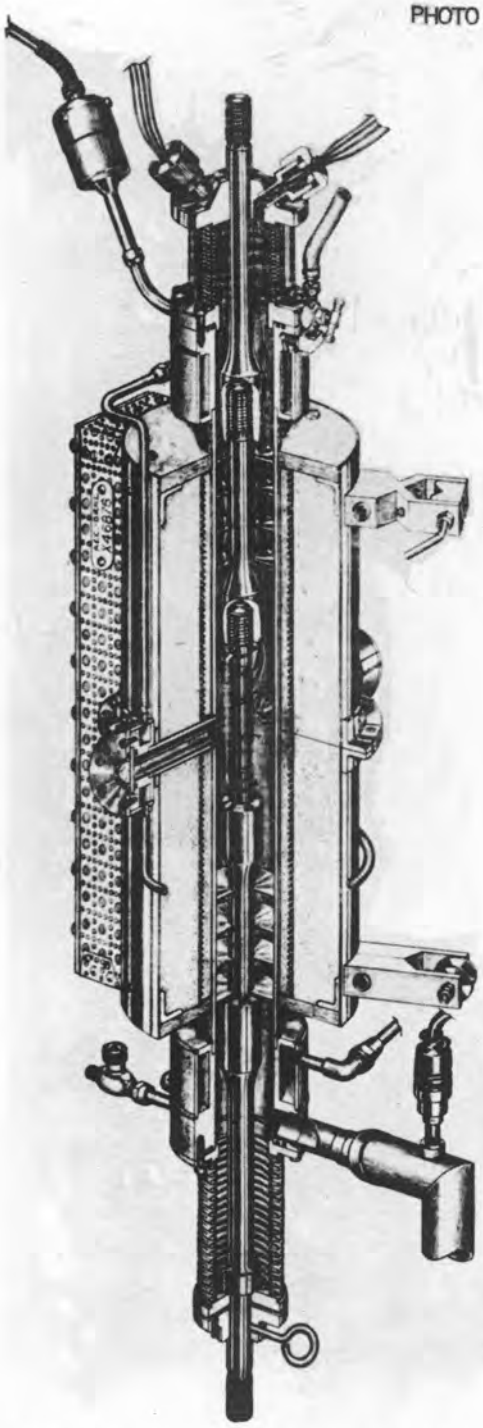

Fig. 3.26 - Furnace for Creep-Rupture Testing in Vacuum or Inert Atmosphere.

chromel-alumel couple was placed in a stainless steel protection tube and used to control the temperature. The furnace was operated at 750°C, 25°C above the iron-uranium eutectic temperature and 12°C above the nickel-uranium eutectic temperature. After about 30 hr the resulting eutectic melting had caused a crater in the uranium bar where the thermocouples made contact, and the end of the bar which had been screwed into the stainless steel grip had completely melted. Figure 3.27 illustrates this eutectic melting.

The testing program was started early in June, primarily to train the nine new technicians. The results obtained during this period have been affected by several small inaccuracies: Temperature gradients were not controlled as well as we hope to control them in the future, all extensions were measured with dial gages external to the furnace, and tests were interrupted as a result of the operators' misjudging the amount of extension occurring overnight. However, even though this period has been primarily for training, some test results have been obtained.

Uranium. Two 0.505-in. bars were each loaded to 12,000, 6000, 4000, and 2000 psi at 500°C and 0.05 μ Hg pressure. The data obtained, which are shown graphically in Fig. 3.28, are given in the following tabulation:

NOMINAL STRESS (psi)	RUPTURE TIME	
12,000	20 min	95% total elongation
6,000	3 to 4 hr	65% total elongation
4,000	90 to 110 hr	75% total elongation
2,000	Still on at 200 and 330 hr, respectively	Creep rate ~0.02% per hour

Fig. 3.27 - Eutectic Melting of Uranium in Contact with Fe-Ni-Cr Alloys.

Additional test samples have been loaded to 3500 and 4500 psi.

Thorium. One of five 0.505-in. bars has been loaded at 300°C and 0.05 μ Hg pressure, to each of the following stress levels: 22,000, 19,000, 16,000, 8,000, and 2,000 psi. The samples, from different lots of Ames thorium, had room-temperature tensile strengths ranging from 30,000 to 39,000 psi. The results of the tests were as follows:

NOMINAL STRESS (psi)	RUPTURE TIME	
22,000	30 min	32% total elongation
19,000	In test 120 hr	Creep rate ~0.0110% per hour
16,000	In test 500 hr	Creep rate ~0.0009% per hour
8,000	In test 750 hr	Creep rate ~0.0004% per hour
2,000	Discontinued at 1000 hr	Creep rate ~0.0005% per hour

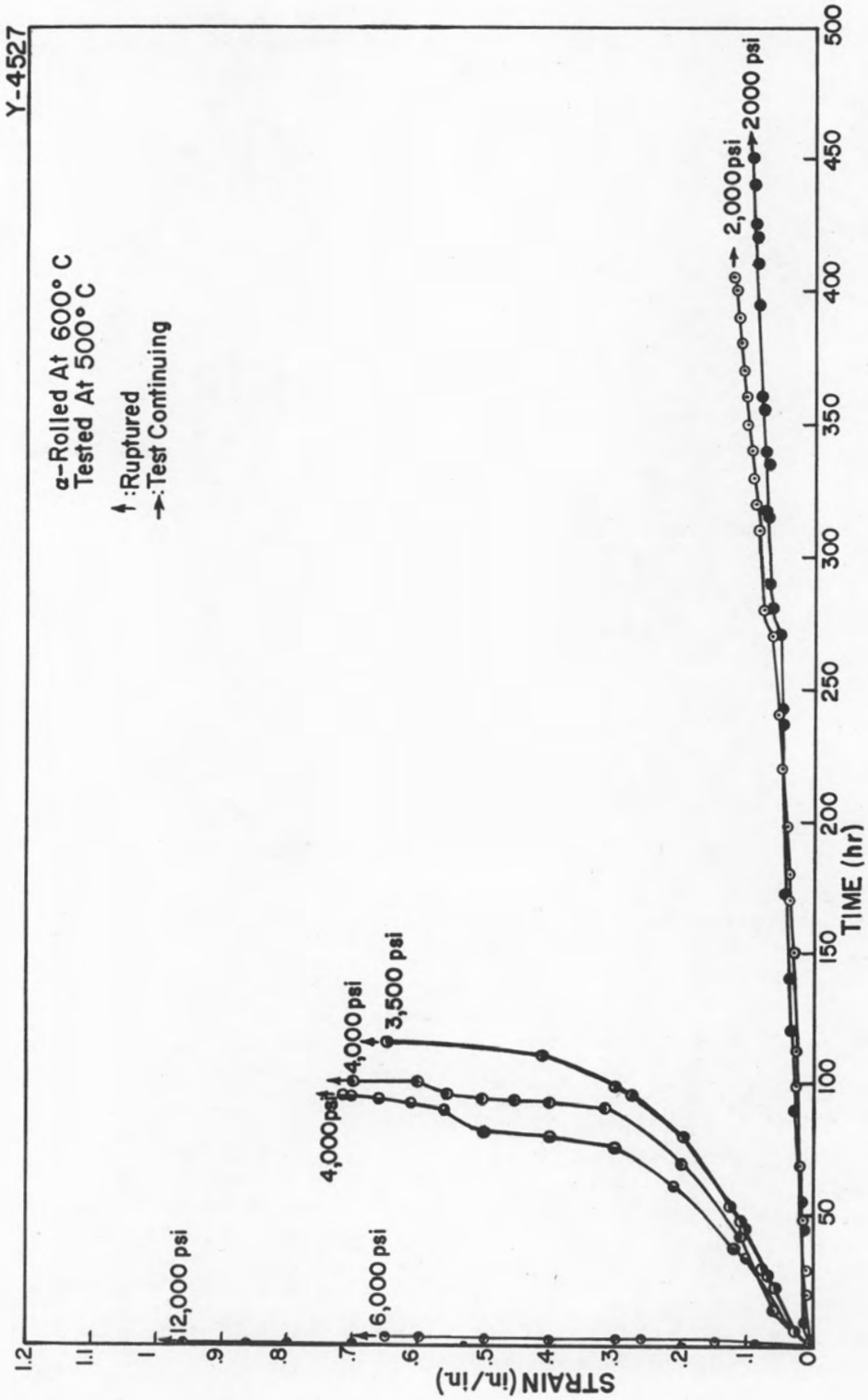

Fig. 3.28 - Strain-Time Curves for Natural Uranium.

Type 316 Stainless Steel. Duplicate sheet specimens (0.500- by 0.065-in. reduced section) have been loaded to 6000, 7000, and 8000 psi at 815°C in an argon atmosphere. There is considerable scatter in the results, and the work is being repeated.

Inconel. Sheet specimens in the as-received temper (0.500- by 0.065-in. reduced section) have been loaded to 5000, 6000, and 8000 psi at 815°C in an argon atmosphere. Duplicate tests check very well and are close to the published data. Similar specimens were heated to 1120°C in vacuum for 2 hr, then air cooled and loaded to 8000 psi at 815°C in argon. There was a very close agreement between the data from duplicate tests although the agreement with published data was poor. International Nickel Co. reports an increased rupture time following this treatment, and our results indicate a much shorter rupture time. Edge cracking was observed in the sheet specimens, and, assuming that International Nickel used bars, this cracking might account for the discrepancy. Metallographic studies have been initiated in an attempt to account for this difference. Loadings at 3000 and 5000 psi are in test.

Columbium. Two specimens were loaded to rupture at 815°C in argon. Rupture occurred at 26,000 psi with about 20% elongation. One specimen loaded to 6000 psi has been in test for 650 hr and has a total elongation of 6.8%.

Stress-Relaxation Testing. Eight simulated stress-relaxation tests for type 316 stainless steel were conducted at stress levels of 5000, 10,000, and 20,000 psi using the Baldwin creep-rupture machine. All tests were made at a temperature of 1500°F. After 16 hr the stress was about 4600 to 4800 psi regardless of the initial stress (Fig. 3.29) level. Stress-relaxation curves are also to be obtained for inconel and nickel A.

Design work for stress-relaxation tests on inconel bolts in sodium at 1500°F has been completed, but construction of the equipment has not been finished.

WELDING LABORATORY

Welding of Inconel. The greater part of the work to date has been confined to basic evaluation of the quality of inconel tube-to-header welded joints. A limited amount of fabrication of typical tube-to-header assemblies has been undertaken and will receive emphasis during the next quarter.

Mechanical Properties of Welds. *Tensile Tests.* The results of room temperature tests of inconel tube-to-header tensile pairs made using manual inert arc, cone arc, and brazing techniques are summarized in Table 3.5. It may be noted that strengths and ductility of manually and cone-arc-welded pairs were of the same order of magnitude and favorably comparable to the strength of the as-received inconel tubing used in the fabrication.

It is interesting to note that welded joints with average penetration of 70% of the header thickness of 0.062 in. exhibited strength and ductility comparable to welds with complete penetration. Failures in both types of joints occurred in the heat-affected zone immediately adjacent to the weld,

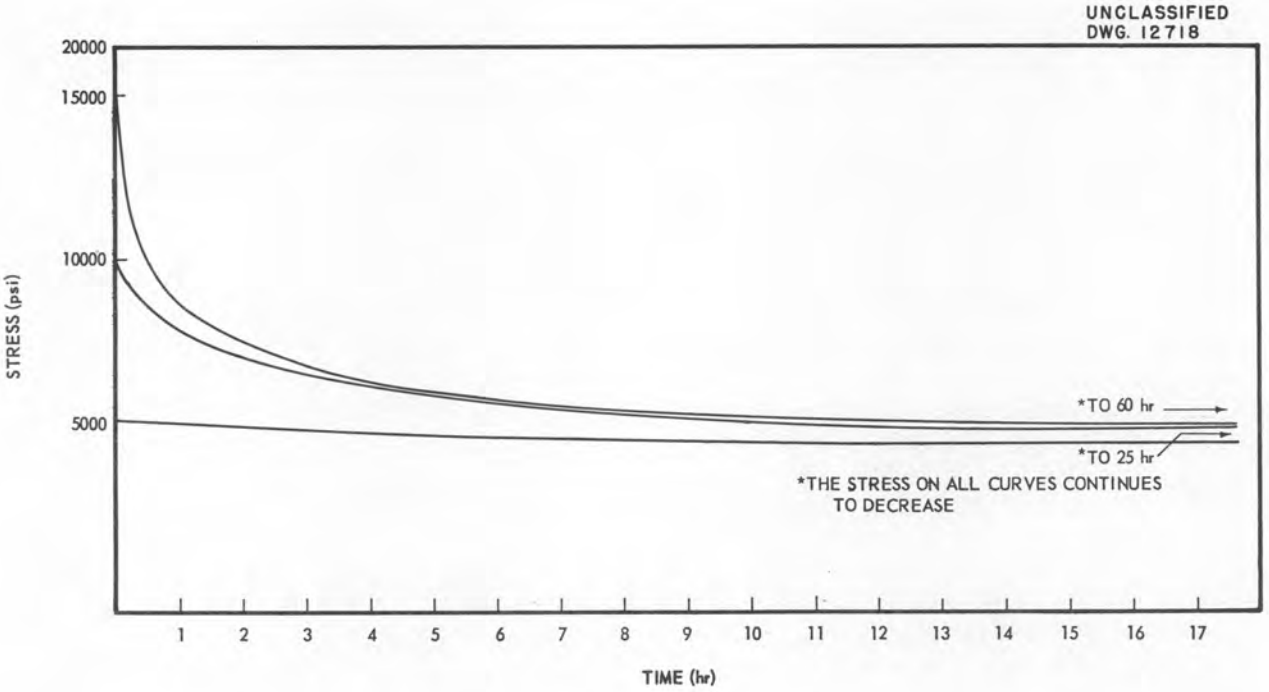

Fig. 3.29 - Relaxation Curves of 316 Stainless Steel at 1500°F.

as would be expected since this area is that of minimum cross-section. Partial penetration requires considerably less critical control of the variables of the cone-arc method. Complete penetration is more difficult to achieve with consistency, and it is expected that even more difficulty will be encountered when experiments with thinner header sheets and smaller tubing are attempted.

Strength values for joints brazed with Nicrobraz in preliminary experiments are included in Table 3.5. The lower tensile strength and somewhat higher elongation in 3 in. of these specimens may be attributed to the annealing received in the brazing operation. Brazing of basic joints for evaluation and comparison with welded joints will receive major consideration in future work.

Two manually inert-arc-welded inconel tube-to-header pairs were tested in liquid sodium at 1000°C for 100 hr before tensile testing to determine the effect on the room-temperature tensile strength. It may be noted that the only effect indicated by this experiment was a slight lowering of the tensile strength and an appreciable increase in elongation due to annealing.

Fatigue Tests. In order to further evaluate the quality of tube-to-header joints, a rotating tubular-beam fatigue test was developed. A photograph of the test apparatus is shown in Fig. 3.30 along with a schematic presentation of the fatiguing motion. The

TABLE 3.5

Room-Temperature Tensile Properties of Inconel Tube-to-Header "Pairs"

DESCRIPTION	NO. OF TESTS	AVERAGE TENSILE* STRENGTH (psi)	AVERAGE ELONGATION** (% in 3 in.)
Manual inert arc weld with complete penetration; tested as welded	3	93,000	23.8
Cone arc weld with complete penetration; tested as welded	3	96,500	21.5
Cone arc weld with average penetration of 70% of 0.062-in. header sheet; tested as welded	4	95,500	26.9
As-received inconel tubing	2	105,000	30.8
Nicrobrazed	2	82,200	28.9
Manual inert arc weld with complete penetration; tested after treatment in liquid sodium at 1000°C for 100 hr	2	89,500	36.9

*Tensile strength based on tube dimensions of 0.187 in. in o.d. and 0.025 in. in wall thickness except for "pairs" treated in liquid sodium. Tubing used was 0.188 in. in o.d. and 0.030 in. in wall thickness.

$$\text{**Percent elongation} = \frac{\text{Final "pair" length} - \text{Initial "pair" length}}{\text{Initial "pair" length}}.$$

test is effectively torsionless since the eccentric cam within which the tube end rides is equipped with roller bearings. Specimen lengths were 5.8 in. long and were rotated at 1125 rpm at a preset deflection.

A limited number of data are presented as an S-N scatter band curve in Fig. 3.31. Further tests are necessary for conclusive evaluation. It may be noted, however, that welds incorporating complete penetration, whether manual inert arc, cone arc, or brazed exhibited superior fatigue life to those joints with partial penetration. This condition was not evident on examination of tensile data. The lower fatigue life of these welds may be attributed to the lack of penetration, and, as a result, the presence of a "notch." The evaluation of fatigue, tensile, and corrosion properties of partially welded cone-arc joints, with the notch eliminated by brazing, will be the subject of future work.

All-Weld-Metal Tensile Tests. The properties of weld deposits in inconel plate are of interest since the ARE reactor shell and other components will be fabricated from thick plate. A limited number of tests have been conducted using ½-in. inconel plate and various filler metals to provide

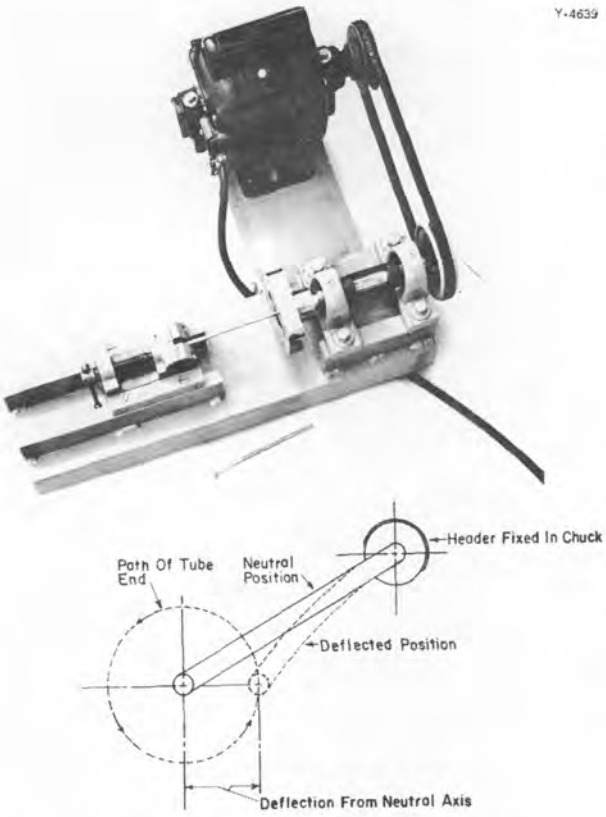

Fig. 3.30 - Fatigue-Testing Apparatus.

all-weld-metal 0.357-in. tensile specimens. The remaining weld deposits were reserved for quantitative analysis and static corrosion tests in liquid sodium and a fluoride.

The results of the room-temperature tensile tests are presented in Table 3.6. It may be noted that the inert-arc-weld deposits exhibited superior physical properties to those of the metal-arc deposit. The use of the manual inert arc, however, to fabricate the reactor shell is impractical. Further tests using Inco No. 132 metal-arc rod will be conducted to compare with the properties of weld deposits from an Aircomatic welder which should be in operation in the next quarter.

Inspection. Inspection of welds of the tube-to-header type involving a relatively intricate geometry and numerous small components is difficult. Radiography has been attempted with single specimens, and deliberate flaws which were located on the radiographs were much more evident with the naked eye. It is expected that the use of a system such as Dye-Chek, followed by microscopic examination of weld surfaces, hydraulic pressure testing of assemblies, and helium leak testing will prove useful in detecting major flaws. This system will be set up as part of future work as a preliminary approach to the problem.

Corrosion of Welds. The effect on the tensile strength of welded inconel tube-to-header specimens has been indicated in an earlier section.

Samples of the weld deposit from specimens 1 and 2 of Table 3.6 were treated in liquid sodium at 1000°C for 100 hr and in a liquid sodium-potassium-uranium fluoride mixture at 816°C for 100 hr. There was no significant loss or gain in weight of any of the samples. Metallographic examination indicated a weld metal immunity to attack by these liquid metals during the interval of test.

Special Tests. A recent problem which has arisen due to a finite departure from the tube-to-header type of reactor involves sealing off of the inconel tubing under a positive helium pressure. Preliminary experiments have been performed which indicate that pressures of 25 psig of helium can be enclosed within inconel tubing by application of mechanical pressure to crimp the tubing. While still under

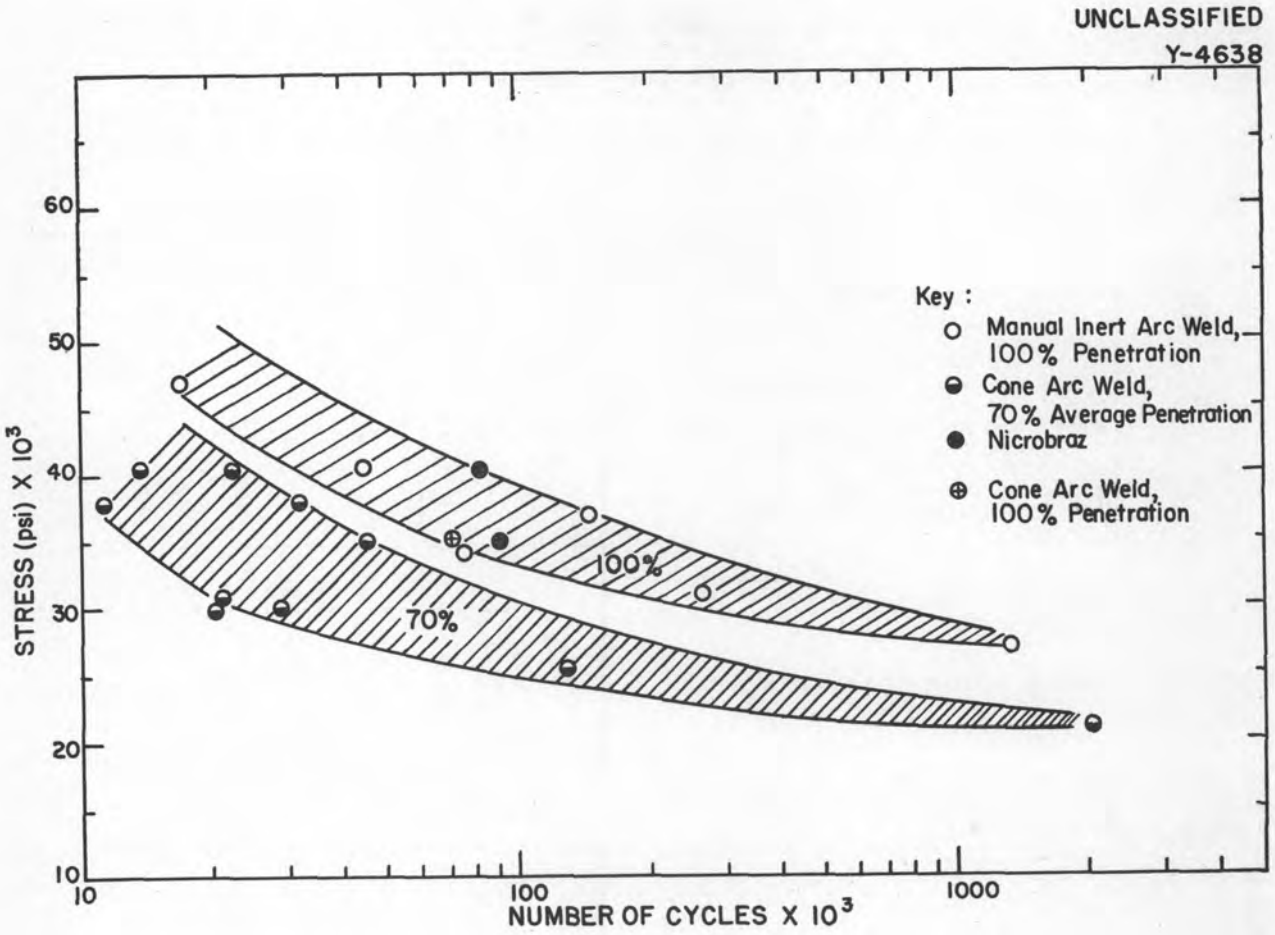

Fig. 3.31 - Effect of Penetration on Fatigue Life of Inconel Tube-to-Header Joints.

mechanical pressure, the tubing is sheared from the pressure source and is then welded shut. Pressure-tight tubes with gages brazed on one end for verification have been subjected to swaging experiments in an attempt to accomplish a uniform cylindrical closure more suitable to the newly proposed ARE design.

CERAMICS LABORATORY

A large number of pieces of equipment have been received and the millwrights should complete the installation by August 10. A number of other pieces of equipment are on order, the principal items of which are a Loomis press, surface grinder, tubular "Globar" furnace, and a band saw. Parts have been ordered for the construction of a vacuum dilatometer, beryllium oxide tube furnace and for a small "Globar" furnace.

Additional space has been secured for the ceramic laboratory and the Engineering Department is making

TABLE 3.6

Inconel All-Weld-Metal Tensile Values

(0.357-in.-diameter Test Specimens; 2 in. Gage Length)

SPECIMEN NO.	DESCRIPTION	TENSILE STRENGTH (psi)	ELONGATION (% in 2 in.)	YIELD STRENGTH 0.2% OFFSET (psi)
1	Inert arc welded; 1/8-in. inconel wire filler metal	100,000	40.5	55,000
2	Metal arc welded; Inco No. 132 1/8-in. rod filler metal	85,500	31	47,200
3	Inert arc welded; Inco No. 62 1/8-in. wire filler metal	98,000	44	55,500

estimates for placing this in a workable condition.

An agreement is being negotiated with the Electrotechnical Laboratory of the Bureau of Mines, Norris, Tennessee, whereby the latter will cooperate with the laboratory in the fabrication of crucibles and other refractory parts, and carry on special investigations of interest to the laboratory. All work which involves the use of beryllia and other beryllium compounds will be done at Norris.

The work of the laboratory is to consist of three parts, namely: basic or long-term research, engineering development, and service work. The former will be concerned mainly with the wetting of metals by oxides, phase studies of systems involving uranium oxide or carbide, and a study of the properties of hafnia. Development problems will be concerned with such projects as the fabrication of fuel rods for high-temperature reactors, valve seats to resist liquid sodium, and cermets for use as structural materials at elevated temperatures. Service work will consist in the fabrication of crucibles and other refractory parts for the Metallurgy Division. Also, a limited amount of work will be done for other divisions. The laboratory has already rendered service in the design of special refractories for vacuum induction furnaces for melting uranium, the making of special lithium fluoride insulators for the calutron, enameled iron gaskets to resist high temperatures, and in the design of a grinding system for refractories impregnated with plutonium.

An excellent ceramic library has been assembled at Y-12 with complete files of the more important ceramic technical journals.

Five pounds of hafnium metal has been produced from hafnium fluoride and will be sent to the Battelle Memorial Institute for further purification.

PHYSICAL CHEMISTRY OF LIQUID METALS

Interaction of Solid and Liquid Metals. A study is being made of the interaction of solid and liquid metals in which major emphasis is placed on the role played in these interactions by the crystallographic orientation of the solid metal surface. Preliminary tests were made of the action of liquid mercury on copper single crystal spheres. This system was chosen because of the great simplicity with which experiments could be conducted. As previously reported (ORNL-1033) it was found that the copper-mercury interaction was a function of the crystallographic orientation of the copper surface.

The success of the experiments on the copper-mercury system has encouraged the investigators to plan a more extensive program of study. This program is designed not only to determine the extent to which crystallographic orientation influences solid metal-liquid metal interactions but also to study the mechanisms by which this influence is exerted. The first type of interaction to be studied is the solution of a solid metal in a liquid metal and the inverse process of the deposition of a solid metal from a liquid metal solution. This type of interaction will be referred to as "solution-deposition" interaction.

The reason for choosing solution-deposition interaction for initial study is that this type of interaction is relatively simple when compared, for example, with interactions involving compound formation. However, it should be realized that solution-deposition interaction is of considerable applied importance. For example, thermal gradient mass transfer in several important liquid metal heat transfer systems takes place by solution of the container walls in a hot zone followed by deposition in a cold zone. This process is sometimes the source of a devastating form of corrosion.

The system which will be investigated first is copper-bismuth. This system should be suitable for study because it fulfills the following criteria: (1) The two metals do not form compounds, and (2) the liquid metal (bismuth) is relatively insoluble in the solid metal (copper). Subsequent studies are planned for other systems fulfilling these criteria.

The first experiments on the interaction of solid copper and liquid bismuth consisted simply in heating copper single crystal spheres in liquid bismuth at 400°C. The bismuth and the surface of the copper spheres were first deoxidized by suitable heating with hydrogen. Then a copper sphere was immersed in liquid bismuth at 400°C under an atmosphere of hydrogen. After heating for a specified time at 400°C the copper was removed from the bismuth at temperature. In these experiments the bismuth was heated in a conventional tube furnace with a simple on-off temperature controller. Therefore, the liquid was subject to thermal gradients and to a thermal cycling of ±3°C. Initially it was felt that the effects introduced by these thermal variations would be small enough to be ignored in qualitative measurements.

Two striking results were obtained when spherical copper crystals were immersed in liquid bismuth at 400°C

for 36 to 48 hr. First, the copper crystals were severely and fairly uniformly attacked. In one instance the crystal remained spherical although considerable copper had been removed. In other instances one side of the sphere was more strongly attacked than the other. On a smaller scale the surfaces of the spheres were slightly roughened. In no instance could any relation be found between the crystallographic orientation and the attack on the crystals. The second result was that a quantity of small copper crystals was deposited in one part of the capsule. These crystals were about 1 mm in diameter. Part of these crystals were well formed octahedra of excellent symmetry with very smooth faces and sharp, well-defined edges. Some octahedra had small secondary faces symmetrically arranged. The only secondary faces which were identified were cube faces. In a few instances the cube faces were large, but they displayed an irregular hopper structure. In no instances were curved surfaces found on the deposited particles.

These experiments were repeated twice with polycrystalline copper cylinders which had been electrolytically polished. In both experiments the results were similar to those obtained with the spherical crystals. In one experiment, however, the deposited copper consisted almost entirely of dendritic crystals.

Finally, an experiment was performed in which a copper single crystal sphere was heated in liquid bismuth at 400°C for 10 min. The crystal was appreciably attacked, but no crystallites were deposited.

The formation of crystallites of copper in the above experiments may have been caused by one or more of the following mechanisms:

1. *Thermal Gradients.* Assume that there existed a thermal gradient in the liquid bismuth and that the initial copper specimen was not in the coldest region of the liquid. The solubility of copper in liquid bismuth decreases with decreasing temperature. Hence, as soon as the bismuth became saturated with dissolved copper there would be a concentration gradient with a maximum value at the surface of the initial copper specimen and a minimum value in the coldest region of the bismuth. This gradient would cause a diffusion of dissolved copper from the initial specimen into the colder regions of the bismuth. However, since the bismuth was already saturated, copper would have to precipitate at the same rate as the rate of diffusion. This would lead to a steady state condition which would be maintained until all the original copper specimen had dissolved and redeposited in colder portions of the bismuth.

It is impossible to give an exact solution in terms of the diffusion equations for the mechanism discussed above because nothing is known at the present time about the supersaturation required for nucleation or the rate of growth of copper crystals for a given degree of supersaturation. That these factors may be of considerable importance is shown by the fact that under certain conditions dendritic growth may be obtained.

2. *Thermal Cycling.* Thermal cycling in which the temperature of the saturated solution of copper in bismuth periodically fluctuated a few degrees owing to improper temperature control could lead to the deposition

of copper crystallites in the following manner: As the temperature of the bismuth increased, part of the original specimen would go into solution; as the temperature decreased, the bismuth would become supersaturated and some of the dissolved copper would be deposited. If the supersaturation required for nucleation within the melt or on the walls of the container was no greater than the supersaturation induced by the cooling portion of the cycle, part of the redeposition of copper would occur at points other than on the original specimen, and hence crystallites would form. As the temperature increased on the next cycle, the crystallites would start to dissolve again but they would not dissolve completely because part of the copper going into solution would be contributed by the original copper specimen. In this manner the crystallites might slowly grow during a number of cycles.

3. *Free Energy Changes.* It is possible that the crystallites possess an intrinsic free energy which is less than that of the original specimen. If this is so, such a free energy difference might serve as a driving force for converting the original specimen into the crystallites.

The deposition of crystallites has been observed in a number of the static corrosion tests which have been made on liquid-metal systems at the Oak Ridge National Laboratory. This phenomenon resembles at least superficially the results reported above for the copper-bismuth system. It has been previously suggested by others that the deposits obtained in the static corrosion tests may be attributed to a free energy difference between the original specimens and the deposited crystallites.

It is clear that before meaningful measurements can be made on the copper-bismuth system, it will be necessary to learn something more concerning the origin of the crystalline deposits. A salt bath has therefore been constructed with which it will be possible to conduct experiments in which the thermal gradients and thermal cycling have been reduced to very small values or in which thermal cycling of a predetermined magnitude may be established. Experiments using this salt bath are now being conducted.

Although it is not known why the deposits were formed in the experiments discussed above, the results have an important fundamental significance. The deposition of copper from a solution of copper in bismuth is, at least under certain conditions, a function of crystallographic orientation. This is shown by the characteristic habit shapes which the deposits assumed.

. . . . .

4. X-RAY-DIFFRACTION LABORATORY

Several new pieces of equipment were installed in the laboratory during this period. A North American Philips diffraction unit, similar to the unit already on hand, has been obtained and placed in operation. Parts and diffraction tubes are interchangeable for our two units, and their camera tracks are identical. A Buerger precision camera, useful principally for crystal structure determinations, has also been placed in operation. A convenient feature of this apparatus is that it employs a goniometer head identical with our Weissenberg camera.

A Debye-Scherrer 114.6-mm camera has been added to the laboratory to replace a camera which had been borrowed from the Chemistry Division.

As was previously reported, an X-ray spectrometer for use with highly radioactive materials has been designed and is being built.

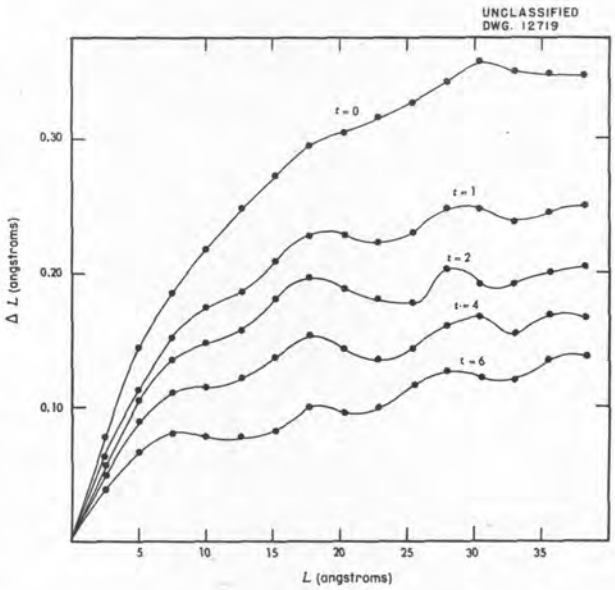

Fig. 4.1 - Root-Mean-Square Change in Length vs. Length for Cold-Worked Copper Filings During Recovery. HKL = 220. Unit time is one day.

RECOVERY FROM COLD WORK IN COPPER

The study of room-temperature recovery from cold work in copper filings has been continued. As before, the Fourier series method of Warren and Averbach was used to study the changes in the diffraction line contour during the recovery period. The analysis for the line for which hkl = 220 has been completed, and the results are shown in Fig. 4.1.

The interpretation of these data is not yet complete. It has been suggested that the almost periodic variations in each of the curves may be due to the approximations involved in evaluating the Fourier coefficients.

Recent conversations with Professor Averbach indicate the necessity for re-evaluating most of the data taken to date.

LOW-TEMPERATURE X-RAY DIFFRACTION

A device for the investigation of X-ray patterns at liquid-nitrogen temperatures has been designed and is now being constructed. The apparatus is intended for use with the North American Philips high-angle spectrometer. It will consist of an inner chamber which will be filled with

liquid nitrogen and will support the specimen and an outer chamber which will be evacuated, thus preventing ice formation on the specimen and providing high thermal efficiency. In addition to the evacuated region between the two chambers, nickel radiation shields will be employed to further increase the effectiveness of the insulation. A small heater will be built into the sample support to obtain temperatures intermediate to room temperature and liquid nitrogen. A beryllium window will be built into the outer chamber to provide an entrance and exit for the X-ray beam.

. . . . .

5. TENSILE PROPERTIES OF PURE METALS

THE STRESS-STRAIN-TIME CURVE AT INFINITE TIME

An approximation to this curve, called the σ_c stress-strain curve rather than $\sigma_{t\to\infty}$ stress-strain curve, has been obtained by tensile testing at exceedingly slow strain rates. The experimental data for the σ_c curves have been shown in a previous report (ORNL-910, p. 50ff). The course of this curve has been confirmed by five additional tests carried out by Argonne National Laboratory and by Ames Atomic Laboratory.

A logarithmic plot of the σ_c curve is reproduced in Fig. 5.1. The slope of the curve $d\sigma_c/d\delta$ has a probable error of ±0.2%. Hence σ_c is probably known within $\pm 0.2(\delta/\sigma_c)\%$ for $\delta > 0.001$. On the other hand, the stress, σ, of any test piece may fall within ±2% of the σ_c curve. Thus once a portion of the stress-strain curve is determined, the whole curve is known within the probable limits $\pm 0.2(\delta/\sigma_c)\%$.

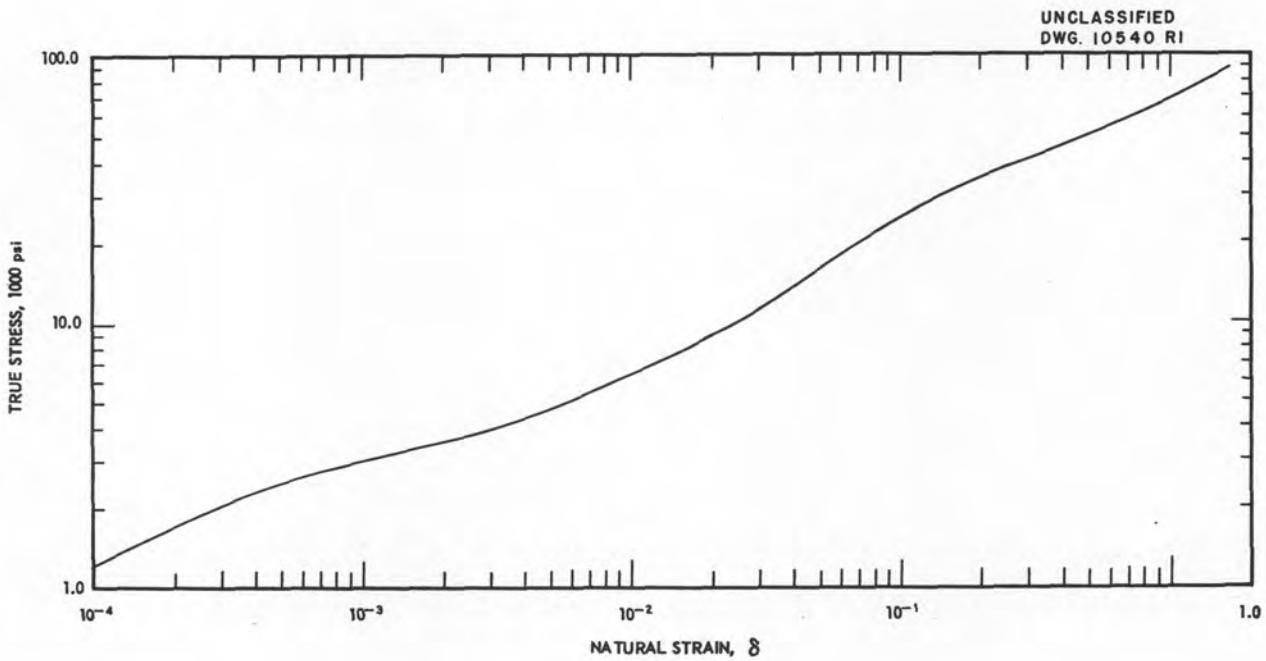

Fig. 5.1 - True Stress-Natural Strain Diagram, Logarithmic. Data obtained by hydraulic type Baldwin Southwark 120,000-lb tensile-testing machine; Tate-Emery load-indicating system; strain measured by SR-4 gages below 10^{-2} and by Peters microformers above 10^{-2}; strain rates, 0.005 in./min; specimens, OFHC copper 0.357 in. in diameter; grain size, 0.03 mm.

EMPIRICAL STRESS, STRAIN, STRAIN RATE, TIME RELATIONS IN PURE METALS

A general equation for isothermal deformation of pure single-phase metals has been proposed. An ideal condition of persistent homogeneity and constant small nonisotropy is assumed.

$$F[\delta(t)] = \sigma(t) =$$

$$\int_0^{t_s} (vf_\delta + f_t + af_v + \dot{a}f_a \ldots)\, dt \qquad (1)$$

where F denotes a functional and $\sigma(t)$ a multivalued function of time, $\sigma(\delta, \dot{\delta}, \ddot{\delta}, \ldots; t)$, in configuration space t; and $\delta = \delta(t)$, $a = \dot{\delta}(t)$, $\dot{a} = \ddot{\delta}(t)$, ..., etc. The functions are analytic and continuous. f_δ, f_t, f_v, etc. are partial derivatives of stress with respect to strain, time, and strain rates, respectively, and v, a, $\dot{a}$, etc. are strain rates and variations in strain rates. Thus each point in configuration space possesses one and only one set of partial derivatives of $\sigma(t)$.

Equation (1) represents tensile testing at arbitrarily varying strain rates. The differential equation of Eq. (1) is linear, of first order in the partials. In general, except in creep, the time derivatives are independently variable coordinates and may be considered as coefficients in the equation

$$\frac{d\sigma}{f_t + vf_\delta + af_v + \dot{a}f_a \ldots} = \frac{dt}{1} = \frac{d\delta}{v}$$

and

$$\frac{d\sigma}{dS} = \frac{f_t + vf_\delta + af_v + \dot{a}f_a \ldots}{\sqrt{1 + v^2 + a^2 + \dot{a}^2 + \ldots}}$$

where $dS^2 = d\delta^2 + dt^2 + dv^2 + da^2 + \ldots$. The coefficients may be obtained from a δ-t plot with little trouble. When the strain rates v do not vary, $a = dv/dt = 0$ and all higher derivatives are zero, and we obtain the equation for tensile testing at constant strain rates.

$$\sigma(t) = \int_0^{t_s} \left[v(f_\delta)_v + (f_t)_v\right] dt = \sigma(v, t) \qquad (2)$$

where v = a constant. Equation (2) represents a constant v section of Eq. (1), called the $(\sigma)_v$ surface. When the strain δ is maintained constant, $v = 0$ and we obtain constant δ sections of the $(\sigma)_v$ surface.

$$\sigma(t) = \int_0^{t_s} (f_t)_v\, dt = \sigma(\delta_0{}^\theta, \delta_k, t) \qquad (3)$$

where δ_k = a constant and $\delta_0{}^\theta$ specifies the course of the strains from 0 to δ_k. When the load is relieved, $\sigma = 0$ but internal stresses ψ remain. This condition is represented by

$$\delta(\psi) = f(\sigma_m, \sigma_0{}^\theta, t, \psi) \qquad (4)$$

where ψ is the average internal stress and σ_m is the external stress at the time of stress release, while $\sigma_0{}^\theta$ denotes the stress-strain-time curve from $t = 0$ to $t = \theta$, the time when the stress is relieved. In order for Eq. (4) to be inferred from Eq. (1), relations between ψ, δ, and σ must be found.

When the stress σ is kept constant $d\sigma = 0$ and Eq. (1) becomes

$$(vf_\delta + f_t + af_v + \dot{a}f_a + \ldots)_{\sigma_0{}^\theta} = 0 \quad (5)$$

where the subscript $\sigma_0{}^\theta$ represents the stress used as well as the loading rate at which this stress is obtained. Equation (5) is a constant σ section of Eq. (1) and represents level curves of the n-dimensional surface described by Eq. (1). The coefficients v, a, $\dot{a}$, etc. now cannot be varied independently of σ. They now are unknown functions and the equation is of higher order in v:

$$f_t + v_{f_\delta} + \dot{v}_{f_v} + \ddot{v}_{f_a} + \ldots = 0.$$

Equation (5) may be written

$$\left(\frac{d\delta}{dt}\right)_\sigma = (v)_\sigma = -\left(\frac{f_t}{f_\delta} + \frac{af_v + \dot{a}f_a + \ldots}{f_\delta}\right)_{\sigma_0{}^\theta}$$

$$= -\left(\frac{f_t}{f_\delta}\right)_v - F(\delta,\ v,\ a,\ \ldots;\ t,\ \sigma_0{}^\theta) \quad (6)$$

and represents the creep rate equation at constant stress; $-(f_t/f_\delta)_v$ are the tangents to the level curves of the functions $\sigma(t)$ of Eq. (2). Equation (6) may be integrated and will then give

$$(\delta)_\sigma = \delta_{(\sigma)_v} - F_1(t,\ \delta,\ \sigma_0{}^\theta).$$

$\delta_{(\sigma)_v}$ may be obtained from the empirically determined relation

$$\sigma - \sigma_c = B\delta^u t^{-b}$$

where σ_c is the asymptotic stress at any strain δ after $t \to \infty$. σ_c, B, u, and b have been determined for copper at 22°C, grain size 0.3 mm.

$$(\delta)_\sigma = \left(\frac{\sigma - \sigma_c}{B} \cdot t^b\right)^{1/u} - F_1(t,\ \delta,\ \sigma_0{}^\theta) \quad (7)$$

Equation (7) indicates that creep curves depend upon loading rates as well as upon stress. This is illustrated in Fig. 5.2, which gives the results of paired creep curves where a pair of curves was obtained at approximately the same stress but this stress was arrived at by widely differing strain rates during the loading period. Three pairs of curves at three different stress levels are shown. Since we have defined a creep curve as a constant stress section of the n-dimensional surface $\sigma(t)$ of Eq. (1), it is readily seen that at constant stress there is a particular creep curve for every loading rate; but at a given stress there is only one level curve of the surface representing stress as functions of strain and time at constant strain rate, which were called $(\sigma)_v$ surfaces in Eq. (2). Figures 5.2 and 5.3 represent projections on a strain-time coordinate plane, of both types of level curves. The creep curves (level curves of the n-dimensional surface) are therefore coincident with the level curves of the $(\sigma)_v$ surface at the instant the stress, which in loading increases from zero to σ, becomes constant, and thereupon they immediately depart from the latter. This relation is expressed by

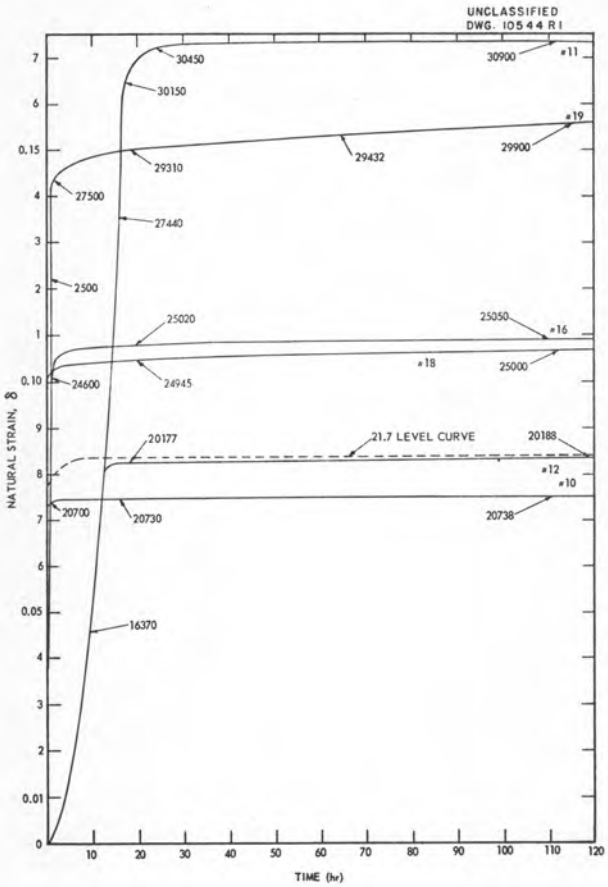

Fig. 5.2 - Creep Curves of OFHC Copper. Room temperature; effect of loading rates and magnitude of strain. The figures at the curves are in pounds per square inch.

Eq. (7); the first term of the right-hand side is the strain-time equation of the level curve of the $(\sigma)_v$ surface at a definite stress, and the sum of the right-hand terms gives the total strains on the creep curve at the same stress. Actually, the creep curves were obtained at constant load and the stresses of any two paired curves are not quite the same; but these variations are very small compared to the large differences in strains on any pair of curves. The creep conditions may be summarized as follows:

1. There is an infinite number of creep surfaces, one for each strain rate in loading, between the shock wave time rate and zero strain rate.
2. There is an infinity of creep curves on each stress level, one for each strain rate in loading.
3. There is only one creep curve after a given strain rate is used in loading to a given stress level.

Equation (5) thus may be written, when the creep rate is denoted by $(v)_\sigma$,

$$(v)_\sigma = f'(\delta,\ t,\ v_0{}^\theta)$$

where $v_0{}^\theta$ stands for any constant strain rate in loading.

$$(v)_\sigma = (d\delta/dt)_\sigma$$

and integration yields

$$(\delta)_\sigma = Kf(\delta,\ t) \qquad (8)$$

which is another form of Eq. (7) which for a given stress can be written

$$(\dot{\delta})_\sigma = K\delta(t) - g[\theta,\ (t - \theta)] \qquad (9)$$

since $F(t,\ \delta,\ \sigma_0{}^\theta)$ is dependent upon the strain accrued in loading from

UNCLASSIFIED
DWG. 12720

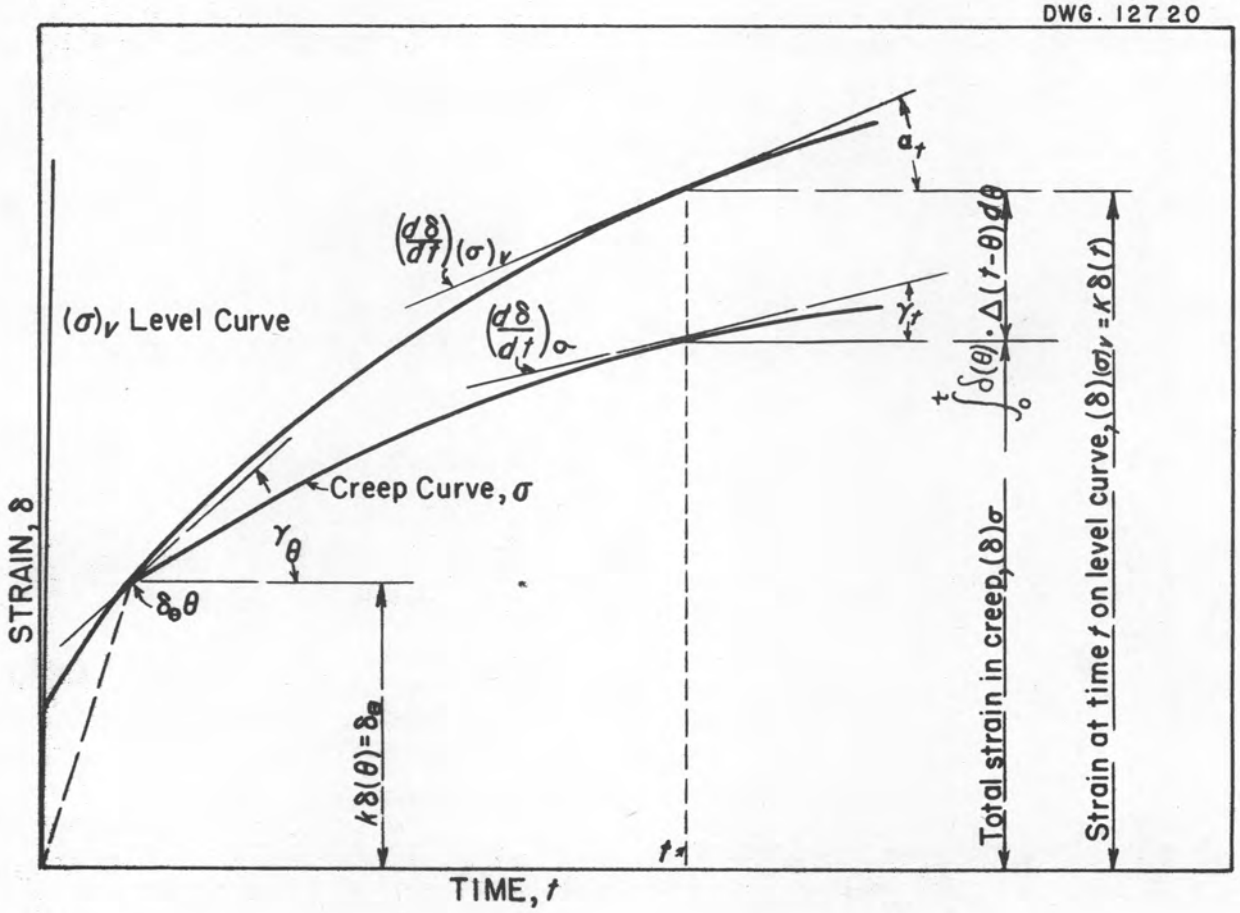

Fig. 5.3 - Relations Between Creep Curves and Level Curves of the $(\sigma)_v$ Surface.

$\sigma = 0$ to $\sigma = \sigma^\theta$ in the period $t = 0$ to $t = \theta$ and upon the strains after $t = \theta$, i.e., during the period after completion of loading $(t - \theta)$.

If this expression embodies a heredity function, analogous to that of Volterra's[1] equation for elastic torque,

$$\omega(t) = KM(t) + \int_0^t M(\tau)\,\phi(t,\tau)\,d\tau$$

and if we make

$$K\,\delta(\tau) = \left(\frac{\sigma - \sigma_c}{B}\,\tau^b\right)^{1/u}$$

(1) Volterra, *Lectures*, Clark University, Worcester, Mass., 1912.

according to the equation[2]

$$(\sigma)_v = B\delta^u t^{-b} + \sigma_c$$

$$(\delta)_\sigma = \left(\frac{\sigma - \sigma_c}{B} t^b\right)^{1/u} - g[\theta, (t - \theta)]$$

then

$$g[\theta, (t-\theta)] = \int_\theta^t \delta[\tau, (t-\tau)] \, d\tau$$

which differs from Volterra's heredity integral by including two variables t and θ instead of the single variable t of Volterra. This seems not unreasonable considering the differences in plastic and elastic phenomena.

. . . . .

(2) ORNL-910, Eq. (2), p. 58.

6. FUNDAMENTAL STUDIES OF ALLOYING

In the alloy systems of copper, silver, and gold with elements from the B subgroups, the equilibrium diagrams are often characterized by the same sequence of phases. These phases have the crystal structures face-centered-cubic, body-centered-cubic, γ brass, and close-packed hexagonal, in the order of increasing solute. When the compositions of these phase diagrams are expressed in terms of electron concentration in accordance with the well-known Hume-Rothery rules, the phase boundaries of many of the diagrams will be found to be superimposed. A theoretical interpretation of this phenomenon has been given by H. Jones[1] on the basis of the energies of the *s-p* valency electrons in the vicinity of the Brillouin zones of the crystal structures.

This theory has explained many alloying effects of the B-subgroup elements, such as the occurrence of defect lattices and the variation of lattice spacings involving Brillouin zone effects. It would be very desirable to extend these concepts to the transition elements. One difficulty, however, is that the number of valency electrons per atom in these metals is not known precisely. The reason for this may be understood in the following discussion of the transition metal theories.

In passing from left to right across the Long Periods of the Periodic Table, the melting points of the elements rise to a maximum and the interatomic distances decrease to a minimum in the vicinity of Groups V-A to VIII. The magnetic susceptibility, on the other hand, remains diamagnetic, or only weakly paramagnetic, for the elements from Groups II-A to VI-A and then becomes strongly paramagnetic or ferromagnetic in Groups VII-A to VIII-A. The explanation of these phenomena has been the subject of two different theories.

In the Mott and Jones[2] theory, the *d* electrons are regarded as interacting only weakly between different atoms. The differences in numbers of these *d* electrons of each type of spin are then adjusted to account for the magnetic properties. The cohesion of the crystal is considered to be due to small numbers of the *s* electrons, which are the valency type. An improvement to this theory was made by Seitz and Johnson,[3] who suggest that the lowering of mean energy of the *d* electrons, as free atoms of transition metals are brought together in a metal crystal, accounts for the additional binding forces. This idea is supported by the band structure calculations of Manning and Chodorow. The center of the filled region of the 5*d* band of wolfram was found by these investigators to be about 8 ev below the mean energy of these levels in the gaseous element.[4] Although this theory explains the increased cohesion of the transition

(1) H. Jones, "The Theory of Alloys in the γ Phase," *Proc. Roy. Soc. London* 144A, 225 (1934).

(2) N. F. Mott and H. Jones, *Theory of the Properties of Metals and Alloys*, p. 189, Oxford University Press, London, 1934.

(3) F. Seitz and R. P. Johnson, "Modern Theory of Solids. II," *J. Applied Phys.* 8, 186 (1937).

(4) F. Seitz, *Modern Theory of Solids*, p. 431, McGraw-Hill, New York, 1940.

metals and can be used to explain the magnetic, electrical, and specific heat properties of Group VIII-A elements and their alloys with Group I-B, its weakness is that it fails to explain in a natural way why the Groups V-A and VI-A elements are diamagnetic or weakly paramagnetic.

The second theory of the transition elements is that of Pauling.[5] In this theory the *d* electrons are regarded as dividing into two bands, of which one band enters the valency cloud by mixing with *s* and *p* electrons, and the other band remains associated with the ionic cores. The number of "atomic" type *d* electrons is chosen to agree with the magnetic properties of the First Long Period. This theory then gives a satisfactory explanation for the increase in the cohesive strength of the elements from Group I to Group VI-A by means of a steadily increasing number of valency electrons. Since the *d* electrons in Groups III-A to VI-A are all valency electrons, the absence of ferromagnetism or strong paramagnetism in these elements is adequately explained. The number of *s-p-d* valency electrons in chromium is 5.78, and this value remains constant throughout the remainder of the transition elements, i.e., manganese, iron, cobalt, and nickel, the additional electrons as one passes to the right along this series being regarded as entering the atomic type *d* band. The weakness of the theory is that its logical extension to the B-subgroup elements gives the following valencies: copper 5.44, zinc 4.44, and gallium 3.44. These values are difficult to reconcile with certain experimental observations, such as the low electronic contribution to the specific heat of copper and the soft X-ray spectra observations of Bearden and others on zinc, and with all the earlier theories of these metals.

It is not possible to decide between these two theories on the basis of present knowledge of energy band structures. The solution to the problem of the transition elements and their alloys would seem to be in the direction of new experimental observations which would be of assistance in the development of a new theory.

The objective of the present program of research will be to investigate the Group IV-A elements: titanium, zirconium, and hafnium. These elements, which have two *s* electrons and two *d* electrons in the ground state, contain fewer *d* electrons than the iron-group elements which have been previously investigated most thoroughly.* Further, they are in that part of the Periodic Table in which the greatest changes in cohesive energy are occurring. A study of these elements should, therefore, be of interest in the general transition metal problem.

The study will begin with the pure elements of Group IV-A, and, in special cases, may be extended to related heavier elements, such as thorium. Professor C. H. Shaw of Ohio State University will investigate the soft-X-ray spectra of these elements. The distribution of the numbers of valency electrons as a function of electron energy may be determined approximately by this means. It is

(5) L. Pauling, "The Nature of the Interatomic Forces in Metals," *Phys. Rev.* 54, 899 (1938).

*It is realized that the occupied states in metal crystals are not necessarily the same as in the free atoms, but this is assumed in the following disucssion as a first approximation.

customary to denote the number of electron states with energy between E and $E + dE$ by the symbol $N(E)\ dE$. When $N(E)$ is plotted as a function of electron energy, the resulting curve is called an $N(E)$ curve. This curve will then be supplemented by measurements of the electronic contribution to specific heat at low temperatures, which is directly proportional to $N(E)$ for electrons of maximum energy. The latter measurements will be made under the supervision of Dr. J. E. Goldman at Carnegie Institute of Technology. These results will then be considered in relation to the number of valency electrons in the metal crystals and in relation to their close-packed hexagonal crystal structures. It is of interest that many other elements with two *s* electrons, such as beryllium, magnesium, calcium, cadmium, and zinc, also have close-packed hexagonal crystal structures. The suggestion is that the *d* electrons in titanium, zirconium, and hafnium are not active in affecting the choice of structure, but it must be freely admitted that many exceptions may be found in a general extension of the same idea to other elements in the Periodic Table.

The experimental research on these pure metals at the Oak Ridge National Laboratory will include a new determination of the melting points of titanium, zirconium, and hafnium. Secondly, the crystal structure of the high-temperature allotrope of hafnium will be investigated by means of a high-temperature camera. Finally, in the course of the Group IV-A investigations, a study of the allotropic modifications of certain other pure metals will be made. This program will begin with measurements of the lattice spacings of thorium at low temperatures. Evidence will be sought for an electronic transition between *d* and *f* states in thorium which would be similar to that hypothesized for cerium by Lawson and Tang.[6] Both cerium and thorium have face-centered-cubic crystal structures at room temperatures, and Bridgman[7] has reported a high-pressure modification in thorium, as well as in cerium. In consideration of the related electronic structures of these two elements, which involve *d* and *f* electronic states of nearly the same energies, a low-temperature allotropic transition in thorium may exist. An examination of the lattice spacings of thorium will show if this is true.

The above work with these pure metals will be extended by investigations of alloys involving these elements. When two metals of different valency are mixed, alloys will result with electron concentrations intermediate to the electron concentrations of the pure elements. The alloys of the Group IV-A elements will be investigated by means of low-temperature specific heat measurements and by soft-X-ray measurements. The soft-X-ray measurements will be useful in determining the effects of alloying on the emission and absorption bands, whereas the variation of electron concentration by means of alloying will permit in certain cases the specific heat measurements to be used to determine a more detailed $N(E)$ curve. The results will then be useful in the interpretation of the solid solubilities, the lattice spacing variations, and the crystal structures

(6) A. W. Lawson and Ting-Yuan Tang, "Concerning the High Pressure Allotropic Modification of Cerium," *Phys. Rev.* 76, 301 (1949).

(7) P. W. Bridgman, "Effects of High Shearing Stress Combined with High Hydrostatic Pressure," *Phys. Rev.* 48, 825 (1935).

observed in a series of phase-diagram studies which will be made at the Oak Ridge National Laboratory. The combinations of elements to be investigated will be of three types, as follows:

TYPE	SOLVENT	SOLUTE
1	Group IV-A element with *s* + *d* electrons	Elements with *s* electrons
2	Group IV-A element with *s* + *d* electrons	Elements with *s* + *p* electrons
3	Group IV-A element with *s* + *d* electrons	Elements with *s* + *d* electrons

Type 1. The magnesium-zirconium system is ideal for studying the effects of alloying an element having two *s* electrons with the Group IV-A element zirconium having two *s* and two *d* electrons. The solid solution of magnesium in zirconium is stated by Nowotny, Wormnes, and Mohrnheim[8] to extend to 90 atom % magnesium. The atoms of both these elements are very nearly the same size, and the electrochemical natures of magnesium and zinc are not too greatly different.

Types 1 and 2. The alloy systems of zirconium with the B-subgroup elements of the Second Long Period, silver, cadmium, indium, tin, and antimony, will be investigated next. The tin-zirconium phase diagram is being determined carefully at the Illinois Institute of Technology. It is proposed to investigate here the phase boundaries of the zirconium-rich terminal solid solutions of the remaining systems. This study should show the effects of alloying B-subgroup solute elements having *s* or *s* + *p* valency electrons with zirconium whose valency electrons are either in *s* + *d* states or in *s* states only. The phase boundaries will be plotted in terms of electron concentration, assuming various values for the valency of zirconium. New factors may be found in alloying A-subgroup elements with those from the B subgroups which were not considered in the theories of the alloys involving elements of B subgroups and the short periods only. One of the objects of these experiments is to identify those factors.

Type 3. Finally, in order to test the effects of alloying Group IV-A elements with other elements which have *s* and *d* valency electrons, solute elements will be taken from Groups III-A, IV-A, V-A, and VI-A. Since elements from all these groups apparently have the same number of *s* electrons per atom, the variation of the proportion of each in an alloy with a Group IV-A element should show the effect of varying the concentration of *d* electrons. In this regard the present program will be concerned in the future for the most part with hafnium systems, since titanium and zirconium systems are being investigated in other laboratories. Among the elements of Group III-A — scandium, yttrium, and lanthanum — the atomic diameter of scandium is the most favorable for alloying with zirconium or hafnium. Either the system hafnium-scandium or the system zirconium-scandium would be a favorable one for future research on a micro scale whenever a small quantity of purified scandium is available. However, for the present the solute elements from Group III-A

[8] H. Nowotny, E. Wormnes, and A. Mohrnheim, "Investigations in the Systems Aluminum-Calcium, Magnesium-Calcium, and Magnesium-Zirconium," *Z. Metallkunde* 32, 39 (1940).

will be neglected, and alloying will be done with solutes from Groups IV-A, V-A, and VI-A. The elements tantalum and wolfram, in Groups V-A and VI-A, respectively, follow hafnium in the same row of the Periodic Table. The systems hafnium-tantalum and hafnium-wolfram will be investigated first in the present program, and the results will be compared with those from the zirconium and titanium systems which are being investigated elsewhere.

In addition, the phase diagrams of the systems titanium-zirconium and hafnium-zirconium will be investigated to determine the effects of alloying Group IV-A elements with other Group IV-A elements. Preliminary investigations of both systems have shown that continuous solid solutions are formed. These alloy systems will provide reference diagrams for comparison with the other systems in which a solute from a different group is involved. A more complete examination of both systems is intended, which would include measurement of lattice spacings and examination for possible superlattices.

. . . . .

7. METALLOGRAPHY OF ZIRCONIUM AND ITS ALLOYS

The metallography laboratories of several AEC installations have initiated a study of zirconium and zirconium alloys as a joint program for the identification of constituents, effects of phase transformation, etc.

The metallography laboratory at ORNL has examined some zirconium-nickel and zirconium-tungsten alloys.

The zirconium stock was 1-in. Westinghouse crystal bar. Arc-melting was used in both consumable- and nonconsumable-electrode methods.

The zirconium-nickel alloys were made by rolling the crystal bar to 0.40 in. and wrapping nickel wire, discontinuously, around the bar in machined grooves. This bar was then used as a consumable electrode. A blank melt of the rolled zirconium was made for comparison. An argon atmosphere was used for all melts.

Analyses for the gases O_2, N, and H_2 were made of the crystal bar as received, the blank melt, and two alloys of 2.07 wt % and 4.08 wt % nickel additions and are shown in Table 7.1.

Heat treatments were made of the blank melt and of the two nickel alloys. Diamond pyramid hardness values and X-ray data were obtained after heat treatment. The hardness values are shown in Table 7.2.

TABLE 7.1

Analyses for Gases in Crystal-Bar Zirconium

	O_2 (wt %)	N (wt %)	H_2 (wt %)
1-in. crystal-bar zirconium	0.009 ± 0.003		
Zirconium as cast	0.012 ± 0.003		
Zirconium +2.07 wt % nickel	0.030 ± 0.005		0.0001
Zirconium +4.08 wt % nickel	0.030 ± 0.005		0.0001

TABLE 7.2

Diamond Pyramid Hardness Values* of Zirconium Alloys, 10 kg Load

HEAT TREATMENT	BLANK MELT	1% NICKEL ALLOY	3.2% NICKEL ALLOY
As cast	64-75	119-128	152-167
800°C for 1 hr, slow cooling	51-54	70-82	121-126
900°C for 1 hr, slow cooling	55-58	95-99	100-108
900°C for 1 hr, water quenching	66-76	116-130	133-152

*Hardness of as-received crystal-bar zirconium = 48-53.

Photomicrographs are shown in Figs. 7.1 through 7.4 of the bar as received,

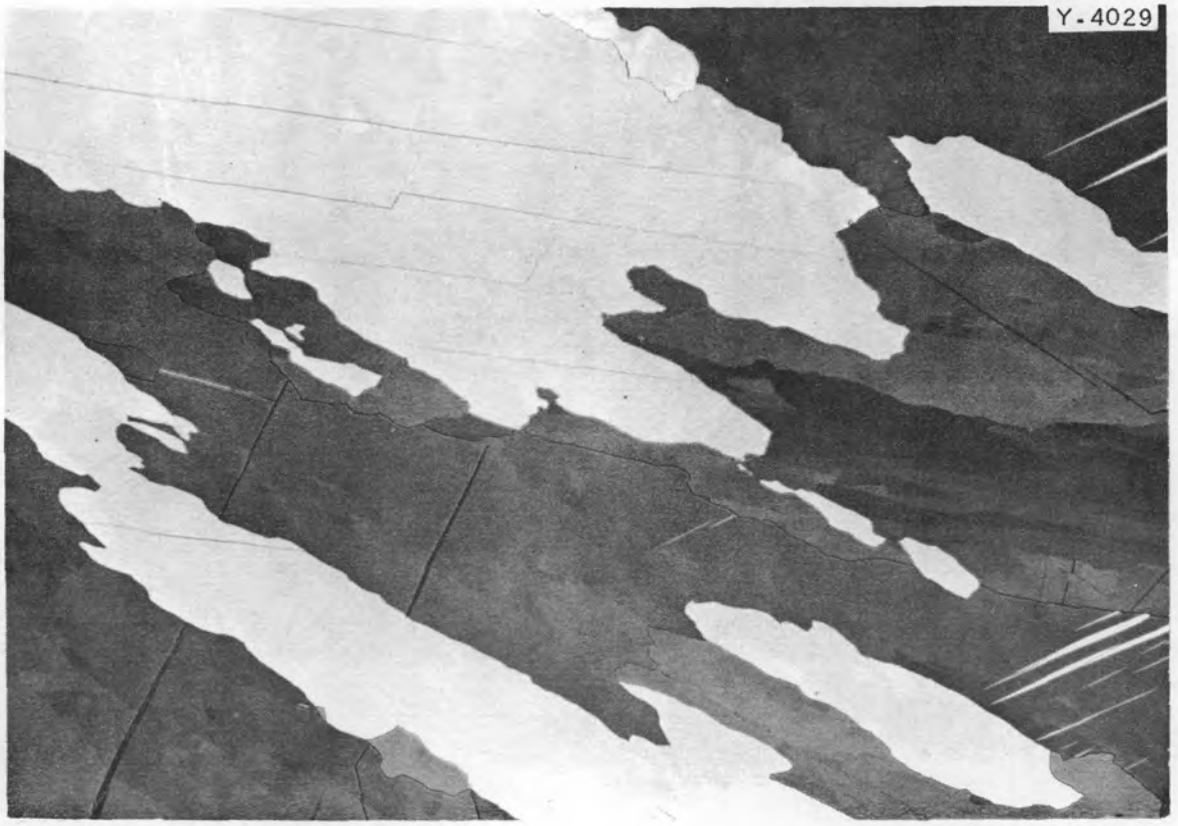

Fig. 7.1 - 1-in. Westinghouse Crystal Bar as Received. 100X. Electrolytically polished; polarized light.

of heat-treated zirconium, and of zirconium-nickel alloys. Specimens were electrolytically polished in a mixture of 1 part of perchloric acid plus 10 parts of glacial acetic acid.

All heat treatments resulted in α-phase zirconium. There was insufficient second phase present in the 2.07 wt % alloy to show on the X-ray spectrometer, but the second phase (probably $ZrNi_3$) was shown in the 4.08 wt % alloy.

The consumable-electrode method could not be used for the zirconium-tungsten alloys since the heat of the arc would not melt the tungsten wire. Consequently, a nonconsumable electrode was used, and tungsten powder was added to the zirconium. This alloy is under examination and will be reported later.

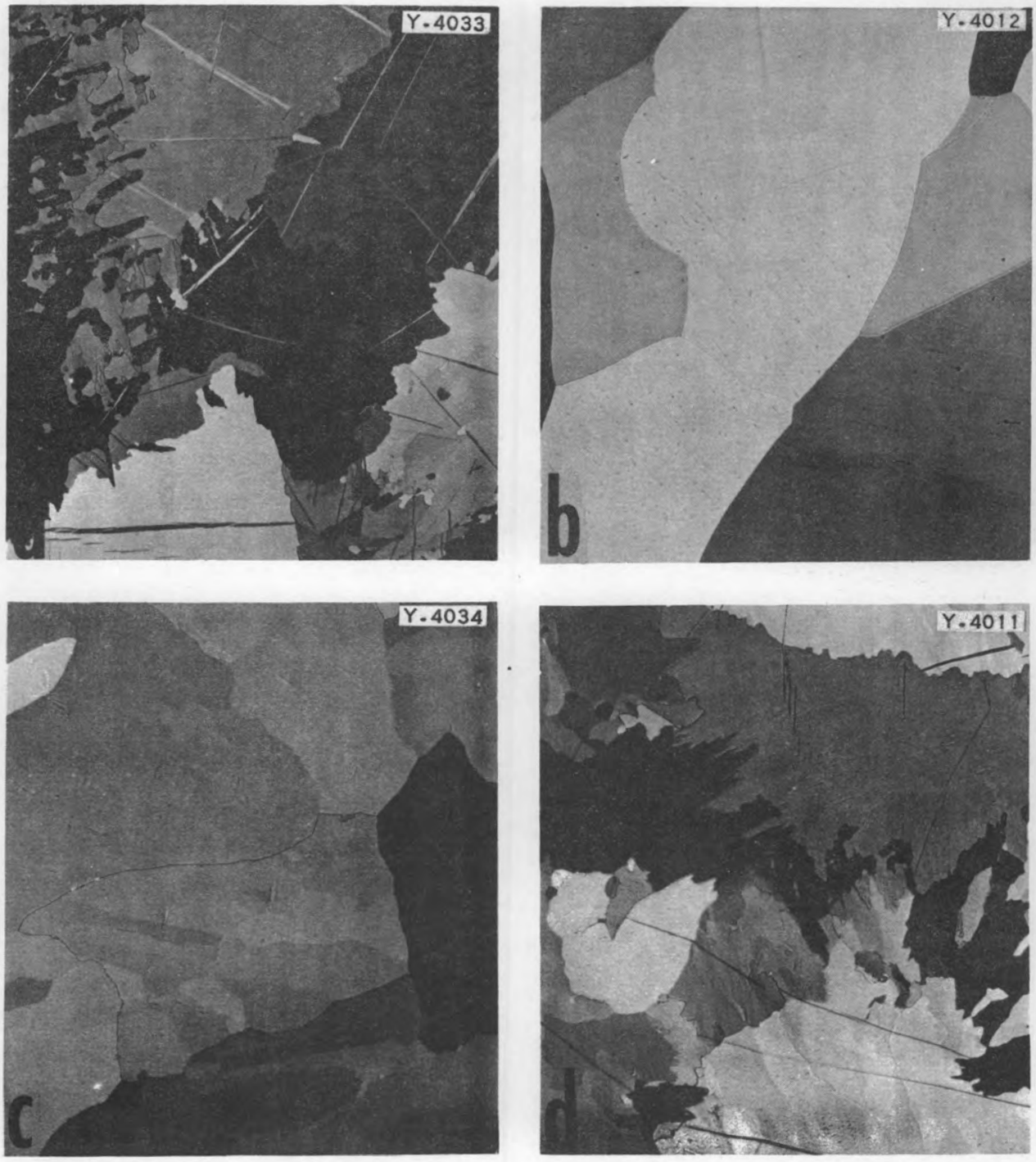

Fig. 7.2 - Zirconium Crystal Bar. 100X. Electrolytically polished; polarized light. (*a*) Arc-melted. (*b*) Arc-melted, 1 hr at 800°C, and slow-cooled. (*c*) Arc-melted, 1 hr at 900°C, and slow-cooled. (*d*) Arc-melted, 1 hr at 900°C, and water-quenched.

UNCLASSIFIED

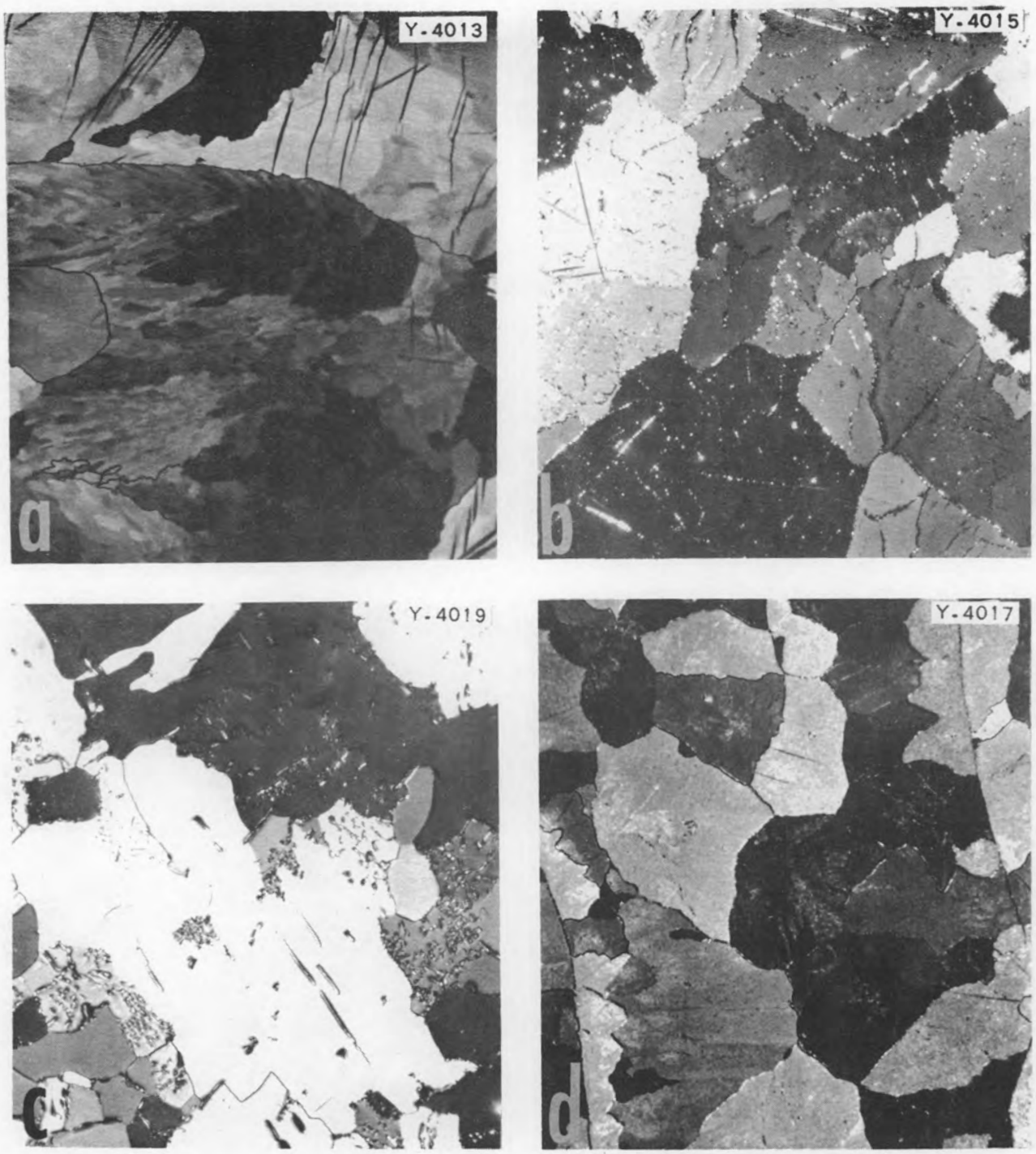

Fig. 7.3 - Zirconium-Nickel Alloy, 2.07 wt % Nickel. 250X. Electrolytically polished; polarized light. (*a*) Arc-melted. (*b*) Arc-melted, 1 hr at 800°C, and slow-cooled. (*c*) Arc-melted, 1 hr at 900°C, and slow-cooled. (*d*) Arc-melted, 1 hr at 900°C, and water-quenched.

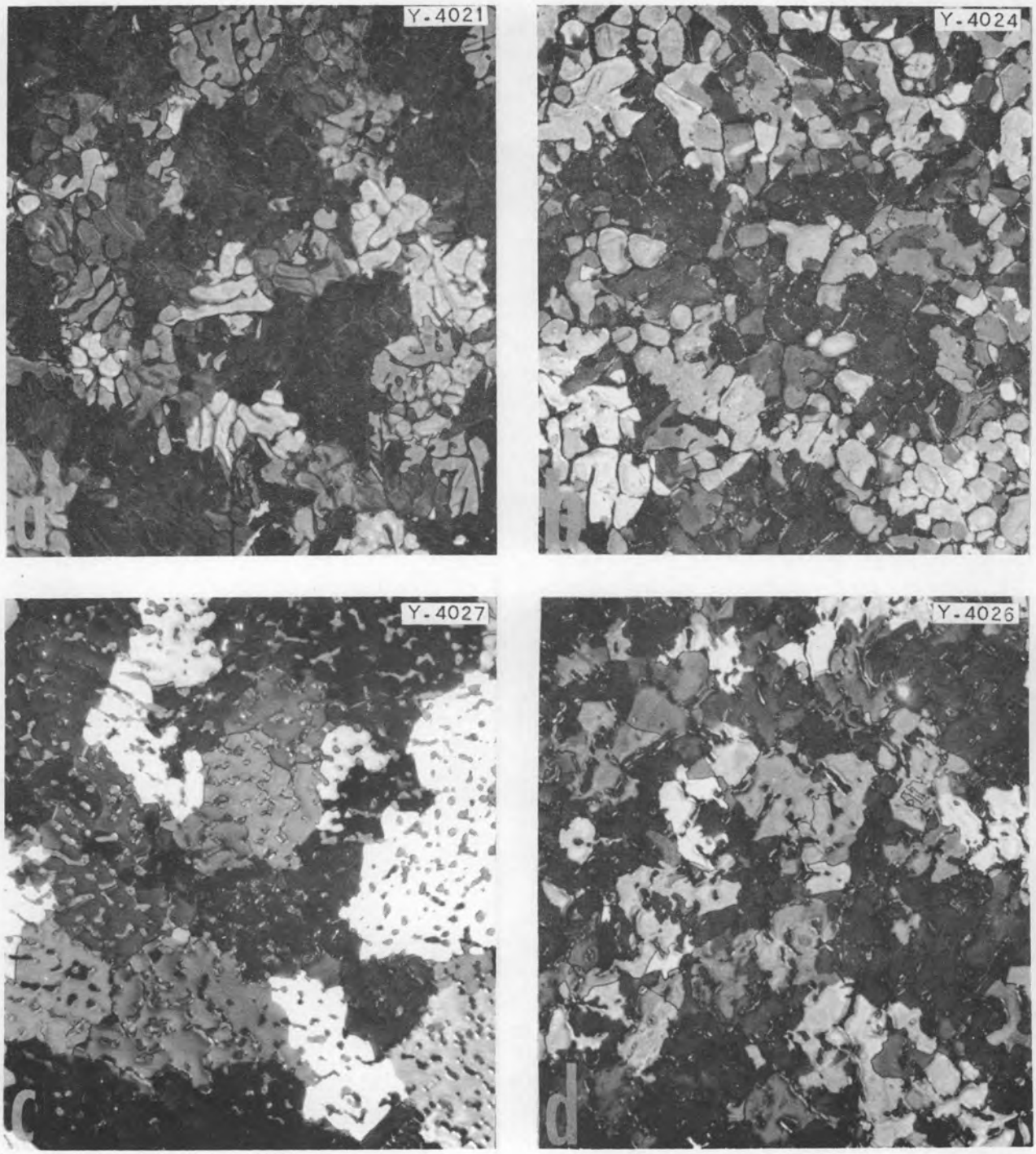

Fig. 7.4 - Zirconium-Nickel Alloy, 4.08% Nickel. 250X. Electrolytically polished; polarized light. (*a*) Arc-melted. (*b*) Arc-melted, 1 hr at 800°C, and slow-cooled. (*c*) Arc-melted, 1 hr at 900°C, and slow-cooled. (*d*) Arc-melted, 1 hr at 900°C, and water-quenched.

8. FUEL ELEMENT FABRICATION

IDAHO UNITS

Late arrival of the enriched uranium metal delayed start-up on the construction of the initial 138 fuel units scheduled for IDOO (Idaho Operations Office) from July 1 to July 15, 1951. During the remainder of the month, however, six units were brazed and the alclad uranium-aluminum alloy plates for nine additional assemblies were prepared.

It now appears that the impurity copper, in an amount less than nominally present in the 99.8% aluminum purity grade, is largely responsible for the consistently high uranium results obtained on analysis of uranium-aluminum alloy melts. In working with the Analytical Chemistry Division on this small but serious discrepancy, it was found that removal of copper by electroplating prior to making the uranium determination results in lowering the uranium content of the alloy approximately 0.5 wt % on an intended 14.2% uranium (800 g of uranium) heat.

BULK SHIELDING FACILITY UNITS

Three modified MTR enriched fuel units were prepared and transferred to the Bulk Shielding Group for use in making gamma-ray spectral measurements on the ANP divided shield.

LITR UNIT

A special nine-plate enriched-fuel unit, designed to permit exposure of radiation study samples to a fast or virgin flux in the LITR, was fabricated for the Physics of Solids Institute.

RaLa UNITS

Twenty-five natural uranium fuel units were fabricated and transferred to the Chemical Technology Division for their dissolving and separation studies on the RaLa program.

. . . . . .

9. SERVICE WORK

MELTING, CASTING, AND FABRICATION FACILITY

Specimens of α-rolled and drawn uranium were cycled 500 times between 100 and 500°C. The α-rolled and drawn material showed normal deformation (approximately 13% elongation) of α-rolled material after cycling. The α-rolled and drawn material that was given a fast β heat treatment showed no elongation or other deformation.

Several hundred feet of 1/8-in. diameter zirconium rod was prepared for the Reactor Experimental Engineering Division for use as welding rod. The rod was made by cold-swaging Westinghouse crystal-bar zirconium from approximately 3/4 to 1/8 in. diameter. The MTA program requires a quantity of zirconium, thorium, and 347 stainless steel wire in sizes of 0.010-, 0.015-, and 0.020-in. diameter. Several feet of zirconium wire 0.018 in. in diameter have been successfully drawn from Westinghouse crystal-bar zirconium. A lacquer dip on a phosphate coating appears to provide good lubrication for drawing to this size. However, sizes smaller than 0.018 in. diameter are offering considerable trouble owing to breakage of the wire.

Uranium disks 1/8 in. thick were cut from Hanford size γ-extruded uranium slugs. Since the slugs were canned, it was necessary to strip the can from the slug and etch the slug prior to cutting.

Brass bars were cold-swaged to ¼ in. and 0.128 in. diameter for G. T. Murray, Physics of Solids Institute. Attempts were made to swage a cadmium bar for Dr. Taylor, Physics of Solids Institute, but the bar cracked after the third pass.

Several uranium melts were prepared and vacuum-cast for extrusion work in connection with the MTA program. Uranium rod was extruded to furnish material to the MTA Group for further work. Approximately 12 ft of ½-in.-diameter rod and several feet of 5/8-in.-diameter rod were prepared. Two duplex extrusions of uranium and zirconium were made to furnish uranium rod with an outside cladding of zirconium. The rods were returned to the MTA Group for examination.

Manganese and nickel steels were prepared for use in the graduate study program under the direction of Dr. E. E. Stansbury.

A number of zirconium alloys were prepared for Dr. Jesse Betterton, Jr. for use in the Fundamental Research Group.

A 2% gold—98% beryllium alloy was prepared for B. S. Borie for study of a possible high-temperature phase of beryllium which is supposedly stabilized at room temperature by the gold addition.

ROLLING MILL

During the past quarter the following service work was completed:

Several zirconium target samples, 3 in. thick, were prepared for cyclotron bombardment studies by the Group at Y-12.

Cold-rolled zirconium plates, 2 by 12 in. in area by 10, 20, and 30 mils thick, were prepared for the Savannah River Operations Office.

Thick-walled inconel piping was converted into thin sheet for use in the ANP brazing experiments.

Several high-purity (99.99% minimum) aluminum target plates were prepared for cyclotron testing at Y-12.

Beryllium foil, 3 by 12 in. in area, 4.5 to 5.0 mils thick, was prepared from Brush sintered metal by hot-rolling for X-ray-diffraction work in the Chemistry Division.

Component parts of water-cooled target assemblies were fabricated for cyclotron bombardment studies on bismuth at Y-12.

Several lithium-aluminum alloy billets prepared at Argonne National Laboratory were vacuum annealed in an attempt to outgas or remove the undesirable hydrogen gas impurity present in the alloy.

X-RAY-DIFFRACTION LABORATORY

During this quarter 423 diffraction patterns were measured as a service activity for other research groups by the X-ray laboratory. This is an increase of more than 40% over the first quarter of 1951. Patterns taken for metallurgy research account for 65% of the service work; for chemistry, 32%; and for physics, 3%.

As in the previous quarter, most of the service work was identification. Some precision lattice parameter measurements and a few preferred orientation studies were made.

CREEP-RUPTURE LABORATORY

Twenty thorium samples were pulled in tension for the Thorium Research Group. Stress-strain curves were obtained on all tests. The tensile strength of five inconel weld specimens and ten inconel tube-to-header specimens was determined for the Welding Section. Twenty-two pipe sections, types 316, 304, 347 stainless steel, and inconel, from sodium harps in the Liquid Metals Corrosion Section were pulled in tension. Nine thin-walled tube sections, types 347 and 310 stainless steel, from sodium harps were also pulled in tension. The tensile strength of five tube-to-header inconel specimens, brazed joints, and seven thin-walled inconel tubes was determined for the Welding Group.

Calibration of the Baldwin tensile testing machine was made with the aid of the Instrument Department. For this work, Morehouse proving rings, calibrated by the Bureau of Standards, were used. The accuracy of the machine was found to be within 0.5%.

Several high-density randomly oriented samples of both copper and bismuth were pressed for the Fundamental Research Section. With bismuth a density of 99% was obtained in the pressed condition. A compact consisting of 55% copper and 45% nickel was also pressed for this group.

Samples of types 304, 310, 316, and 347 stainless steel and inconel were decarburized by a wet hydrogen treatment similar to that discussed in the last report (ORNL-1033). Twenty lengths of inconel tubing were given various heat treatments in nonoxidizing atmospheres for use in liquid-metal corrosion and welding work.

SECRET

RESTRICTED DATA

This document contains restricted data as defined in the Atomic Energy Act of 1946.

CAUTION

This document contains information affecting the National Defense of the United States. Its transmission or the disclosure of its contents in any manner to any unauthorized person is prohibited and may result in severe criminal penalties under applicable Federal laws.

SECRET